



ELSEVIER

Available online at www.sciencedirect.com

SCIENCE @ DIRECT®

Journal of Non-Crystalline Solids xxx (2006) xxx–xxx

JOURNAL OF  
NON-CRYSTALLINE SOLIDS

www.elsevier.com/locate/jnoncrsol

Review

# Homogeneous crystal nucleation in silicate glasses: A 40 years perspective

Vladimir M. Fokina<sup>a,\*</sup>, Edgar D. Zanotto<sup>b</sup>, Nikolay S. Yuritsyn<sup>c</sup>,  
Jörn W.P. Schmelzer<sup>d</sup>

<sup>a</sup> Vavilov State Optical Institute, ul. Babushkina 36-1, 193171 St. Petersburg, Russia

<sup>b</sup> LaMaV – Vitreous Materials Laboratory, Federal University of São Carlos, 13565-905 São Carlos, SP, Brazil

<sup>c</sup> Grebenshchikov Institute of Silicate Chemistry, Russian Academy of Sciences, ul. Odoevskogo 24-2, 199155 St. Petersburg, Russia

<sup>d</sup> Institut für Physik, Universität Rostock, 18051 Rostock, Germany

Received 18 June 2005; received in revised form 27 January 2006

## 13 Abstract

14 We review a plethora of relevant experimental results on internal homogeneous crystal nucleation in silicate glasses obtained in the  
15 last four decades, and their analyses in the framework of the classical nucleation theory (CNT). The basic assumptions and equations of  
16 CNT are outlined. Particular attention is devoted to the analysis of the properties of the critical nuclei, which, to a large extent, govern  
17 nucleation kinetics. The main methods employed to measure nucleation rates are described and the possible errors in the determination  
18 of the crystal number density (and, correspondingly, in nucleation rates) are discussed. The basic regularities of both time and temper-  
19 ature dependencies of nucleation rates are illustrated by numerous experimental data. Experimental evidence for a correlation between  
20 maximum nucleation rates and reduced glass transition temperatures is presented and theoretically justified. Special attention is given to  
21 serious problems that arise in the quantitative description of nucleation rates when using the CNT, for instance: the dramatic discrepancy  
22 between calculated and measured nucleation rates; the high value of the crystal nuclei/melt surface energy,  $\sigma_{cm}$ , if compared to the  
23 expected value estimated via Stefan's rule; the increase of  $\sigma_{cm}$  with increasing temperature; and the discrepancies between the values  
24 of the surface energy and the time-lag for nucleation when independently estimated from nucleation and growth kinetics. The analysis  
25 of the above mentioned problems leads to the following conclusion: in contrast to Gibbs' description of heterogeneous systems under-  
26 lying CNT, the bulk thermodynamic properties of the critical nuclei generally differ from those of the corresponding macro-phase result-  
27 ing simultaneously in significant differences of the surface properties as compared with the respective parameters of the planar interfaces.  
28 In particular, direct experimental evidence is presented for compositional changes of the crystal nuclei during formation of the critical  
29 nuclei and their growth from critical to macro-sizes. In addition, detailed examinations of crystal nucleation and growth kinetics show a  
30 decrease of both the thermodynamic driving force for nucleation and of the critical nuclei/liquid interfacial energy, as compared with the  
31 respective properties of the macro-phase. However, despite significant progress in understanding crystal nucleation in glasses in the past  
32 four decades, many problems still exist and this is likely to remain a highly interesting subject for both fundamental and applied research  
33 for a long time.

34 © 2006 Published by Elsevier B.V.

35 **Keywords:** Crystallization; Glass ceramics; Nucleation; Crystals; Glass transition; Oxide glasses; Silicates; Thermodynamics

## 1. Introduction

Glasses can be defined as non-crystalline solids that  
undergo a *glass transition* in the course of their prepara-  
tion. One of the most important and traditional (but not  
the only) method of vitrification consists in supercooling

\* Corresponding author. Address: ul. Nalichnay 21, ap.7, 199406 St. Petersburg, Russia. Tel.: +7 812 355 30 38.

E-mail address: vfokin@pisem.net (V.M. Fokina).

42 a liquid escaping crystallization. Thus, when a liquid is  
 43 cooled down at sufficiently high rates, crystallization can  
 44 occur to a limited degree or can be completely arrested  
 45 down to temperatures corresponding to very high viscosi-  
 46 ties, in the range  $\eta \geq 10^{13} - 10^{12}$  Pa s  $\approx \eta(T_g)$ , where  $T_g$  is  
 47 the glass transition temperature. Below this temperature,  
 48 the viscosity is so high that large-scale atomic rearrange-  
 49 ments of the system are no longer possible within the  
 50 time-scale of typical experiments, and the structure  
 51 freezes-in, i.e., the structural rearrangements required to  
 52 keep the liquid in the appropriate metastable equilibrium  
 53 state cannot follow any more the change of temperature.  
 54 This process of freezing-in the structure of an undercooled  
 55 liquid transforming it into a glass is commonly denoted as  
 56 *glass transition*. Typical glass-forming liquids, such as sili-  
 57 cate melts, are usually characterized by: (i) relatively high  
 58 viscosities ( $\eta > 100$  Pa s) at the melting point or liquidus  
 59 and (ii) a steep increase of the viscosity with decreasing  
 60 temperature. These properties favor vitrification. The  
 61 mechanism above sketched leads to the conclusion that  
 62 the glass structure must be similar to that of the parent  
 63 undercooled liquid at temperatures near  $T_g$  and, indeed,  
 64 this similarity has been experimentally observed.

65 Glass is thermodynamically unstable with respect to the  
 66 undercooled liquid, i.e., there is no energy barrier between  
 67 the glass and its corresponding undercooled (metastable)  
 68 liquid. At a first glance, the high stability of the glassy state  
 69 reflects only a relaxation problem; the system cannot  
 70 evolve to a metastable state due to the kinetic inhibition  
 71 of this process at low temperatures. On heating, relaxation  
 72 of the glass structure may occur to reach first a metastable  
 73 liquid state corresponding to the given temperature and  
 74 then, eventually, go over into the crystalline state. The lat-  
 75 ter evolution process, as will be shown below, involves  
 76 overcoming of a thermodynamic potential barrier. At  
 77 room temperature glasses can exist for extremely long peri-  
 78 ods of time because their high viscosity inhibits structural  
 79 rearrangements required for crystal nucleation and growth.  
 80 However, when a glass is heat-treated for a sufficiently long  
 81 time at temperatures within or above the glass transition  
 82 range, devitrification readily starts, as a rule, from the sur-  
 83 face and sometimes in the bulk via heterogeneous or homo-  
 84 geneous nucleation (see below).

85 Nucleation, or the process of formation of the precu-  
 86 rsors of the crystalline phases, may occur by different mech-  
 87 anisms. Commonly one divides these processes into  
 88 homogeneous and heterogeneous nucleation. Homoge-  
 89 neous nucleation is a stochastic process occurring with  
 90 the same probability in any given volume (or surface) ele-  
 91 ment. Alternatively, nucleation occurring on preferred  
 92 nucleation sites, e.g., such as pre-existing interfaces, previ-  
 93 ously nucleated phases, and surface defects, is denoted as  
 94 heterogeneous nucleation. Depending on the location  
 95 where nucleation takes places, volume (bulk) and surface  
 96 crystallization can be distinguished.

97 Glass-forming melts are interesting models for studies of  
 98 nucleation, growth and overall crystallization phenomena.

Their high viscosities result in relatively low (measurable) 99  
 rates of crystallization, which may permit detailed studies 100  
 of nucleation and growth kinetics. Homogeneous nucle- 101  
 ation can sometimes be observed at deep undercoolings 102  
 ( $T/T_m < 0.6$ ) because glass-forming melts are excellent sol- 103  
 vents for solid impurities that thus only exist as ionic spe- 104  
 cies when the liquid is vitrified. In addition, the rapid 105  
 increase of viscosity with decreasing temperature makes it 106  
 possible to ‘freeze-in’ different states of the crystallization 107  
 process by quenching previously heat-treated specimens 108  
 to room temperature. Hence, as it was figuratively said in 109  
 Ref. [1], ‘glasses did and may serve as the *Drosophila* of 110  
 nucleation theory in order to test different approaches’. 111  
 Moreover, silicate glass is one of the oldest materials pro- 112  
 duced by mankind, having its origin about 6000 years 113  
 ago in ancient Mesopotamia [2], but are still gaining tech- 114  
 nological importance. 115

116 It is evident from the above discussion that crystalliza- 117  
 tion and glass formation are competitive processes. In this 118  
 way, in order to avoid uncontrolled crystallization of glassy 119  
 articles one needs to know the main factors that govern 120  
 crystal nucleation and growth. On the other hand, con- 121  
 trolled nucleation and crystallization of glasses underlay 122  
 the production of glass-ceramics invented in the mid- 123  
 1950s [3], which are widely used in both domestic and 124  
 high-technology applications. By the foregoing reasons, 125  
 the investigation of glass crystallization kinetics is of great 126  
 interest from both practical and theoretical points of view. 127  
 Since, in many respects, the nucleation stage determines the 128  
 pathways of overall crystallization, in this review we will 129  
 focus our attention on nucleation, with particular emphasis 130  
 on the analysis of relevant experimental results in the 131  
 framework of the classical nucleation theory (CNT). 132  
 Hereby we will restrict ourselves to selected data for homo- 133  
 geneous nucleation obtained mainly with silicate glasses. 134

135 The present paper is organized as follows: In Section 2, 136  
 the basic equations of CNT are briefly summarized, which 137  
 are then employed for nucleation data analysis. Section 3 138  
 presents the main methods that may be employed to exper- 139  
 imentally determine nucleation rates. Section 4 is devoted 140  
 to experimental findings concerning transient and steady- 141  
 state crystal nucleation in glasses. In particular, evidence 142  
 for a strong correlation between nucleation rates and 143  
 reduced glass transition temperature is given. An analysis 144  
 of the problems arising in the application of CNT to exper- 145  
 imentally observed nucleation rate data is performed in 146  
 Section 5. The paper is completed by concluding remarks. 147

## 2. Basic assumptions and equations of classical nucleation theory (CNT) 148

### 2.1. Historical notes 149

150 In its original form, classical nucleation theory is based 151  
 on the thermodynamic description of heterogeneous sys- 152  
 tems developed by Gibbs [4]. Following Gibbs, a real inho- 153  
 mogeneous system is replaced by a model system consisting 154

153 of two homogeneous phases divided by a mathematical  
154 surface of zero thickness. While the properties of the ambi-  
155 ent phase are known, the bulk properties of the critical  
156 clusters are determined via Gibbs' equilibrium conditions.  
157 A detailed analysis shows that the cluster bulk properties  
158 determined in such way are widely identical to the proper-  
159 ties of the newly evolving macroscopic phase coexisting in  
160 stable equilibrium with the ambient phase at a planar inter-  
161 face. The free energy of the heterogeneous system – consist-  
162 ing of a cluster of the newly evolving phase in the ambient  
163 phase – is expressed as the sum of the bulk contributions of  
164 the nucleus and the ambient phase. These bulk terms are  
165 supplemented by interfacial contributions, the main one  
166 is given by the product of the interfacial area and specific  
167 surface energy.

168 When applying the theory to cluster formation, these  
169 surface terms initially result in an increase of the character-  
170 istic thermodynamic potential, which leads to the existence  
171 of a critical cluster size. Only clusters with sizes larger than  
172 the critical size are capable to grow up to macroscopic  
173 dimensions in a deterministic way. The change of the char-  
174 acteristic thermodynamic potential resulting from the for-  
175 mation of clusters of critical size is commonly denoted as  
176 the work of critical cluster formation. This quantity reflects  
177 the thermodynamic aspects in the description of nucleation.

178 In addition to thermodynamic aspects of nucleation, the  
179 dynamics of cluster formation and growth must be appro-

180 priately incorporated into the theory. Different approaches  
181 have been employed depending on the particular problem  
182 being analyzed. The application of CNT to the formation  
183 of crystals originates from the work of Kaischew and  
184 Stranski [5]. These authors investigated this problem for  
185 the case of crystal formation from supersaturated vapor  
186 employing the approach developed by Volmer and Weber  
187 [6] for vapor condensation. Further advances in CNT  
188 including nucleation in the condensed systems, which are  
189 the focus of the present review, were connected with the  
190 work of Becker and Döring [7], Volmer [8], Frenkel [9],  
191 Turnbull and Fisher [10], Reiss [11] and others. Photo-  
192 graphs of some of these pioneers of nucleation theory are  
193 shown in Fig. 1.

194 According to CNT, the description of homogeneous and  
195 heterogeneous nucleation can be basically performed by  
196 the same methods. We will present first the results for  
197 homogeneous nucleation and afterwards will introduce  
198 the modifications required to account for the effect of insol-  
199 soluble solid impurities and interfaces that may lead to heter-  
200 ogeneous nucleation.

## 2.2. Homogeneous nucleation

201  
202 As we already discussed, homogeneous nucleation sup-  
203 poses the same probability of critical nucleus formation  
204 in any given volume or surface element of the system under



Fig. 1. From top left to right bottom: J.W. Gibbs, G. Tammann, M. Volmer, R. Kaischew, J. Frenkel, and D. Turnbull.

205 study. According to CNT (see, e.g., Refs. [12,13]), the  
206 steady-state homogeneous volume nucleation rate can be  
207 written as  
208

$$I_{st} = I_o \exp \left[ -\frac{W_* + \Delta G_D}{k_B T} \right], \quad (1)$$

$$I_o = 2N_1 \frac{k_B T}{h} \left( \frac{a^2 \sigma_{cm}}{k_B T} \right)^{1/2}.$$

211 This equation determines the so-called steady-state nucle-  
212 ation rate,  $I_{st}$ , i.e., the number of supercritical clusters  
213 formed per unit time in a unit volume of the system. The  
214 pre-exponential term,  $I_o$ , depends only weakly on tempera-  
215 ture (if compared to the exponential function) and varies  
216 between  $10^{41}$  and  $10^{43} \text{ m}^{-3} \text{ s}^{-1}$  for different condensed sys-  
217 tems [14]. In Eq. (1)  $k_B$  and  $h$  are the Boltzmann and  
218 Planck constants, respectively;  $N_1 \sim 1/a^3$  is the number of  
219 structural (formula) units, with a mean size  $a$ , per unit vol-  
220 ume of melt;  $\sigma_{cm}$  is specific surface free energy of the crit-  
221 ical nucleus-melt interface;  $\Delta G_D$  is the activation free  
222 energy for transfer of a ‘structural unit’ from the melt to  
223 a nucleus (kinetic barrier). To a first approximation, the ki-  
224 netic barrier for glass-forming liquids is often replaced by  
225 the activation free energy for viscous flow,  $\Delta G_\eta$ .  $W_*$  is the  
226 thermodynamic barrier for nucleation, i.e., the increase in  
227 the free energy of a system due to the formation of a nu-  
228 cleus with critical size,  $r_*$ . The critical nucleus size can be  
229 determined from the condition

$$\frac{\partial W}{\partial r} = 0, \quad W = c_1 r^2 \sigma_{cm} - c_2 r^3 \Delta G_V, \quad (2)$$

232 where  $\Delta G_V = G_l - G_c$  is the difference between the free  
233 energies of liquid and crystal per unit volume of the crystal  
234 (i.e., the thermodynamic driving force for crystallization)  
235 and  $c_1$  and  $c_2$  are shape factors. In the case of a spherical  
236 nucleus, we obtain the expressions  
237

$$r_* = \frac{2\sigma_{cm}}{\Delta G_V} \quad (3)$$

240 and

$$W_* = \frac{16\pi}{3} \frac{\sigma_{cm}^3}{\Delta G_V^2}. \quad (4)$$

244 The thermodynamic driving force for crystallization is  
245 given by  
246

$$\Delta G_V V_m = \frac{\Delta H_m}{T_m} (T_m - T) + \int_T^{T_m} \Delta C_p dT' - T \int_T^{T_m} \frac{\Delta C_p}{T'} dT', \quad (5)$$

249 where  $V_m$  is the molar volume,  $\Delta H_m$  and  $T_m$  are the molar  
250 heat of melting and the melting temperature of the crystal,  
251 respectively, and  $\Delta C_p = C_p^l - C_p^c$  is the difference between  
252 the molar heat capacities of liquid and crystal at constant  
253 pressure. The experimental values of  $\Delta G_V$  are normally  
254 bounded by the approximations usually assigned to Turn-  
255 bull (Eq. (6)) and Hoffman (Eq. (7)) that assume  $\Delta C_p = 0$   
256 and  $\Delta C_p = \text{constant}$ , respectively [13],

$$\Delta G_V(T) = \Delta H_V \left( 1 - \frac{T}{T_m} \right), \quad (6)$$

$$\Delta G_V(T) = \Delta H_V \left( 1 - \frac{T}{T_m} \right) \frac{T}{T_m}. \quad (7) \quad 259$$

Here  $\Delta H_V$  is the melting enthalpy per unit volume of the  
260 crystal. One should note, however, that Eq. (6) was first  
261 employed by Thomson and Volmer (cf. Ref. [8]).  
262

Eq. (1) describes the time-independent steady-state  
263 nucleation. Such nucleation regime occurs if a stationary  
264 size distribution of the newly evolving subcritical ( $r < r_*$ )  
265 and critical ( $r = r_*$ ) nuclei is established in the system.  
266 The cooling rates typically employed for glass formation  
267 from the melt, and the heating rates of small glass speci-  
268 mens to any given temperature  $T$  under investigation are  
269 commonly too high to maintain a steady-state distribution  
270 of nuclei in the system. Hence, some time period is needed  
271 for a reconstruction of the initial nuclei distribution  
272 towards the time-independent distribution corresponding  
273 to the temperature of study. During this period the nucle-  
274 ation rate varies and approaches a steady-state value given  
275 by Eq. (1).  
276

The time required to establish steady-state nucleation in  
277 a system is commonly denoted as the time-lag for nucle-  
278 ation,  $\tau$ . It characterizes the duration for the onset of the  
279 steady-state distribution, and hence the evolution of the  
280 nucleation rate,  $I(t)$ , towards a steady-state value,  $I_{st}$ . In  
281 the cases when the initial concentration of critical and  
282 sub-critical nuclei may be neglected,  $\tau$  and  $I(t)$  can be  
283 expressed by Eqs. (8) and (9), respectively [15,16],  
284  
285

$$\tau = \frac{16h}{\pi} \frac{\sigma_{cm}}{\Delta G_V^2 a^4} \exp \left( \frac{\Delta G_D}{k_B T} \right), \quad (8)$$

$$I(t) = I_{st} \left[ 1 + 2 \sum_{m=1}^{\infty} (-1)^m \exp \left( -m^2 \frac{t}{\tau} \right) \right]. \quad (9) \quad 287$$

Integration of Eq. (9) results in the following expression for  
288 the time-dependence of the number of super-critical nuclei  
289 per unit volume of the system,  $N_V$ ,  
290  
291

$$\frac{N_V(t)}{I_{st} \tau} = \left[ \frac{t}{\tau} - \frac{\pi^2}{6} - 2 \sum_{m=1}^{\infty} \frac{(-1)^m}{m^2} \exp \left( -m^2 \frac{t}{\tau} \right) \right]. \quad (10) \quad 293$$

For sufficiently long times,  $t$ , as compared with  $\tau$  this  
294 expression can be approximated by  
295  
296

$$N_V(t) = I_{st} \left( t - \frac{\pi^2}{6} \tau \right). \quad (11) \quad 298$$

For the experimental estimation of  $\tau$ , it is convenient to  
299 use the induction period,  $t_{ind}$ , defined via Eq. (12) as  
300  
301

$$\tau = \frac{6}{\pi^2} t_{ind}. \quad (12) \quad 303$$

The induction period,  $t_{ind}$ , is easily determined as the inter-  
304 section of the asymptote (Eq. (11)) with the time-axis. An-  
305 other more correct way to estimate  $I_{st}$  and  $\tau$  is by fitting the  
306 experimental values of  $N(t)$  to Eq. (10).  
307

### 308 2.3. Heterogeneous nucleation

309 The existence of foreign solid particles and phase  
310 boundaries may favor nucleation. This effect is due mainly  
311 to the diminished thermodynamic barrier as compared to  
312 that for homogeneous nucleation, owing to a decrease of  
313 the contribution of the effective surface energy to the work  
314 of critical cluster formation. For example, the thermody-  
315 namic barrier for nucleation in the case of condensation  
316 on planar interfaces is given by [12]

$$318 W_*^{\text{het}} = W_* \Phi, \quad \Phi = \frac{1}{2} - \frac{3}{4} \cos \theta + \frac{1}{4} \cos^3 \theta. \quad (13)$$

319 Depending on the value of the wetting angle,  $\theta$ , the param-  
320 eter  $\Phi$  varies from zero to unity. The value of  $\Phi$  depends on  
321 the mechanism of nucleation catalysis.

322 In order to adapt the expression for the steady-state  
323 nucleation rate, Eq. (1), to the description of heterogeneous  
324 nucleation, the number of ‘structural’ units per unit vol-  
325 ume,  $N_1$ , which appears in the pre-exponential term of  
326 Eq. (1), must be replaced by the number,  $N^S$ , of ‘structural  
327 units’ in contact with the catalyzing surface per unit vol-  
328 ume. Hence, in the case of heterogeneous nucleation, the  
329 following equation can be written for the steady-state  
330 nucleation rate:

$$332 I_{\text{st}}^{\text{het}} \cong N^S \frac{k_B T}{h} \exp \left[ -\frac{W_* \Phi + \Delta G_D}{k_B T} \right]. \quad (14)$$

333 Catalyzing surfaces may be represented, for instance, by  
334 dispersed solid particles that act as nucleation sites. In this  
335 case, their curvature and number may strongly affect the  
336 nucleation kinetics [14,17]. The exhaustion of available  
337 nucleation sites due to crystal nucleation leads to satur-  
338 ation of the kinetic curve  $N$  versus  $t$ . If, however, for some  
339 reason such saturation is not achieved, the knowledge of  
340 the  $N(t)$ -dependence is not sufficient to conclude what type  
341 of nucleation took place.

## 342 3. Experimental methods to estimate nucleation rates

### 343 3.1. General problem

344 At high undercoolings corresponding to the range of  
345 measurable homogeneous (volume) nucleation rates in typ-  
346 ical glass-forming liquids, the critical nuclei are undetect-  
347 able by common experimental techniques, hence they  
348 must first be developed to a visible size to allow one to  
349 determine (e.g., using a microscope) their number density,  
350  $N$ , as a function of time, allowing then to estimate the  
351 nucleation rate as  $I = dN/dt$ . In order to perform such  
352 task, different methods have been developed.

### 353 3.2. Double-stage (‘development’) method

354 If the overlapping of the nucleation and growth rate  
355 curves is weak (i.e., the crystal growth rates are very low  
356 at temperatures corresponding to high nucleation rates),  
357 the observation of the nucleated crystals and the estimation

of the crystal number density is a quite difficult task. For  
these cases, about a hundred years ago, Gustav Tammann  
(who was studying crystallization of organic liquids) pro-  
posed the following procedure, which is now known as  
the Tammann or ‘development’ method [18]. Crystals  
nucleated at a low temperature,  $T_n$ , are grown up to micro-  
scopic sizes at a higher temperature,  $T_d > T_n$ . The develop-  
ment temperature  $T_d$  has to meet the following conditions  
for nucleation ( $I$ ) and growth ( $U$ ) rates:  $I(T_d) \ll I(T_n)$  and  
 $U(T_d) \gg U(T_n)$ . After a lapse of seventy years, Ito et al.  
[19] and Filipovich and Kalinina [20] independently applied  
Tammann’s method to the study of crystal nucleation  
kinetics in lithium disilicate glasses. Since then, this method  
has been widely employed for glass crystallization studies.  
Some problem inherent in this method and connected with  
the possible dissolution of some part of the originally  
formed (at the nucleation temperature) nuclei at the devel-  
opment temperature will be discussed later.

### 358 3.3. Single-stage methods

#### 359 3.3.1. The direct method

When there is considerable overlap of the  $I(T)$  and  $U(T)$ -  
curves, the number density of crystals can be measured  
directly after single-stage heat treatments at  $T_n$ . Then, the  
obtained  $N(T_n, t)$ -curve will be shifted (relatively to the true  
one) to higher times by a time  $t_o = (r_{\text{res}} - r_*)/U(T_n) \cong r_{\text{res}}/$   
 $U(T_n)$  that is needed to grow the crystals up to the micro-  
scope resolution limit,  $\varepsilon = 2r_{\text{res}}$  [21]. Finally, one must cor-  
rect the number densities to account for stereological  
errors. This procedure will be described in Section 3.4.

#### 360 3.3.2. Crystal size distribution analysis

Continuous nucleation and growth normally result in a  
broad distribution of crystal sizes, i.e., the first nucleated  
crystal has the largest size and so forth. If the crystal  
growth rate is known, one can calculate the ‘birth dates’  
of crystals belonging to different size groups and then plot  
a  $N(t)$ -curve. Toshev and Gutzow derived the basic form-  
ulas relating the size distribution of spherical isolated  
particles embedded in a continuous matrix with that of  
their circular intersections on a sample cross-section for  
both steady-state and transient volume nucleation [22].  
For surface crystallization the size distribution is easily  
constructed from direct measurements. This method,  
known as Köster’s method, also works in the case of heter-  
ogeneous nucleation from a finite number of active centers  
when the latter are depleted in a relative short time, and  
further advancement of crystallization only occurs via crys-  
tal growth. It has been systematically employed to study  
the surface nucleation rates in metallic [23] and silicate  
glasses [24].

### 361 3.4. Stereological corrections

The use of reflected light microscopy can lead to large  
errors in the determination of the number of crystals per

410 unit volume due to the stereological methods employed to  
 411 calculate volume properties (size distributions, numbers,  
 412 etc.) based on statistical evaluations performed on cross-  
 413 sections through the specimens. Thus a significant fraction  
 414 of the cut crystals (in the cross-sections) can be smaller  
 415 than the resolution limit of the microscope used, which  
 416 may lead to an underestimation of the crystal numbers  
 417 and, consequently, of the determined values of nucleation  
 418 rates. In Refs. [25,26], equations were derived for the frac-  
 419 tional underestimation,  $f$ , of the number of spherical parti-  
 420 cles per unit volume and of the nucleation rates, as  
 421 obtained from stereological techniques for reflected light  
 422 microscopy or SEM, for typical cases of crystal nucleation  
 423 in glasses. The following two cases bound the most com-  
 424 mon experimental situations: (i) a monodisperse system  
 425 of spherical particles that can result from instantaneous  
 426 heterogeneous nucleation; (ii) a uniform size distribution  
 427 of spherical particles from the critical size to  $D_M$ , where  
 428  $D_M$  is the largest diameter of the clusters in the distribu-  
 429 tion. Such distribution is typical for simultaneous nucle-  
 430 ation and growth with constant rates in a single-stage  
 431 heat treatment. The equations for these cases are:

432 *Case (i). Monodisperse systems:*

$$434 \quad f = \frac{2}{\pi} \arcsin(\sigma_1), \quad (15)$$

435 *Case (ii). Uniform size distribution from the critical size to*  
 436  *$D_M$ :*

$$438 \quad f = 1 - \left\{ \frac{2}{\pi} [\cos \theta_1 [1 - \ln(1 + \sin \theta_1)] + \theta_1 + \sigma_1 \ln \sigma_1 - \sigma_1] \right\}. \quad (16)$$

439 In above equations,  $\theta_1 = \arccos \sigma_1$ ,  $\sigma_1 \equiv \varepsilon/D_M$ , and  $\varepsilon$  is the  
 440 resolution limit of the microscope used. Comparison with  
 441 experimental nucleation data for two silicate glasses dem-  
 442 onstrated that these equations predict well the observed  
 443 underestimations of the number of spherical particles.  
 444 Fig. 2 shows the function  $f$  for cases (i) and (ii).

445 To minimize these errors employing reflected light opti-  
 446 cal microscopy methods, one should use high magnification  
 447 objective lenses or SEM. Alternatively, transmission meth-  
 448 ods could be used because they lead to much smaller errors  
 449 than reflection techniques.

450 Similar underestimates occur when one tries to deter-  
 451 mine volume fractions crystallized, and these may be sub-  
 452 jected to significant errors when the largest grain size of  
 453 the distribution is close to the microscope resolution limit  
 454 [26]. For transformations occurring from a fixed number  
 455 of nuclei, the systematic errors are smaller than those  
 456 observed in the continuous nucleation case, but can still  
 457 be significant when reflected light microscopy is used.  
 458 Transmission methods are more time-consuming, but lead  
 459 to much smaller errors than reflection techniques.

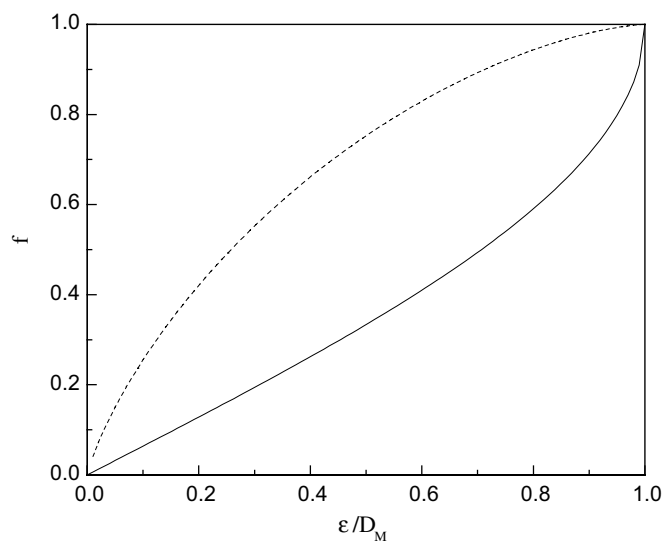


Fig. 2. Fractional underestimation of the number of spherical particles versus the ratio between the microscope resolution limit and the largest particle diameter. Solid and dashed curves refer to cases (i) and (ii), respectively.

### 3.5. Probabilistic approach for the analysis of the nucleation process

462 For the sake of completeness we should briefly mention  
 463 a method based on the stochastic nature of nucleation [27].  
 464 The appearance of critical nuclei is a stochastic event that  
 465 can be characterized by an average waiting period,  $\bar{\tau}$ ,  
 466

$$468 \quad \bar{\tau} = \frac{1}{IV}, \quad (17)$$

469 where  $I$  is the nucleation rate and  $V$  is the volume of the  
 470 system under study.

471 Since the probability of critical nucleus formation due to  
 472 a successful series of attachment and separation reactions is  
 473 very low, nucleation can be treated as a Poissonian process.  
 474 Hence the probability of appearance of one critical nucleus  
 475 in a time period  $\tau^1$  is  
 476

$$478 \quad P_1(\tau^1) = \lambda \tau^1 \exp(-\lambda \tau^1), \quad (18)$$

479 where  $\lambda = 1/\bar{\tau}$ .

480 In cases of high nucleation rates, their measurement is  
 481 normally limited to relatively low undercoolings that corre-  
 482 spond to high values of the crystal growth rate. Thus, the first  
 483 few super-critical nuclei trigger crystallization of the whole  
 484 sample. Fitting the experimental distribution of waiting times  
 485 of the first nucleus,  $\tau^1$ , to Eq. (18) one can estimate an aver-  
 486 age waiting period,  $\bar{\tau}$ , and then the nucleation rate from Eq.  
 487 (17). Such analysis has been employed, e.g., for metals dis-  
 488 persed in the form of small drops when the use of other meth-  
 489 ods is connected with difficulties (see, e.g., [13,28]).

### 3.6. Overall crystallization kinetics

490  
 491 Crystal nucleation followed by subsequent growth  
 492 results in the overall crystallization of the sample. This

493 process can be described by determining the volume frac- 535  
 494 tion of the transformed phase,  $\alpha(t)$ . The formal theory of 536  
 495 overall-crystallization kinetics under isothermal conditions 537  
 496 was developed in the late 1930s by Kolmogorov [29], John- 538  
 497 son and Mehl [30], and Avrami [31], and is well-known as 539  
 498 the JMAK theory. According to this theory, the volume 540  
 499 fraction of the new phase is given by

$$502 \quad \alpha(t) = 1 - \exp \left[ -g \int_0^t I(t') \left[ \int_{t'}^t U(t'') dt'' \right]^3 dt' \right], \quad (19)$$

503 where  $g$  is a shape factor, which is equal to  $4\pi/3$  for spher- 547  
 504 ical crystals. If the nucleation ( $I$ ) and growth ( $U$ ) rates are 548  
 505 constant throughout the transformation (e.g., steady-state 549  
 506 homogeneous stoichiometric nucleation), Eq. (19) can be 550  
 507 rewritten as

$$510 \quad \alpha(t) = 1 - \exp \left[ -\frac{gIU^3 t^4}{4} \right]. \quad (20)$$

511 When the number of growing crystals,  $N_0$ , does not 551  
 512 change with time (as it is typical for fast heterogeneous 552  
 513 nucleation on a finite number of active sites), Eq. (19) 553  
 514 transforms to

$$517 \quad \alpha(t) = 1 - \exp[-gN_0U^3t^3]. \quad (21)$$

518 Avrami proposed that, in general, the following relation 559  
 519 should be used:

$$522 \quad \alpha(t) = 1 - \exp(-Kt^n). \quad (22)$$

523 In typical applications, Eq. (22) is employed in the form

$$526 \quad \ln(-\ln(1 - \alpha)) = \ln K + n \ln t. \quad (23)$$

527 The values of  $K$  and  $n$  can be estimated then by fitting the 563  
 528 experimental data of  $\alpha(t)$  to Eq. (23). Thus the coefficient  $K$  564  
 529 includes  $I$  and  $U$ , or  $N_0$  and  $U$ . The Avrami coefficient,  $n$ , 565  
 530 depends on both nucleation and growth mechanisms, and 566  
 531 can be written for the case of three-dimensional growth as 567  
 532

$$534 \quad n = k + 3m, \quad (24)$$

where  $k$  and  $m$  are taken from the formulas  $N \sim t^k$  and 535  
 $r \sim t^m$  describing the variation of crystal number ( $N$ ) and 536  
 crystal size ( $r$ ) with time. 537

The knowledge of the Avrami coefficient,  $n$ , is helpful to 538  
 understand the mechanism of phase transformation at a 539  
 given temperature. When it is possible to independently 540  
 measure the crystal growth rate, one can then calculate 541  
 the nucleation rate from the coefficient  $K$ . This method is 542  
 not as precise as direct measurements, but can give useful 543  
 information about nucleation in advanced stages of crystal- 544  
 lization, when the application of other methods is hindered 545  
 (see Section 5). 546

For the simplest cases of constant nucleation rate (or 547  
 constant number of crystals) and linear growth, Eqs. (20) 548  
 and (21) have been tested by using  $I_{st}$ ,  $U$ , and  $N_0$  data inde- 549  
 pendently measured by optical microscopy in glasses of 550  
 stoichiometric compositions  $2\text{Na}_2\text{O} \cdot \text{CaO} \cdot 3\text{SiO}_2$  [32] and 551  
 $\text{Na}_2\text{O} \cdot 2\text{CaO} \cdot 3\text{SiO}_2$  [33]. Good agreement was obtained 552  
 between the values of  $gIU^3$  (or  $gN_0U^3$ ), calculated from fit- 553  
 ting the  $\alpha(t)$ -data to the JMAK equation, and directly mea- 554  
 sured values. Recently, the JMAK-equation was also 555  
 successfully employed, together with measured crystal 556  
 growth rates, to estimate extremely high nucleation rates 557  
 in a stoichiometric glass of fresnoite composition [34]. 558

#### 4. Interpretation of nucleation experiments by the classical 559 nucleation theory 560

##### 4.1. Non-steady state (transient) nucleation 561

##### 4.1.1. Estimation of the time-lag in nucleation 562

Typical  $N(T_n, T_d, t)$ -curves obtained by the ‘develop- 563  
 ment’ method are shown in Fig. 3. As we already men- 564  
 tioned, only the nuclei that achieve the critical size, 565  
 $r_*(T_d)$ , during heat treatment at  $T_n$  can grow at the devel- 566  
 opment temperature  $T_d$ . The other nuclei have a high prob- 567  
 ability to dissolve at  $T_d$ . As the result, the number of 568  
 crystals nucleated at given conditions and developed at 569  
 $T_d$  has, strictly speaking, to decrease with increasing  $T_d$  570

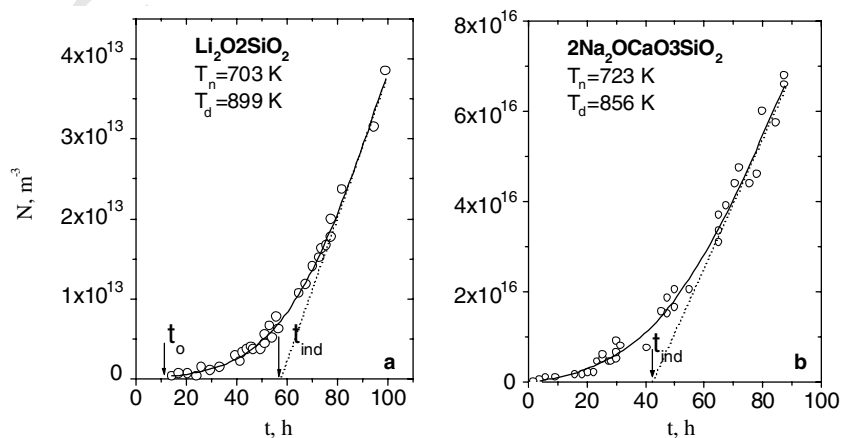


Fig. 3. Typical curves of the number density of  $\text{Li}_2\text{O} \cdot 2\text{SiO}_2$  (a) and  $2\text{Na}_2\text{O} \cdot \text{CaO} \cdot 3\text{SiO}_2$  (b) crystals in glasses of respective stoichiometric compositions versus time of nucleation obtained by the ‘development’ method [35,36].

(see Figs. 4 and 5). The total number of supercritical crystals,  $N$ , nucleated at a temperature,  $T_n$ , in a time,  $t$ , is given by

$$N(T_n, r_*(T_n), t) = \int_0^t I(T_n, t') dt' \quad (25)$$

The number of crystals nucleated in the same conditions, but having sizes larger than the critical size,  $r_*(T_d)$ , and which are, consequently, capable to grow at  $T_d$ , is given by

$$N(T_n, r_*(T_d), t) = \int_0^{t-t_0} I(T_n, t') dt' \quad (26)$$

where  $t_0$  is the period of time that critical nuclei of size  $r_*(T_n)$  need in their growth to reach the size  $r_*(T_d)$ . This time interval is determined by

$$t_0(T_n, T_d) = \int_{r_*(T_n)}^{r_*(T_d)} \frac{dr}{U(T_n, r)} \quad (27)$$

Eqs. (25) and (26) yield

$$N(T_n, r_*(T_n), t) = N(T_n, r_*(T_d), t + t_0) \quad (28)$$

Hence,  $N(T_n, r_*(T_n), t)$  plots are similar to  $N(T_n, r_*(T_d), t)$ -plots with the difference that the latter is shifted along the time-axis by a time  $t_0$ . Thus, the development method can provide the correct value of the steady-state nucleation rate, but overestimates the induction time for nucleation by  $t_0$ .

The period during which heat treatment at the nucleation temperature  $T_n$  does not influence crystallization at  $T_d$  can be identified with  $t_0$  (given by Eq. (27); here we neglect the time of the first critical nucleus formation). This time is indicated by an arrow in Fig. 3(a). According to Eq. (27), the higher the growth rate  $U$  at the nucleation temperature,  $T_n$ , and the closer is  $T_d$  to  $T_n$  ( $r_*(T_n)$  is correspondingly closer to  $r_*(T_d)$ ), the lower is  $t_0$ . Hence, for a strong overlap of the nucleation and growth rate curves, the value of  $t_0$  is not very high and can often be neglected. Fig. 3(b) confirms this assumption for a  $2\text{Na}_2\text{O} \cdot \text{CaO} \cdot 3\text{SiO}_2$  glass. On the other hand, when the overlap of the nucleation and growth rate curves is weak, as observed for lithium disilicate glass, one has to reduce the measured value of  $t_{\text{ind}}(T_n, T_d)$  by a time  $t_0(T_n, T_d)$  (see Fig. 3(a)) to estimate  $t_{\text{ind}}(T_n)$ . The value of  $t_{\text{ind}}(T_n)$  can be roughly estimated via extrapolation of the  $t_{\text{ind}}(T_n, T_d)$ -values for the  $N(T_n, T_d, t)$ -curves, obtained at different  $T_d$ , to  $t_{\text{ind}}$  corresponding to  $T_d = T_n$ . Fig. 5(a) presents examples of such  $N(T_n, T_d, t)$ -curves for lithium disilicate glass. Fig. 5(b) shows the values of  $t_{\text{ind}}$ , taken from these curves, versus development temperature. When  $T_d$  approaches  $T_n = 453^\circ\text{C}$ ,  $t_{\text{ind}}$  is about 1.9 h (the average value of the linear and quadratic polynomial extrapolations). Hence, one can approximately estimate  $t_0$  as  $t_0(T_d, T_n) = t_{\text{ind}}(T_n, T_d) - t_{\text{ind}}(T_n)$ , e.g., for  $T_d = 530^\circ\text{C}$  and  $T_n = 453^\circ\text{C}$   $t_0$  is about 0.9 h. A similar value is obtained by extrapolating the initial section of the  $N(t)$ -curve 1 (see also curve 5) to  $N = 0$ . Thus, according to Eq. (12), one can assume that Eq. (29) holds, i.e.,

$$\tau(T_n) = \frac{6}{\pi^2} (t_{\text{ind}}(T_n, T_d) - t_0(T_n, T_d)) \quad (29)$$

Kinetic  $N(t)$ -curves, such as those presented by Fig. 3, can be plotted in dimensionless coordinates  $(N(T, t - t_0)/I_{\text{st}}(T)\tau(T))$  versus  $(t - t_0)/\tau(T)$ . Fig. 6(a) shows that these coordinates allow one the combination of data for different glasses and different temperatures in the same plot. The experimental points are quite close to the theoretical master curve calculated with Eq. (10). This curve corresponds to increasingly higher nucleation rates towards the steady-state value,  $I_{\text{st}}$ . The evolution of the nucleation rate calculated by Eq. (9) is shown in Fig. 6(b).

As we already mentioned in Section 3.3, if one employs the single-stage method, the induction periods obtained from experimental  $N(T_n, t)$ -curves must be reduced by a period of time  $t_0 \approx r_{\text{res}}/U(T_n)$ . An example of such curve, obtained for Au-catalyzed nucleation in  $\text{NaPO}_3$  glass, is

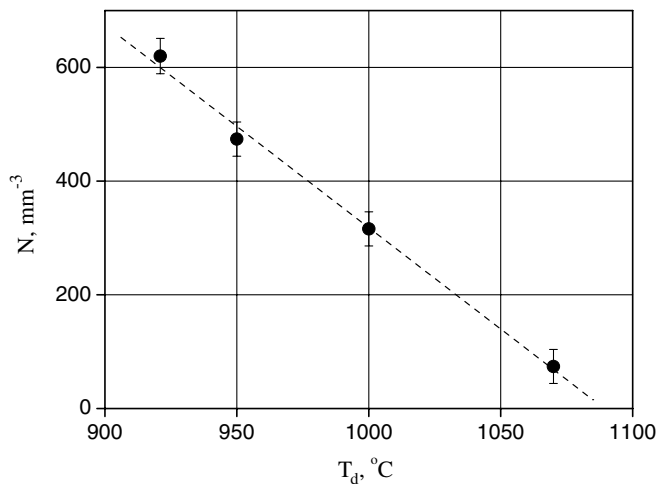


Fig. 4. Number density of crystals versus development temperature in a lithium aluminum silicate glass subjected to nucleation treatment for 5 min at  $T_n = 785^\circ\text{C}$  [37].

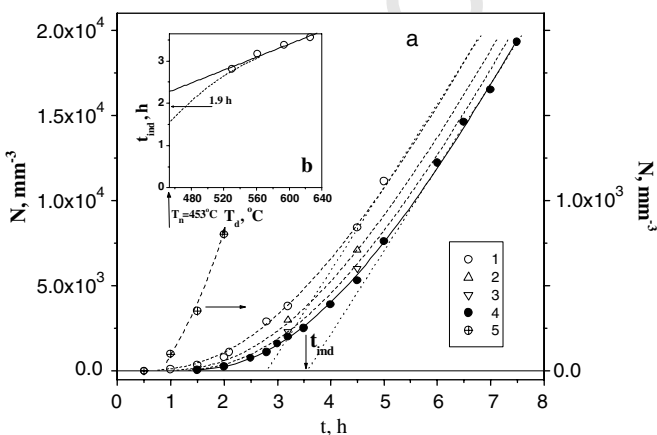


Fig. 5. (a) Number density of  $\text{Li}_2\text{O} \cdot 2\text{SiO}_2$  crystals developed at  $T_d = 530^\circ\text{C}$  (curves 1 and 5),  $560^\circ\text{C}$  (curve 2),  $594^\circ\text{C}$  (curve 3), and  $626^\circ\text{C}$  (curve 4) as a function of nucleation time at  $T_n = 453^\circ\text{C}$  [38]. (b) Induction time versus development temperature.

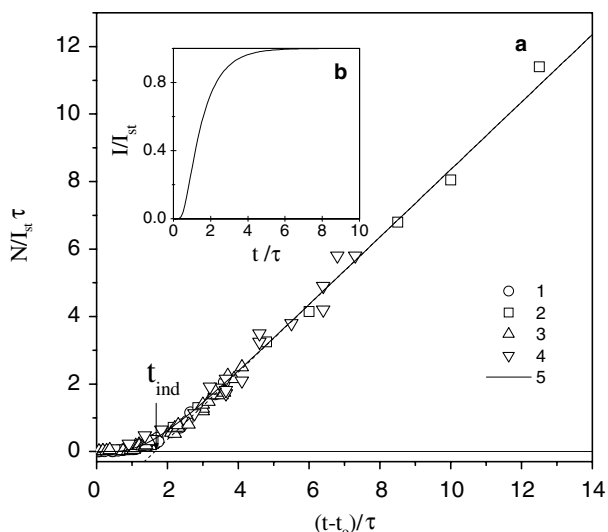


Fig. 6. (a)  $N/(I_{st}\tau)$  versus reduced time for glasses  $\text{Li}_2\text{O}\cdot 2\text{SiO}_2$  (curves 1 and 2), and  $2\text{Na}_2\text{O}\cdot \text{CaO}\cdot 3\text{SiO}_2$  (curves 3 and 4) [35] for  $T = 430^\circ\text{C}$  (curve 1),  $465^\circ\text{C}$  (curve 2),  $465^\circ\text{C}$  (curve 3) and  $470^\circ\text{C}$  (curve 4). Curve 5 was calculated from Eq. (10). (b) Reduced nucleation rate versus reduced time calculated from Eq. (9).

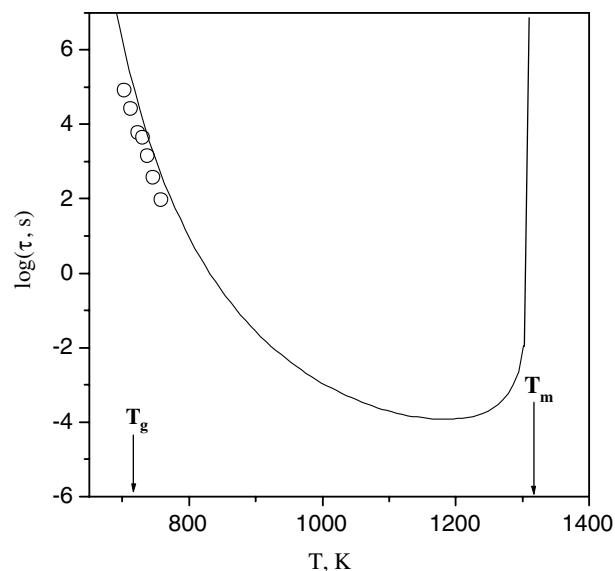


Fig. 8. Temperature dependence of the time-lag for nucleation. Circles refer to experimental data for  $\text{Li}_2\text{O}\cdot 2\text{SiO}_2$  glass [41]. The full line was calculated by Eq. (8).

646 shown in Fig. 7. The dashed line indicates the case of  
 647 steady-state nucleation where the shift,  $t_0$ , is taken into  
 648 account. The comparison of this line with experimental  
 649 data gives clear evidence for the transient character of the  
 650  $N(t)$ -curves. It should be emphasized that one of the first  
 651 experimental demonstrations of transient nucleation in  
 652 glasses was presented in Ref. [39].

653 4.1.2. Temperature dependence of the time-lag for nucleation

654 According to Eq. (8), when the degree of undercooling  
 655 increases, the time-lag  $\tau$  passes through a minimum. This  
 656 behavior is due to the interplay between the decrease of

657  $1/\Delta G_V^2$  and the increase of the exponential term. This mini-  
 658 mum is located at a low undercooling. Since, in the case of  
 659 glass-forming silicate melts, detectable (internal) homoge-  
 660 neous nucleation rates are observed only at very deep  
 661 undercoolings,  $\Delta T/T_m \geq 0.4$  [40], at these undercoolings  
 662 only an increase of the time-lag with increasing undercool-  
 663 ing is observed. Fig. 8 illustrates this trend for lithium disilicate  
 664 glass. The circles refer to experimental data. The solid  
 665 line is determined according to Eq. (8) with  $\sigma_{cm} = 0.2 \text{ J/m}^2$   
 666 assuming that the activation free energy  $\Delta G_D$  is equal to  
 667 that for viscous flow,  $\Delta G_\eta$ . For deep undercoolings the  
 668 validity of this last assumption has been a subject of contro-  
 669 versial discussion, however, it is commonly assumed to  
 670 be valid for  $T > 1.2T_g$  (see, e.g., [42]).

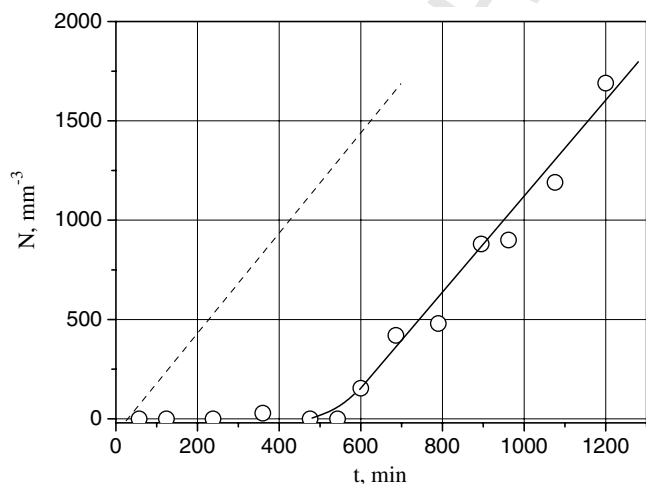


Fig. 7. Number density of crystals in  $\text{NaPO}_3$  glass doped with 0.45% Au versus time of heat treatment at  $T = 332^\circ\text{C}$  obtained by a single-stage method [39]. The dashed line refers to the steady-state nucleation rate. The shift due to the time required to grow the crystals to visible sizes is taken into account.

671 4.1.3. Transient nucleation with a pre-existing nucleus  
 672 size distribution

673 So far we discussed transient nucleation assuming the  
 674 absence of an appreciable number of pre-existing nuclei.  
 675 This assumption is quite reasonable for interpreting time-  
 676 lag phenomena for glasses obtained via fast quenching of  
 677 the melt. In contrast, preliminary annealing of a glass at  
 678 some temperature,  $T_1$ , for sufficiently long times,  $t \geq \tau(T_1)$ ,  
 679 results in the formation of a cluster distribution that acts as  
 680 an initial distribution at the temperature  $T_2$ . Then this dis-  
 681 tribution evolves towards a steady-state distribution corre-  
 682 sponding to the temperature  $T_2$ , complicating the time-  
 683 dependence of the nucleation rate.

684 For example, for lithium disilicate glass annealed at  $T_1$ ,  
 685 the nucleation rate at  $T_2 > T_1$  passes through a maximum  
 686 before reaching the steady-state value. Fig. 9 shows the  
 687  $N(t)$ -curves at  $T_2 = 465^\circ\text{C}$  for a rapidly quenched parent  
 688 glass (curve 1) and for glasses that had been previously  
 689 annealed at  $T_1 = 430^\circ\text{C}$  (curves 2 and 3). All curves were

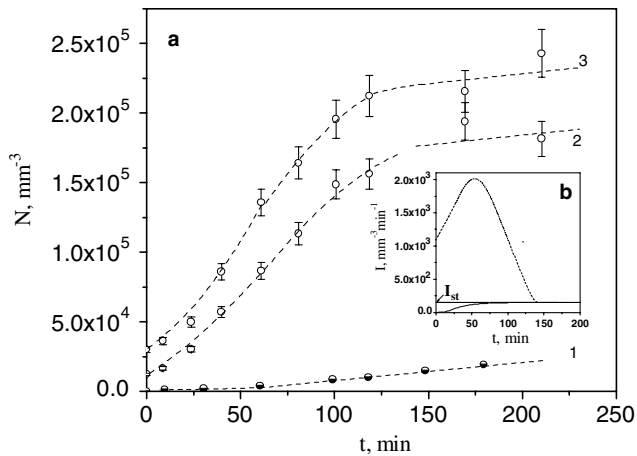


Fig. 9. (a) Number density of  $\text{Li}_2\text{O}\cdot 2\text{SiO}_2$  crystals obtained via the ‘development’ method ( $T_d = 626^\circ\text{C}$ ) versus time of nucleation at  $T_n = 465^\circ\text{C}$ . Curve 1 refers to the quenched glass. Curves 2 and 3 refer to glasses subjected to preliminary treatment at  $T = 430^\circ\text{C}$  for 65 h (curve 2) and 89 h (curve 3) [43]. (b) Nucleation rate versus time. Solid and dashed lines correspond to curves 1 and 3 from (a), respectively.

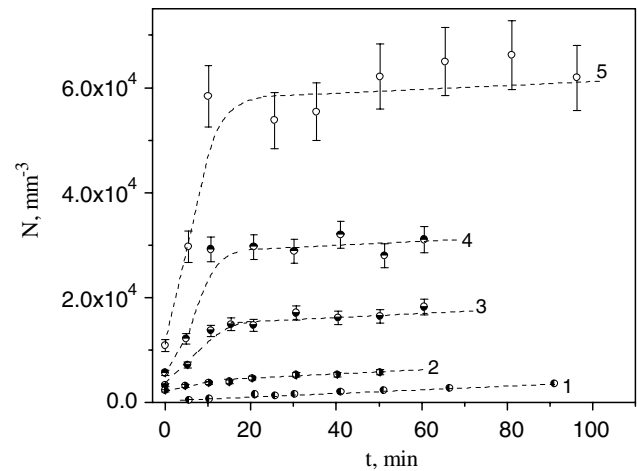


Fig. 10. Number density of  $\text{Li}_2\text{O}\cdot 2\text{SiO}_2$  crystals obtained via the ‘development’ method ( $T_d = 626^\circ\text{C}$ ) versus time of nucleation at  $T_n = 485^\circ\text{C}$ . Curve 1 quenched glass, curves 2–5 glasses subjected to preliminary treatment at  $T = 473^\circ\text{C}$  (curve 2),  $451^\circ\text{C}$  (curve 3),  $440^\circ\text{C}$  (curve 4), and  $430^\circ\text{C}$  (curve 5) for the following times:  $t = 0.75$  h (curve 2),  $4.5$  h (curve 3),  $18$  h (curve 4), and  $65$  h (curve 5) which exceed the time-lags at  $T$  [43].

690 obtained by the ‘development’ method at  $T_d = 626^\circ\text{C}$ .  
 691 Curves 2 and 3 demonstrate, as compared with curve 1, a  
 692 strong increase in the number of crystals, and only for  
 693 times higher than about 120 min the nucleation rate  
 694 reaches steady-state conditions corresponding to the tem-  
 695 perature  $T_2$ . The evolution of the nucleation rate corre-  
 696 sponding to curve 3 is shown in Fig. 9(b).

697 Such unusual behavior of the nucleation kinetics is  
 698 caused by the transition of an initial distribution formed  
 699 at  $T_1$  for sizes less than  $r_*(T_d)$  into the steady state cluster  
 700 size distribution corresponding to  $T_2$ . Since the number of  
 701 nuclei having sizes  $r \geq r_*(T)$  increases with decreasing tem-  
 702 perature, down to  $T = T_m/3$ , a strengthening of the effect of  
 703 the preliminary heat treatment with decrease of  $T_1$  should  
 704 be expected. This is indeed the case as shown in Fig. 10.  
 705 The presented effects of the multistage heat treatments were  
 706 well-described by the numerical modeling of the cluster  
 707 evolution performed in the framework of the classical  
 708 nucleation theory [44–46] with the exception of the heat  
 709 treatments involving the temperature  $T_1 = 430^\circ\text{C}$  [45].  
 710 Since the values of the parameters needed for the simula-  
 711 tions were estimated via a fitting procedure this disagree-  
 712 ment could be caused by the error in the  $I_{st}(430^\circ\text{C})$   
 713 estimation or viscosity data taken from other authors. Nev-  
 714 ertheless, the simulations clearly show that the nucleation  
 715 kinetics is governed by the evolution of the nuclei  
 716 distribution.

## 717 4.2. Steady-state nucleation

### 718 4.2.1. Temperature dependence of steady-state nucleation 719 rates

720 Some examples of steady-state nucleation rates,  $I_{st}$ , mea-  
 721 sured from the slope of the linear part of the  $N(t)$ -plots,  
 722 such as those shown in Fig. 3, are presented in Fig. 11 as  
 723 a function of reduced temperature. The values of  $I_{st}(T)$  pass

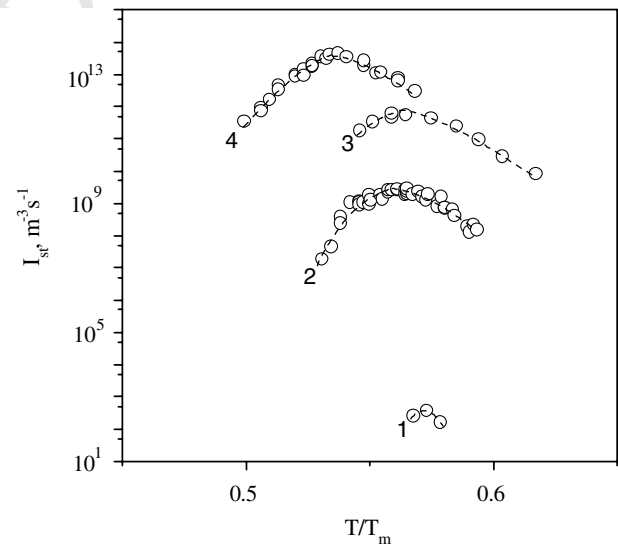


Fig. 11. Steady-state nucleation rate versus reduced temperature for some stoichiometric glasses: (curve 1)  $3\text{MgO}\cdot\text{Al}_2\text{O}_3\cdot 3\text{SiO}_2$  [47]; (curve 2)  $\text{Li}_2\text{O}\cdot 2\text{SiO}_2$  [35]; (curve 3)  $\text{Na}_2\text{O}\cdot 2\text{CaO}\cdot 3\text{SiO}_2$  [48]; (curve 4)  $2\text{Na}_2\text{O}\cdot\text{CaO}\cdot 3\text{SiO}_2$  [36].

724 through a maximum at a temperature  $T_{\text{max}}$ . The  
 725 magnitudes of  $I_{st}(T_{\text{max}}) \equiv I_{\text{max}}$  vary from  $5 \times 10^{13}$  to  $3 \times$   
 726  $10^2 \text{ m}^{-3} \text{ s}^{-1}$  and cover practically the whole range of avail-  
 727 able measurements of nucleation rates in silicate glasses  
 728 with stoichiometric compositions.

729 The reason for the existence of the nucleation rate maxi-  
 730 mum follows from a simple analysis of Eq. (1). Since the  
 731 pre-exponential term,  $I_0$ , depends only weakly on tempera-  
 732 ture, the temperature dependence of the nucleation rate is  
 733 determined mainly by the thermodynamic and kinetic bar-  
 734 riers for nucleation. A temperature decrease produces two

735 effects: a decrease of the thermodynamic barrier due to an  
 736 increase in the thermodynamic driving force for crystalliza-  
 737 tion, leading to a higher nucleation rate, and an increase of  
 738 the kinetic barrier, leading to a lower nucleation rate (the  
 739 kinetic barrier is, as mentioned earlier, often replaced by  
 740 the activation free energy for viscous flow). As a result of  
 741 these two opposite tendencies, one finds a maximum of  
 742 the steady-state nucleation rate at a temperature  $T_{\max}$ ,  
 743 which is located well below  $T_m$ .

744 Eq. (4) for the thermodynamic barrier can be rewritten  
 745 as

$$746 \frac{W_*}{k_B T} = C_1 \frac{1}{T_r(1 - T_r)^2}, \quad C_1 = \frac{16\pi}{3} \frac{\alpha_{ST}^3 \Delta H_m}{RT_m}, \quad T_r \equiv \frac{T}{T_m}. \quad (30)$$

749 Here we used the linear approximation for the thermody-  
 750 namic driving force, Eq. (6), and the following semi-empir-  
 751 ical equation:

$$752 \sigma_{cm} = \alpha_{ST} \frac{\Delta H_m}{V_m^{2/3} N_A^{1/3}} \quad (31)$$

755 for the specific surface energy of the nucleus/melt interface  
 756 proposed by Skapski and Turnbull [49,50]. In Eq. (31),  
 757  $\Delta H_m$  is the melting enthalpy per mole,  $V_m$  is the molar vol-  
 758 ume,  $N_A$  is Avogadro's number, and  $\alpha_{ST}$  is an empirical  
 759 dimensionless coefficient, smaller than unity, reflecting the  
 760 fact that surface atoms have less neighbors than bulk  
 761 atoms. Assuming that  $\Delta G_D$  is of the same order of magni-  
 762 tude as the activation free energy for viscous flow,  $\Delta G_\eta$ , one  
 763 can write the kinetic barrier as

$$764 \frac{\Delta G_D(T)}{k_B T} = \frac{C_2}{T_r - T_{or}}, \quad C_2 \equiv \frac{2.30B}{T_m} \cong 30(T_{gr} - T_{or}),$$

$$766 T_{or} \equiv \frac{T_o}{T_m}, \quad T_{gr} \equiv \frac{T_g}{T_m}, \quad (32)$$

767 where  $T_o$  and  $B$  are the empirical coefficients of the Vogel–  
 768 Fulcher–Tammann (VFT) equation and  $T_g$  is the glass  
 769 transition temperature. The application of the VFT-rela-  
 770 tion implies the assumption of a temperature-dependent  
 771 activation free energy,  $\Delta G_\eta$ . In the definition of  $C_2$  we took  
 772 into account the fact that  $\Delta G_\eta/(k_B T) \cong 30$  at  $T = T_g$ .

773 Fig. 12 shows  $I_{st}(T_r)$ -curves calculated with Eqs. (1),  
 774 (30), and (32), reasonable estimates of the pre-exponential  
 775 term and values of the parameters  $C_1$  and  $C_2$ , as indicated  
 776 in the figure caption. One can see that the decrease in the  
 777 kinetic barrier, caused by a decrease in  $C_2$  at a fixed value  
 778 of  $C_1$ , results in a shift of the nucleation rate maximum to  
 779 lower temperatures (cf. curves 1–4). The reduced tempera-  
 780 ture  $T_r \equiv T/T_m = 1/3$  is a lower limit to  $T_r^{\max} \equiv T_{\max}/T_m$   
 781 obtained when the kinetic barrier tends to zero (cf. curve  
 782 5). This shift is accompanied by a strong increase in the  
 783 magnitude of  $I(T_{\max}) \equiv I_{\max}$ . When the thermodynamic  
 784 barrier is diminished, at fixed values of  $C_2$ , by decreasing  
 785 the parameter  $C_1$  (which is proportional to  $\alpha_{ST}$  and the  
 786 reduced melting enthalpy  $\Delta H'_m = \Delta H_m/RT_m$ ), the value

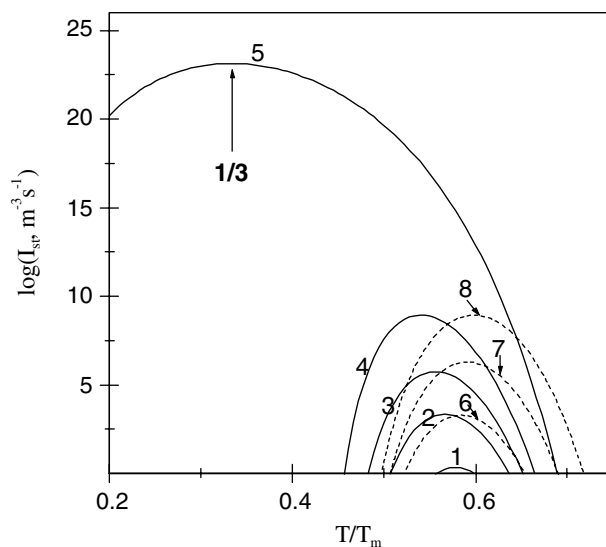


Fig. 12. Temperature dependence of homogeneous nucleation rates. The curves were calculated with Eqs. (1), (30), and (32) with a pre-exponential term  $I_o = 10^{42} \text{ m}^{-3} \text{ s}^{-1}$  and following values of the parameters characterizing the temperature independent parts of the thermodynamic ( $C_1$ ) and kinetic ( $C_2$ ) barriers:  $C_1 = 6.5$  (curves 1–5), 5.8 (curve 6), 5.1 (curve 7), 4.5 (curve 8);  $C_2 = 6$  (curves 1 and 6–8), 4.8 (curve 2), 3.9 (curve 3), 2.8 (curve 4), 0 (curve 5).

of  $I_{\max}$  also increases (curves 1 and 6–8), but the value of  $T_{\max}$  shifts to higher temperatures.

The effect of variation of the kinetic barrier on the nucleation rate can be qualitatively illustrated for lithium disilicate [51] and sodium metasilicate [52] glasses with different  $\text{H}_2\text{O}$  content (a few percent of water often result in a significant decrease of viscosity) as shown in Fig. 13. A decrease in the thermodynamic barrier can be also caused by a decrease in the effective crystal/melt interfacial energy as in the case of heterogeneous nucleation. As a result, as was shown in Ref. [53], the temperature  $T_{\max}$  for heterogeneous surface nucleation is displaced to higher values as compared with homogeneous nucleation.

#### 4.3. Correlation between nucleation rate and glass transition temperature

The methods discussed in Section 3 to measure nucleation kinetics are both difficult to perform and time consuming. Also, owing to several restrictions, they cannot always be employed. Hence, the knowledge of any correlation between nucleation rate and easily measurable properties of glasses is highly desirable. As one example, well before the development of nucleation theory for condensed systems, Tammann called attention to the following tendency: the higher the melt viscosity at the melting temperature, the lower is its crystallizability [54].

Almost eighty years after Tammann's pioneering research work, James [55] and Zanotto [56], based on numerous experimental nucleation rate data for several silicate glasses, concluded that glasses having a reduced glass transition temperature,  $T_{gr} \equiv T_g/T_m$ , higher than  $\sim 0.58$ –

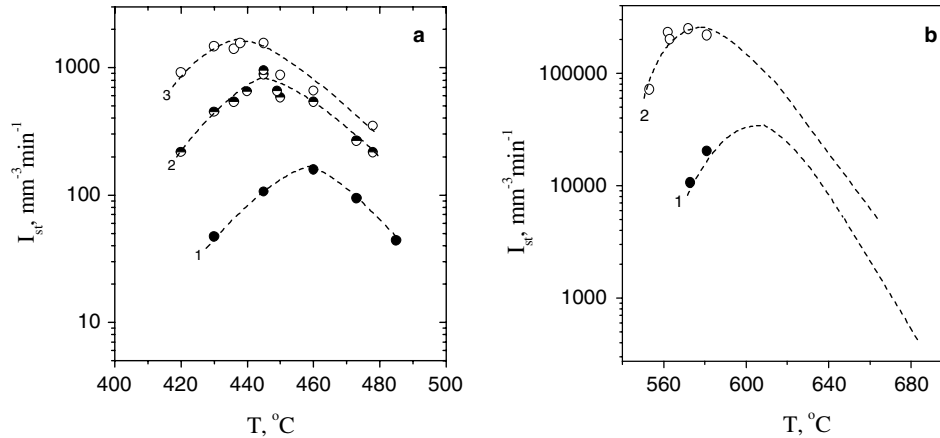


Fig. 13. Temperature dependencies of the steady-state nucleation rates in  $\text{Li}_2\text{O} \cdot 2\text{SiO}_2$  [51] (a) and  $\text{Na}_2\text{O} \cdot 2\text{CaO} \cdot 3\text{SiO}_2$  [52] (b) glasses containing different amounts of  $\text{H}_2\text{O}$ : (a) 0.05 mol% (curve 1), 0.12 mol% (curve 2), and 0.20 mol% (curve 3); (b) 0.01 mol% (curve 1), 0.2 mol% (curve 2).

817 0.60, display only surface (mostly heterogeneous) crystalliza-  
 818 tion; while glasses showing volume (homogeneous) nucleation  
 819 have values  $T_{gr} < 0.58$ –0.60. Since at temperatures  $T < T_m$   
 820 the nucleation rate is always positive, the absence of vol-  
 821 ume nucleation for glasses having  $T_{gr} > 0.60$  merely indi-  
 822 cates undetectable nucleation on laboratory time/size  
 823 scales. Hence, an increase in the nucleation rate with  
 824 decreasing  $T_{gr}$  could be expected. Indeed, a drastic increase  
 825 of the magnitude of  $I_{max}$  with decreasing  $T_{gr}$  has been dem-  
 826 onstrated by Deubener [57]. Fig. 14 presents a plot of the  
 827  $I_{max}(T_{gr})$ -dependence, which has been extended in Ref.  
 828 [58] and in the present work. In a relatively narrow range  
 829 of  $T_{gr}$  (from 0.47 to 0.58) shown by 55 glasses of stoichiomet-  
 830 ric and non-stoichiometric compositions, belonging to  
 831 eight different silicate systems, the nucleation rates drop by  
 832 about 17 orders of magnitude! When  $T_{gr}$  increases, the

kinetic inhibition of nucleation proceeds at higher temper- 833  
 atures and at higher values of the thermodynamic barrier 834  
 due to lower values of the thermodynamic driving force. 835  
 As a consequence, nucleation becomes practically unde- 836  
 tectable at  $T_{gr} > 0.58$ . This result confirms the findings of 837  
 James [55] and Zanotto [56]. The lines in Fig. 14 are calcu- 838  
 lated from CNT (Eqs. (1), (30), and (32)) with reasonable 839  
 values of the parameters  $C_1$  and  $C_2$  indicated in the figure 840  
 caption. Remember that  $C_1$  and  $C_2$  characterize the temper- 841  
 ature independent parts of the thermodynamic and kinetic 842  
 barriers for nucleation, respectively. Since Eq. (32) 843  
 contains two independent parameters  $C_2$  and  $T_{or}$ , the vis- 844  
 cosity and, correspondingly,  $T_{gr}$ , was varied in two differ- 845  
 ent ways, by keeping either  $C_2$  (solid line) or  $T_{or}$  (dashed line) 846  
 fixed. In the most interesting temperature range 847  
 ( $0.5 < T_r < 0.6$ ) these different ways of varying  $T_{gr}$  lead 848  
 to similar results. The lines reflect correctly the experimentally 849  
 observed general trend. However, in applying the men- 850  
 tioned rule to particular systems one has to act with some 851  
 precaution since a substantial variation of the thermody- 852  
 namic barrier can result in a considerable variation of  $I_{max}$  853  
 for glasses having similar values of  $T_{gr}$ . For instance, fres- 854  
 noite ( $2\text{BaO} \cdot \text{TiO}_2 \cdot 2\text{SiO}_2$ ) and wollastonite ( $\text{CaO} \cdot \text{SiO}_2$ ) 855  
 glasses have  $T_{gr}$  about 0.57, while the values of the param- 856  
 eter  $\alpha_{ST}$  are 0.4 and 0.6, respectively. The latter fact leads to 857  
 a strong difference in the values of the thermodynamic bar- 858  
 riers and correspondingly to a strong difference in  $I_{max}$ . 859  
 Also nucleation of metastable phases, such as  $\text{BaO} \cdot 2\text{SiO}_2$ , 860  
 is possible as shown in Ref. [59]. 861

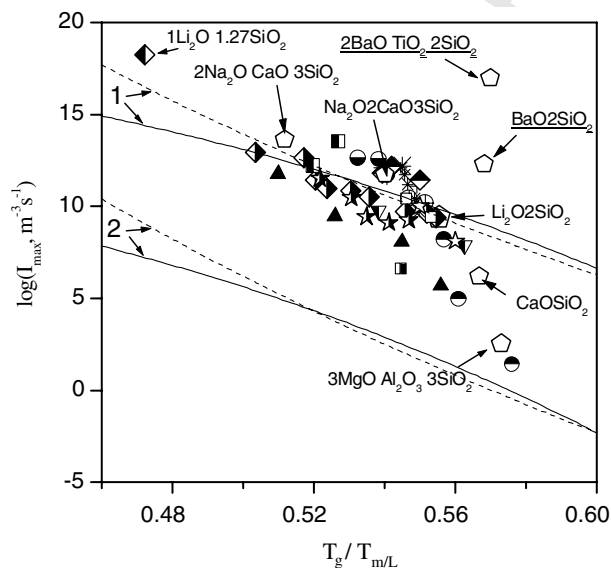


Fig. 14. Maximum nucleation rate as a function of reduced glass transition temperature for 55 silicate glasses. The lines are calculated from CNT with  $C_1 = 4.5$  (curve 1) and  $6.5$  (curve 2). Solid lines refer to  $C_2 = 4.5$  and  $T_{or} = T_{gr} - C_2/30$ ; dashed lines to  $T_{or} = 0.4$  [58].

An important parameter is the location of  $T_{max}$ . It is 862  
 commonly accepted that  $T_{max}$  is close to  $T_g$ . However, it 863  
 was shown in Ref. [58] that the ratio  $T_{max}/T_g$  depends on 864  
 $T_{gr}$ .  $T_{max}/T_g$  is higher than one (i.e.,  $T_{max}$  exceeds  $T_g$ ) at 865  
 low  $T_{gr}$ , approaches one at about  $T_{gr} \sim 0.55$ , and then 866  
 becomes smaller than one. This trend results in an addi- 867  
 tional increase of the kinetic barrier at  $T_{max}$  with increasing 868  
 $T_{gr}$  caused by the increase of  $\eta(T_{max})$ . 869

Computations of  $I_{st}(T)$  temperature dependencies simi- 870  
 lar to those published in Ref. [58] and presented here were 871

872 performed by Turnbull in the 1960s (see, e.g., Ref. [60]).  
 873 However, at that time, with the exception of the measure-  
 874 ments of Tammann [61] and Mikhnevich [62] for organic  
 875 liquids, nucleation rate data were not available in wide  
 876 temperature ranges including  $T_{\max}$ . In order to verify the  
 877 existence of a correlation between  $I_{\max}$  and  $T_{\text{gr}}$ , as pro-  
 878 posed here, an abundance of experimental points must be  
 879 available. This is now the case (cf. Fig. 14).

## 880 5. Nucleation rate data and CNT: some serious problems

### 881 5.1. Different approaches for the interpretation of 882 experimental data by CNT

883 As shown in the previous sections, in its original form  
 884 CNT provides a good qualitative description of nucleation  
 885 rate data for silicate glasses, however, serious problems  
 886 arise when one tries to employ this theory for a quantita-  
 887 tive interpretation of experimental data.

888 If one uses the Stokes–Einstein equation to connect the  
 889 kinetic barrier of nucleation with the glass viscosity one can  
 890 rewrite Eq. (1) for the steady-state nucleation rate as  
 891

$$893 I_{\text{st}} = K_{\eta} \frac{1}{\eta} \exp\left(-\frac{W^*}{k_B T}\right), \quad K_{\eta} = I_o \frac{h}{4l^3}, \quad (33)$$

894 where the size parameter  $l$  has the order of the Si–O bond  
 895 length. Hereby, the diffusivity across the crystal/liquid  
 896 interface is replaced by the volume diffusivity.

897 The use of the Stokes–Einstein equation in Eq. (33) can  
 898 be avoided if one estimates the kinetic barrier from the  
 899 nucleation time-lag. In this case, Eq. (1) takes the following  
 900 form:  
 901

$$903 I_{\text{st}} = K_{\tau} \frac{1}{\Delta G_V^2 t_{\text{ind}}} \exp\left(-\frac{W^*}{k_B T}\right), \quad K_{\tau} = I_o \frac{8h\sigma_{\text{cm}}}{3a^4}. \quad (34)$$

904 In the analysis of crystallization kinetics in glass-forming  
 905 systems, it is commonly accepted – in accordance with  
 906 CNT and Gibbs' classical description of heterogeneous sys-  
 907 tems – to use the properties of the newly evolving macro-  
 908 phase as reference states for the description of the bulk  
 909 properties of the critical nucleus. Additionally one has to  
 910 properly specify the value of the specific interfacial energy,  
 911  $\sigma_{\text{cm}}$ . Since measurements of the interfacial energy of the  
 912 crystals in their own melt are confronted with serious diffi-  
 913 culties, one usually employs the easily measurable thermo-  
 914 dynamic driving force for crystallization of the macro-  
 915 phase for the determination of the work of critical cluster  
 916 formation. Hereby,  $\sigma_{\text{cm}}$  is commonly taken as a fit param-  
 917 eter and is treated, to a first approximation, as a size-inde-  
 918 pendent (capillarity approximation) and temperature  
 919 independent quantity. The respective values of  $\sigma_{\text{cm}}$  are de-  
 920 noted in Tables 1 and 2 as  $\sigma_{\text{cm}}^*$ . These approximations allow  
 921 one to estimate both the magnitude of the pre-exponential  
 922 term,  $I_o$ , in Eq. (1) and the value of crystal-melt surface en-  
 923 ergy,  $\sigma_{\text{cm}}$ , from a fit of experimental data ( $I_{\text{st}}$ ,  $\eta$ , or  $t_{\text{ind}}$ ).  
 924 According to Eqs. (33), (34), and (4),  $\ln(I_{\text{st}}\eta)$  and

Table 1

Ratio of experimental and theoretical pre-exponential, and surface energy values calculated by CNT for different glasses [40]

Glass	$\Delta C_p = 0$		$\Delta C_p = f(T)$	
	$\log(I_o^{\text{exp}}/I_o^{\text{theo}})$	$\sigma_{\text{cm}}^*$	$\log(I_o^{\text{exp}}/I_o^{\text{theo}})$	$\sigma_{\text{cm}}^*$
$\text{Li}_2\text{O} \cdot 2\text{SiO}_2$	15	0.19	19	0.20
$\text{Na}_2\text{O} \cdot 2\text{CaO} \cdot 3\text{SiO}_2$	18	0.17	72	0.19
$2\text{Na}_2\text{O} \cdot \text{CaO} \cdot 3\text{SiO}_2$	27	0.15	139	0.17

The specific interfacial energy is given in  $\text{J m}^{-2}$ .

Table 2

Liquid–crystal surface energies (in  $\text{J m}^{-2}$ ) calculated from nucleation and growth data [69]

Glass	$\sigma_{\text{cm}}$	$\sigma_{\text{cm}}^*$	$\sigma_{\text{cm}}^{**}$	$K$	$\sigma_{\text{cm}}^r$
$\text{Li}_2\text{O} \cdot 2\text{SiO}_2$	1.4	0.20	0.152–0.156 (450 °C < $T$ < 485 °C)	0.19–0.23	0.050–0.060
$\text{Na}_2\text{O} \cdot 2\text{CaO} \cdot 3\text{SiO}_2$	1.5	0.18	0.099–0.110 (580 °C < $T$ < 685 °C)	0.13	0.026

925  $\ln(I_{\text{st}} t_{\text{ind}} \Delta G_V^2)$  versus  $1/(T \Delta G_V^2)$  plots should yield straight  
 926 lines. Their intercepts and slopes can be employed to evalu-  
 927 ate  $I_o$  and  $\sigma_{\text{cm}}^*$ , respectively. However, these approxima-  
 928 tions lead to the following problems:

- (i) The use of Eq. (33) [55,63] and Eq. (34) [64] leads to  
 929 drastic discrepancies between the experimental,  $I_o^{\text{exp}}$ ,  
 930 and theoretical,  $I_o^{\text{theo}}$ , values of the pre-exponential  
 931 factor. This discrepancy was first observed for crystal  
 932 nucleation in undercooled Ga [65] and Hg [66]. In  
 933 order to illustrate this issue, Table 1 shows the  
 934  $(I_o^{\text{exp}}/I_o^{\text{theo}})$ -ratio, and surface energy values for some  
 935 stoichiometric silicate glasses calculated from  
 936  $\ln(I_{\text{st}} t_{\text{ind}} \Delta G_V^2)$  versus  $1/(T \Delta G_V^2)$  plots for temperatures  
 937 above the glass transition range. To trace these plots,  
 938 both the linear (Turnbull) approximation (Eq. (6))  
 939 and the experimental values (Eq. (5)) of the thermo-  
 940 dynamic driving force for crystallization of the stable  
 941 macro-phases were used. The discrepancy between  
 942 theory and experiment is strongly affected by the  
 943 choice of  $\Delta G_V$  (see also Appendix A, where an anal-  
 944 ysis similar to that given in Ref. [13] is performed).  
 945 The experimental values of  $\Delta G_V$  are close to Turn-  
 946 bull's approximation in the case of  $\text{Li}_2\text{O} \cdot 2\text{SiO}_2$  glass,  
 947 and to Hoffman's approximation in the case of  
 948  $2\text{Na}_2\text{O} \cdot 1\text{CaO} \cdot 3\text{SiO}_2$  glass. These equations normally  
 949 bound the experimental values of  $\Delta G_V$  [13], and the  
 950  $(I_o^{\text{exp}}/I_o^{\text{theo}})$ -ratio increases as one passes from Turn-  
 951 bull's to Hoffman's approximation. However, inde-  
 952 pendently of the particular choice of the expression  
 953 of the thermodynamic driving force, i.e., with any  
 954 reasonable approximation or with experimental val-  
 955 ues of  $\Delta G_V$ , the mentioned discrepancy remains quite  
 956 large.  
 957

(ii) The values of the surface energy,  $\sigma_{\text{cm}}$ , calculated as described above (in the deeply undercooled regime close to  $T_g$ ), are lower than the melt–vapor surface energy,  $\sigma_{\text{mv}}$ , which can be measured directly [67,68] (above the equilibrium melting point) by a factor of about 0.5–0.6. These values must then be corrected since  $\sigma_{\text{cm}}$  refers to nuclei of critical size,  $r_*$ , while  $\sigma_{\text{mv}}$  refers to planar melt/vapor interfaces. In the case of lithium disilicate glass, for instance, corrections made with the Tolman equation, Eq. (35), for the size effect, increase this factor to 0.8 [69]. Such high values of  $\sigma_{\text{cm}}$ , as compared with  $\sigma_{\text{mv}}$ , strongly overestimate its real magnitude. Indeed, according to Stefan’s rule [70], one would expect the ratio  $\sigma_{\text{cm}}/\sigma_{\text{mv}}$  to be approximately equal to  $\sigma_{\text{cm}}/\sigma_{\text{mv}} \cong \Delta H_{\text{cm}}/\Delta H_{\text{mv}} \ll 1$ , where  $\Delta H_{\text{cm}} \equiv \Delta H_m$  and  $\Delta H_{\text{mv}}$  are the melting enthalpy of the crystalline phase and enthalpy of evaporation, respectively.

It follows that the widespread believe – the driving force of critical cluster formation can be determined correctly via the classical Gibbs’ approach and all necessary corrections have to be incorporated into the theoretical description via the introduction of appropriate values of the specific interfacial energy – is challenged by above given analysis and has to be reconsidered. In the following sections, possible reasons for the failure of CNT in application to a quantitative description of nucleation experiments will be analyzed in detail.

### 5.2. Temperature and size-dependence of the nucleus/liquid specific surface energy

The discrepancy between experimental and theoretical values of  $I_0$  can be avoided if one calculates  $\sigma_{\text{cm}}$  from nucleation data ( $I_{\text{st}}$  and  $t_{\text{ind}}$  or  $\eta$ ) employing the theoretical expression for  $I_0$ . This procedure slightly decreases the values of  $\sigma_{\text{cm}}$  and leads to a weak increase of  $\sigma_{\text{cm}}$  with increasing temperature [71] ( $d\sigma/dT \sim (0.06\text{--}0.16) \times 10^{-3} \text{ J/m}^2 \text{ K}$ ) regardless of the way of estimating the kinetic barrier. As far as we know, Turnbull [66] was the first to draw attention to this fact. At a first sight such kind of temperature dependence of  $\sigma_{\text{cm}}$  (i.e., an increase of the surface tension with increasing temperature obtained via the mentioned treatment of nucleation experiments) is in conflict with the theoretical expectations of most, but not all, authors (see the discussion below). Commonly the opinion is favored that, from a thermodynamic point of view, a decrease of  $\sigma_{\text{cm}}$  (for planar interfaces ( $\sigma_\infty$ )) with temperature should be expected [72–74], at least, in the temperature range where crystallization processes may occur [74]. It follows that we are confronted here with a contradiction between the discussed interpretation of experimental results and general theoretical expectations.

As will be shown now this contradiction can be partly removed by taking into account a possible curvature (or nucleus size) dependence of the surface energy. Recall that

the specific surface energy estimated from nucleation rate data refers to nuclei of critical size. Curvature corrections are expected to reduce the effective value of the surface energy. When the critical nucleus size increases with increasing temperature, the effect of curvature corrections decreases (see Eq. (35)), leading to higher effective values of the surface energy.

To a first approximation, Tolman’s equation (that was originally derived for a liquid drop in equilibrium with its vapor) can be used to decouple these size and temperature effects. The Tolman equation reads

$$\sigma(r_*) = \frac{\sigma_\infty}{\left(1 + \frac{2\delta}{r_*}\right)}, \quad (35)$$

where the Tolman parameter  $\delta$  is a measure of the (unknown) width of the interfacial region between the coexisting phases.

Employing this relation, the work of formation of a spherical critical nucleus may be written as

$$W_* = \frac{16\pi}{3} \frac{\sigma_\infty^3}{\left(1 + \frac{2\delta}{r_*}\right)^3 \Delta G_V^2}, \quad (36)$$

where

$$r_* = \frac{2\sigma_\infty}{\Delta G_V} - 2\delta \quad (37)$$

holds.

Fig. 15 shows the average values of  $(d\sigma_\infty/dT)$  at  $T \geq T_g$  versus the Tolman parameter. Using experimental nucleation data for  $\text{Li}_2\text{O} \cdot 2\text{SiO}_2$  glass, fits of  $\sigma_\infty$  have been performed for different values of  $\delta$  employing Eq. (34). For this glass, as  $\delta$  increases  $(d\sigma_\infty/dT)$  progressively decreases and becomes negative for  $\delta > 2.4 \times 10^{-10} \text{ m}$ . Thus, reasonable values of the Tolman parameter may be chosen such that  $\sigma_\infty$  decreases with increasing temperature, in line with

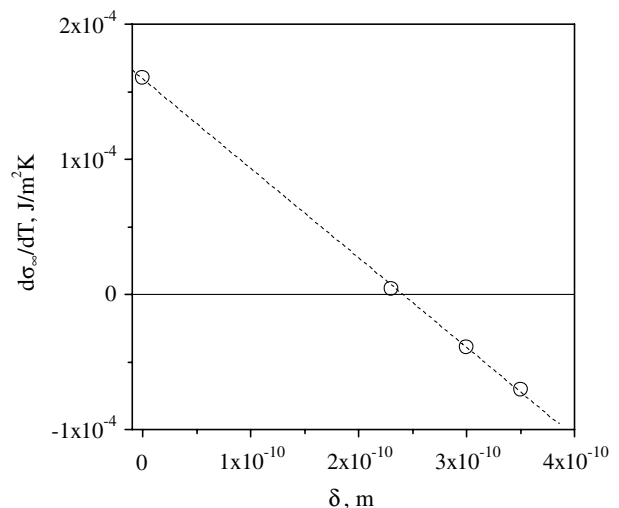


Fig. 15.  $(d\sigma_\infty/dT)$  versus Tolman’s parameter for  $\text{Li}_2\text{O} \cdot 2\text{SiO}_2$  crystals in a glass of the same composition. The kinetic barrier for nucleation was estimated from the nucleation time-lag.

1046 the theoretical predictions of Refs. [72,73]. Similar results  
1047 were obtained for a  $\text{Na}_2\text{O}\cdot 2\text{CaO}\cdot 3\text{SiO}_2$  glass [71].

1048 For completeness of the discussion, we would like to  
1049 mention also another interpretation of the increase of  $\sigma_{\text{cm}}$   
1050 with increasing temperature widely discussed in Ref. [75].  
1051 The argumentation is based on model considerations sup-  
1052 posing an increased ordering of the liquid near the crystal.  
1053 These ideas were expressed first by Turnbull [66] and result  
1054 in an entropy decrease. Employing some plausible assump-  
1055 tions, the positive temperature coefficient of  $\sigma_{\text{cm}}$  can be  
1056 accounted for then by the mentioned entropy loss. Run-  
1057 ning ahead we could also suppose that the temperature  
1058 dependence of  $\sigma_{\text{cm}}$  is the result of a possible change of  
1059 the critical nucleus composition and/or structure with its  
1060 size.

1061 However, regardless of the above possible interpretations  
1062 the values of the specific surface energy estimated from  
1063 nucleation rate data in the framework of the classical Gibbs'  
1064 approach remain too high when compared with the respective  
1065 melt–vapor surface energies. Consequently, the problem  
1066 posed at the end of the preceding section remains unsolved  
1067 by these considerations.

### 1068 5.3. Estimation of crystalliquid specific surface energies 1069 via dissolution of subcritical nuclei

1070 Essentially all known methods to determine the nucleus-  
1071 undercooled liquid surface energy are based on nucleation  
1072 experiments involving certain additional assumptions.  
1073 However, in order to test the classical nucleation theory  
1074 or to make theoretical predictions, independent estimates  
1075 of the specific surface energy are required. Such an inde-  
1076 pendent method of estimating  $\sigma_{\text{cm}}$  for clusters of near-crit-  
1077 ical sizes has been developed recently [69]. The results are  
1078 summarized below.

1079 The new method is based on the dissolution phenome-  
1080 non (discussed in Sections 3 and 4) of subcritical nuclei  
1081 with an increase in temperature. As we already have  
1082 shown, an  $N(T_n, r_*(T_n), t)$ -plot coincides with the  
1083  $N(T_n, r_*(T_d), t)$ -plot, with the only difference that the latter  
1084 is shifted along the time-axis by a time  $t_o$  (Eq. (27)). Then,  
1085 kinetic  $N(T_n, t)$ -curves obtained with different development  
1086 temperatures  $T_{d1}$  and  $T_{d2} > T_{d1}$  should be shifted with  
1087 respect to each other by a time  $\Delta t_o = t_{o2} - t_{o1}$ . Fig. 5 shows  
1088 an example of such kinetic curves. The following equation:  
1089

$$1091 \Delta t_o = \int_{r_*(T_{d1})}^{r_*(T_{d2})} \frac{dr}{U(T_n, r)} = \frac{1}{U(T_n, \infty)} [r_*(T_{d2}) - r_*(T_{d1}) + r_*(T_n) \ln \left( \frac{r_*(T_{d2}) - r_*(T_n)}{r_*(T_{d1}) - r_*(T_n)} \right)] \quad (38)$$

1092 was derived in Ref. [38] to estimate this shift. In the deriva-  
1093 tion of Eq. (38) a size-dependent crystal growth velocity  
1094 [76] was used of the form

$$1095 U(T, r) = U(T, \infty) \left[ 1 - \frac{r_*(T)}{r} \right]. \quad (39)$$

Employing Eq. (3) for the critical nucleus size and assum-  
ing that  $\sigma_{\text{cm}}$  depends only slightly on temperature, Eq.  
(38) can be rewritten as

$$1100 \sigma_{\text{cm}} = \frac{1}{2} \frac{\Delta t_o U(T_n, \infty)}{\left[ \frac{1}{\Delta G_V(T_{d2})} - \frac{1}{\Delta G_V(T_{d1})} + \frac{1}{\Delta G_V(T_n)} \ln \left[ \frac{\frac{\Delta G_V(T_{d2})}{\Delta G_V(T_{d1})} \frac{\Delta G_V(T_n)}{\Delta G_V(T_n)}}{\frac{\Delta G_V(T_{d1})}{\Delta G_V(T_n)}} \right] \right]}. \quad (40) \quad 1103$$

1104 Hence, it is possible to calculate the average value of  $\sigma_{\text{cm}}$  in  
1105 the temperature range  $T_n - T_{d2}$  from experimental values of  
1106  $\Delta t_o$ ,  $U(T_n, \infty)$  and  $\Delta G_V$ . Note that in doing so neither nucle-  
1107 ation rate nor time-lag data are required. The values of  $\sigma_{\text{cm}}$   
1108 calculated by this method for  $\text{Li}_2\text{O}\cdot 2\text{SiO}_2$  and  $\text{Na}_2\text{O}\cdot 2\text{-}$   
1109  $\text{CaO}\cdot 3\text{SiO}_2$  glasses are collected in Table 2, which also  
1110 shows values estimated with the assumption of a size and  
1111 temperature independent specific surface energy,  $\sigma_{\text{cm}}^*$  (see  
1112 also Table 1) and  $\sigma_{\text{cm}}^{**}$  employing the theoretical values of  
1113  $I_o$ . The values of  $\sigma_{\text{cm}}$  calculated via Eq. (40) significantly  
1114 exceed the corresponding values calculated from a fit of  
1115 nucleation rate data to CNT ( $\sigma_{\text{cm}}^*$ ,  $\sigma_{\text{cm}}^{**}$ ). According to  
1116 CNT such high values of  $\sigma_{\text{cm}}$  lead to vanishing nucleation  
1117 rates. However, nucleation processes do occur and are in-  
1118 deed observed in deeply undercooled glasses!

1119 In order to find out the origin of this discrepancy, one  
1120 should realize that the methods discussed above do not  
1121 provide us with the surface energy directly, but instead only  
1122 give its combination with the thermodynamic driving force.  
1123 In particular,  $\sigma_{\text{cm}}$  is calculated from the measured values of  
1124  $\Delta t_o$  and  $U(T_n, \infty)$  via (see Eq. (40))

$$1125 \Delta t_o = \frac{2}{U} \sigma_{\text{cm}} f \left( \frac{1}{\Delta G_V} \right) \quad (41) \quad 1127$$

and  $\sigma_{\text{cm}}^{**}$  (as well as  $\sigma_{\text{cm}}^*$ ) from the thermodynamic barrier  
for nucleation

$$1128 W_* \sim \frac{(\sigma_{\text{cm}}^{**})^3}{\Delta G_V^2}. \quad (42) \quad 1130$$

1131 One should recall again that, in line with Gibbs' thermo-  
1132 dynamic description of heterogeneous systems, the thermo-  
1133 dynamic driving force for crystallization of macro-crystals  
1134 has been used to estimate the surface energy of critical and  
1135 near-critical nuclei. Provided, this assumption is correct  
1136 then we obtain correct values of the specific interfacial  
1137 energy. However, if this assumption occurs to be incorrect  
1138 then also the estimates of the surface energy are not cor-  
1139 rect. In such case, in order to arrive at correct values of  
1140 the work of critical cluster formation for nucleation, the  
1141 value of the surface energy has to be chosen appropriately  
1142 becoming merely a fit parameter. Hence, the above dis-  
1143 crepancy may result from the difference between  
1144 the macroscopic values of the thermodynamic driving  
1145 force,  $\Delta G_\infty$ , employed and the correct driving force of crit-  
1146 ical cluster formation and growth,  $\Delta G_V$ , which is deter-  
1147 mined by the real physical state of the critical and near-  
1148 critical clusters. Since the identity of the driving force of  
1149 critical cluster formation with the respective macroscopic  
1150

values is the only assumption employed in the analysis it has to be removed in order to solve the discussed in this and earlier sections discrepancies. Then we have to admit that the bulk properties of critical and near-critical clusters do not coincide with the properties of the respective macroscopic phases and are not determined correctly employing Gibbs' classical thermodynamic approach. As a direct consequence from this assumption, it follows that both surface energy and thermodynamic driving force must be considered as unknown quantities.

Let us analyze now the above mentioned results introducing a coefficient  $K(r)$  that connects the (supposed) real thermodynamic driving force,  $\Delta G_V$ , with the respective value for the macro-phase,  $\Delta G_\infty$ , as

$$\Delta G_V = K(r)\Delta G_\infty. \quad (43)$$

The coefficient  $K(r)$  reflects the fact that the thermodynamic driving force for critical nuclei may differ from that of the corresponding macro-phase. If one denotes by  $\sigma_{cm}^r$  the true value of the surface energy estimated with account of Eq. (43) and takes into consideration that  $U \sim \Delta G_V$ , the following equations connecting  $\sigma_{cm}^r$  with  $\sigma_{cm}$  and  $\sigma_{cm}^{**}$  are obtained from Eqs. (41) and (42)

$$\sigma_{cm}^r = K(r)^2 \sigma_{cm}, \quad \sigma_{cm}^r = K(r)^{2/3} \sigma_{cm}^{**}. \quad (44)$$

Eq. (44) yield

$$K = \left( \frac{\sigma_{cm}^{**}}{\sigma_{cm}} \right)^{2/3}. \quad (45)$$

Thus, both methods provide the same value of crystal/melt surface energy if the reduced thermodynamic driving force,  $\Delta G_V = K(r)\Delta G_\infty$ , is employed. The values of  $K$  presented in Table 2 show a considerable reduction of the thermodynamic driving force for nucleation and growth of critical and near-critical nuclei as compared with that for the macro-crystal growth ( $K < 1$ ). Employing this self-consistently determined value of the driving force, different estimates for the specific surface energy are obtained as compared with the case when the classical Gibbs' approach for the determination of the driving force is used. It should be emphasized that the value of  $\sigma_{cm}^r$  (see Table 2) is smaller than that of  $\sigma_{cm}^*$  and  $\sigma_{cm}^{**}$ . Hence, in this way, the decrease of the thermodynamic driving force results in values of the interfacial energy that are significantly more reasonable (taking Stefan's rule into account). We can conclude, consequently, that the discussed so far grave problems in the theoretical interpretation of crystallization can be removed if one assumes that the state of critical and near-critical clusters is different from the state of the newly evolving macro-phase. That is the classical Gibbs' approach does not give, consequently, in general a correct description of the bulk properties of critical and near-critical clusters.

Arriving at such conclusion, two classes of problems arise: First, one has to discuss whether there exist alternative theoretical concepts favoring this point of view or not

and whether it is possible to generalize eventually Gibbs' approach in order to remove mentioned defect in Gibbs' classical treatment. Second, one has to search for the physical origin of such differences in the state of the critical clusters as compared with the respective bulk phases and for additional arguments and experimental results confirming such point of view. Such analysis will be performed in the subsequent sections.

#### 5.4. Bulk properties of critical clusters and properties of the newly evolving macroscopic phase: some results of theoretical analyses

##### 5.4.1. Gibbs' theory of heterogeneous systems: basic postulates, advantages and shortcomings

In the theoretical interpretation of experimental results on the dynamics of first-order phase transitions starting from metastable initial states, up to now the classical nucleation theory has been predominantly employed treating the respective process in terms of cluster formation and growth and employing Gibbs' theory of capillarity. This preference is due to the advantage of Gibbs' approach to the description of thermodynamically heterogeneous systems allowing one to determine the parameters of the critical clusters and the work of critical cluster formation in the nucleation rate expression in a relatively simple way which is based on the knowledge of macroscopic bulk and surface properties of the ambient and newly evolving phases.

In his classical analysis [4], Gibbs describes heterogeneous systems (in application to the problems under consideration, we discuss a cluster of a newly evolving phase in the ambient phase) via an idealized model system. In this model, the real system is described as consisting of two homogeneous phases divided by a mathematically sharp interface. The thermodynamic characteristics of the system are represented as the sum of the contributions of both homogeneous phases and correction terms, the so-called superficial quantities, which are assigned to the interface. They reflect the diffuseness of the interface in the framework of Gibbs' model approach. In contrast to alternative statements [77,78] we believe that such approach is theoretically well-founded and correct provided one is able to determine the superficial quantities in an appropriate way for any real system.

In order to further develop the theoretical concept attempting to solve this task, Gibbs formulated a fundamental equation for the superficial (or interfacial) thermodynamic parameters (specified by the subscript  $\sigma$ ) which is widely similar to the fundamental equation for homogeneous bulk phases. For spherical interfaces we restrict our considerations to, it reads [4]

$$dU_\sigma = T_\sigma dS_\sigma + \sum \mu_{i\sigma} dn_{i\sigma} + \sigma dA + C dc, \quad (46)$$

where  $U$  is the internal energy,  $S$  the entropy,  $T$  the temperature,  $\mu_i$  the chemical potential,  $n_i$  the number of particles or moles of the different components ( $i = 1, 2, \dots, k$ ),  $\sigma$  the surface or interfacial tension,  $A$  the surface area, and

1263  $c = (1/R)$  the curvature of the considered surface element,  
 1264 while  $C$  is a thermodynamic parameter determining the  
 1265 magnitude of changes of the internal energy with variations  
 1266 of the curvature of the considered surface element.  $R$  is the  
 1267 radius of curvature of the considered surface element.

1268 An integration of this equation results in

$$1271 U_{\sigma} = T_{\sigma} S_{\sigma} + \sum \mu_{i\sigma} n_{i\sigma} + \sigma A. \quad (47)$$

1272 A combination of both equations yield the Gibbs adsorp-  
 1273 tion equation in the general form

$$1276 S_{\sigma} dT_{\sigma} + \sum n_{i\sigma} d\mu_{i\sigma} + A d\sigma = C dc. \quad (48)$$

1277 In order to assign well-defined values to the superficial  
 1278 quantities and cluster size, as an essential requirement of  
 1279 Gibbs' theory the location of the dividing surface has to  
 1280 be specified. In application to nucleation processes, usually  
 1281 the surface of tension is employed. It is defined, utilizing  
 1282 Gibbs' fundamental equation for the superficial quantities,  
 1283 via the equation  $C = 0$ . For this particular dividing surface,  
 1284 the surface tension does not depend explicitly on the curva-  
 1285 ture. Moreover, it follows that in the classical Gibbs'  
 1286 approach the surface tension depends on  $(k + 1)$  indepen-  
 1287 dent state variables.

1288 With Eq. (47) and the well-known expressions for the  
 1289 internal energy of homogeneous bulk phases, we get the  
 1290 following expression for the internal energy of the whole  
 1291 system (e.g., [79–81])

$$1294 U = T_{\alpha} S_{\alpha} - p_{\alpha} V_{\alpha} + \sum \mu_{i\alpha} n_{i\alpha} + T_{\beta} S_{\beta} - p_{\beta} V_{\beta} \\ + \sum \mu_{i\beta} n_{i\beta} + T_{\sigma} S_{\sigma} + \sum \mu_{i\sigma} n_{i\sigma} + \sigma A. \quad (49)$$

1295 Here  $p$  is the pressure,  $V$  the volume, the subscript  $\alpha$  spec-  
 1296 ifies the parameters of the cluster phase, the subscript  $\beta$  re-  
 1297 fers to the parameters of the ambient phase.

1298 In application to nucleation, the state of the ambient  
 1299 phase is known. In this way, in order to employ Gibbs' the-  
 1300 ory, the bulk state of the cluster phase has to be specified.  
 1301 This procedure is performed in Gibbs' classical treatment  
 1302 for *equilibrium states of heterogeneous substances*, exclu-  
 1303 sively (the title of his paper, Ref. [4], is 'On the equilibrium  
 1304 of heterogeneous substances'), a cluster of critical size in  
 1305 the ambient phase being a particular realization of a ther-  
 1306 modynamic equilibrium state. By employing the general  
 1307 conditions for thermodynamic equilibrium [4], two of the  
 1308 three basic sets of the equilibrium conditions are obtained

$$1311 T_{\alpha} = T_{\beta} = T_{\sigma}, \quad \mu_{i\alpha} = \mu_{i\beta} = \mu_{i\sigma}, \quad i = 1, 2, \dots, k, \quad (50)$$

1312 allowing one to uniquely determine the state parameters of  
 1313 the cluster phase from the knowledge of the state of the  
 1314 ambient phase.

1315 The bulk properties of the critical clusters of the newly  
 1316 evolving phase are determined, consequently, in Gibbs'  
 1317 approach uniquely via the equilibrium conditions Eq.  
 1318 (50) for temperature and chemical potentials of the differ-  
 1319 ent components in the two coexisting bulk phases. Hereby  
 1320 the question is not posed whether or not these state param-  
 1321 eters represent a correct description of the bulk state

parameters of the cluster. It is commonly believed that this  
 is the case. However, Gibbs himself made a comment that,  
 in general, the properties of the critical clusters may differ  
 from the predictions obtained in his approach. It follows  
 further from the Gibbs method that, for the critical clus-  
 ters, the interfacial tension referred to the surface of ten-  
 sion is uniquely determined by the state parameters of  
 either the ambient or the cluster phase (cf. Eqs. (48) and  
 (50)). Consequently, once the parameters of the ambient  
 phase are given, the surface tension does not depend –  
 according to Gibbs' classical method – on the state param-  
 eters of the cluster phase. Moreover, the superficial temper-  
 ature and chemical potentials are determined by the  
 respective parameters of the bulk phases as well.

As it turns out [80–82], Gibbs' method leads to state  
 parameters of the critical cluster's bulk phase which are  
 widely identical, at least, in application to phase formation  
 in condensed phases, to the properties of the newly evol-  
 ving macroscopic phases. Modifications of these properties,  
 due to differences in the pressure of small clusters as com-  
 pared with the equilibrium coexistence of both phases at  
 planar interfaces, as given by the Young–Laplace equation  
 (the third equilibrium condition),

$$p_{\alpha} - p_{\beta} = \frac{2\sigma}{r_*} \quad (51)$$

is commonly of minor importance here although the pres-  
 sure differences may be large. With the numerical estimates  
 $p_{\beta} = p_{\text{at}} \sim 10^5 \text{ N/m}^2$ ,  $\sigma \sim 0.1 \text{ J/m}^2$ ,  $r_* \sim 10^{-9} \text{ m}$  (at high  
 under-cooling), we get  $\Delta p \sim 2 \times 10^8 \text{ Pa}$  or  $2000 p_{\text{at}}$ . How-  
 ever, the effect of pressure on the density is small due to  
 the low compressibility of the cluster bulk phase. This re-  
 sult – the wide similarity of the properties of the critical  
 cluster with the properties of the evolving macroscopic  
 phases – is an essential general feature of Gibbs' classical  
 theory not only in application to crystallization. It leads  
 – as discussed in detail here above – to contradictions in  
 the interpretation of experimental results and as we will  
 see below to contradictions with the results of computer  
 simulations and density functional computations of the  
 properties of critical clusters showing a quite different  
 behavior, in particular, for higher supersaturations. So,  
 why Gibbs' theory can be applied at all to nucleation?  
 The following answer can be given.

In application to nucleation, not the knowledge of the  
 properties of the critical clusters is commonly of major  
 interest but instead the value of the work of critical cluster  
 formation,  $W_*$ . This quantity is determined in Gibbs'  
 description generally via  $W_* \propto \sigma^3 / (p_{\alpha} - p_{\beta})^2$  [4] or in a fre-  
 quently good approximation via  $W_* \propto \sigma^3 / (\Delta G_V)^2$  (cf. Eq.  
 (4)). For any state of the ambient phase, the driving force  
 of critical cluster formation, which can be considered to  
 be proportional to either  $(p_{\alpha} - p_{\beta})$  or  $\Delta G_V$ , is determined  
 uniquely via the equilibrium conditions Eq. (50). In this  
 way, as far as the process proceeds via nucleation with a  
 well-defined value of the work of critical cluster formation,  
 one can always find a value of the interfacial tension lead-

ing to the correct result for  $W_*$ . Such possibility exists independently on whether the driving force is determined in an appropriate way corresponding to the real situation. In general, the interfacial tension (or the specific interfacial energy in application to formation of crystalline critical nuclei) is different from its macroscopic value. This deviation from the macroscopic value is connected then with the idea of a curvature (or supersaturation) dependence of the surface tension. But in such approach,  $\sigma$  loses its meaning of a physical quantity. As we previously mentioned it becomes a fit parameter that compensates the inappropriate choice of the bulk reference states for the description of the critical clusters.

The failure of Gibbs' classical approach for the determination of the bulk properties of the critical clusters is connected with another disadvantage that has seldom been noticed. This classical approach is in deep conflict with the conventional method of determination of saddle points or extremums of hyper-surfaces of any dimension. In order to find these singular points of such surfaces, following the standard methods, one has to first formulate the respective equations for any arbitrary state of the system and then to apply the extremum conditions. In application to cluster formation, we would have first to formulate the thermodynamic potentials for any well-defined thermodynamic (including non-equilibrium) states of a cluster or ensembles of clusters in the ambient phase and then to search for saddle points. This is the general procedure, which is also employed in any density functional computations of the work of critical cluster formation (see the subsequent discussion).

However, Gibbs never tried in his fundamental paper [4] even to formulate the problem of the determination of the thermodynamic potential of a cluster or ensembles of clusters of non-critical sizes in the otherwise homogeneous ambient phase. His method is, consequently, in conflict with the standard theoretical procedure. It follows as another consequence that Gibbs' original treatment cannot supply one with a recipe to determine the state of sub- and supercritical clusters in a well-founded theoretical way. Any description of cluster growth processes, which is based on Gibbs' theory, involves additional assumptions, which may or may not be appropriate. Consequently, a problem arises whether it is possible to develop a generalisation of Gibbs' thermodynamic treatment allowing one to describe critical cluster formation in a theoretically more founded way and supplying one simultaneously with a regular method of theoretical determination of the properties of sub- and supercritical clusters. However, before developing the respective generalization, we briefly summarize some alternative methods of theoretical description and their results concerning the problems under consideration.

#### 5.4.2. Continuum's approaches to the determination of the properties of heterogeneous systems: van der Waals' and modern density functional approaches

About two decades after the formulation of Gibbs' theory, van der Waals [83,84] developed an alternative contin-

uum's approach to the description of heterogeneous systems. In this approach, the interface is characterized by a continuous change of the intensive thermodynamic state parameters from the respective values in one to those characterizing the other of the coexisting phases. The van der Waals method of description of heterogeneous systems was reinvented about 60 years later by Cahn and Hilliard [85] and applied for the description of the properties of critical clusters in nucleation and for the development of the basic ideas of the classical theory of spinodal decomposition.

In the van der Waals and Cahn–Hilliard approach, the Gibbs free energy of a heterogeneous system is given in the simplest version as

$$G(p, T, x) = \int \left[ g(p, T, x(\vec{r})) + \kappa(\nabla x(\vec{r}))^2 \right] dV. \quad (52)$$

For any given concentration profile, the value of the Gibbs free energy can then be found by integrating the volume density,  $g$ , of the Gibbs free energy supplemented by the surface term,  $\kappa(\nabla x(\vec{r}))^2$ , over the whole volume,  $V$ , of the system, i.e., any well-defined function,  $x(r)$ , results in some definite value of the Gibbs free energy. Critical clusters refer to saddle points of the thermodynamic potentials. Consequently, in order to determine the change of the Gibbs free energy in critical cluster formation, one has to search for such concentration or density profiles, for which the respective conditions for a saddle point of the thermodynamic potential  $G$  are fulfilled. From a mathematical point of view, the thermodynamic potential is determined, consequently, as a functional of the density or concentration profile giving the name to the method of computation of the work of critical cluster formation (density functional methods; i.e., saddle points are determined via the search for an extremum of the respective functional).

In application to nucleation-growth processes (phase transformations originating from metastable initial states), Cahn and Hilliard came to the conclusion that the bulk state parameters of the critical clusters may deviate considerably from the respective values of the evolving macrophases and, consequently, from the predictions of Gibbs' theory. These results of the van der Waals and Cahn–Hilliard-approach were reconfirmed later-on by more advanced density functional computations (cf., e.g., Refs. [86–88]) allowing one to determine the thermodynamic potential by choosing some well-defined interaction potentials between the particles of the system under consideration. Similar to the van der Waals and Cahn–Hilliard approach, the spatial distribution of the order parameter field is computed and it is assumed that the different phases and their states can be described by varying the value of the order parameters.

As an example, the composition of a critical cluster in phase formation in a binary solution is shown in Fig. 16 [80]. The supersaturation is changed by varying the molar fraction,  $x$ , of one of the components in the ambient phase inside the range from the binodal to the spinodal curves,

1434  
1435  
1436  
1437  
1438  
1439  
1440  
1441  
1442  
1443  
1444  
1445  
1446  
1447  
1448  
1449  
1450  
1451  
1452  
1453  
1454  
1455  
1456  
1457  
1458  
1459  
1460  
1461  
1462  
1463  
1464  
1465  
1466  
1467  
1468  
1469  
1470  
1471  
1472  
1473  
1474  
1475  
1476  
1477  
1478  
1479  
1480  
1481  
1482  
1483  
1484  
1485  
1486  
1487  
1488  
1489  
1490

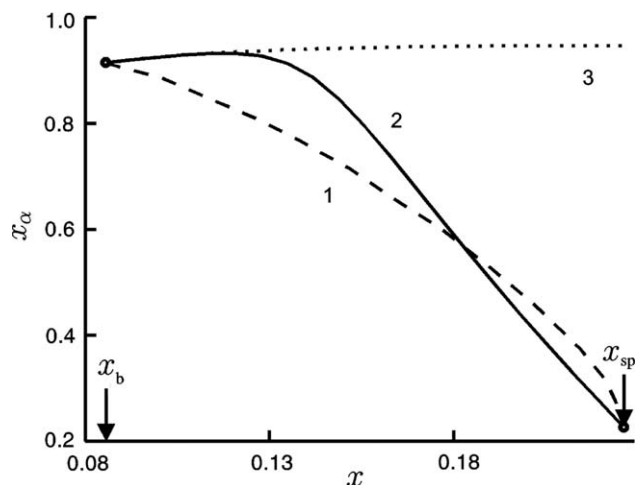


Fig. 16. Composition of the critical cluster,  $x_{\alpha}$ , as a function of the supersaturation for segregation processes in solutions [80]. The molar fraction,  $x$ , of the segregating component in the ambient solution can be considered as a measure of supersaturation, which varies in the range between the binodal ( $x_b$ ) and spinodal ( $x_{sp}$ ) curves. The dotted curve (curve 3) refers to results of computations of the critical cluster parameters obtained via Gibbs' classical method; the dashed curve (curve 1) to the newly developed generalized Gibbs approach and the full curve (curve 2) to results of density functional calculations of the density in the center of the critical cluster obtained via the van der Waals square gradient method.

1491 i.e., for metastable initial states of the ambient phase. The  
 1492 results of the classical Gibbs approach to the determination  
 1493 of the properties of the critical clusters are given by a dot-  
 1494 ted curve (curve 3). It is evident that the composition of the  
 1495 critical clusters – determined in such a way – practically  
 1496 does not depend on supersaturation and is widely equal  
 1497 to the value in the newly evolving macroscopic phase.  
 1498 The full curve (curve 2) shows the results for the cluster  
 1499 composition in the center of the critical cluster as obtained  
 1500 via the van der Waals and Cahn–Hilliard square gradient  
 1501 approximation as described by Eq. (52). It is evident that  
 1502 both approaches lead, in general, to very different results.  
 1503 Qualitatively similar results are obtained when the van  
 1504 der Waals and Cahn–Hilliard approach or more advanced  
 1505 density functional computations are applied to the descrip-  
 1506 tion of crystallization [77,89,90], i.e., the state of the critical  
 1507 cluster differs, in general, from the state of the newly evol-  
 1508 ving macroscopic phase.

1509 Both Gibbs' and the van der Waals or more advanced  
 1510 density functional methods of description of thermody-  
 1511 namically heterogeneous systems are considered commonly  
 1512 as well-established theories. Nevertheless, only one of them  
 1513 (if any) can be correct in the prediction of the properties of  
 1514 the critical clusters. Moreover, the Gibbs and van der  
 1515 Waals approaches lead to contradicting each other results  
 1516 in the description of the behavior of phase separating sys-  
 1517 tems in the vicinity of the classical spinodal curve (cf. Ref.  
 1518 [91]). In this way, one is confronted here with internal con-  
 1519 tradictions in two well-established theories, which must be,  
 1520 hopefully, resolved.

1521 The question which of both mentioned theories  
 1522 describes more correctly the properties of the critical clus-

1523 ters can be answered from a theoretical point of view based  
 1524 on the analysis of the results of computer simulation meth-  
 1525 ods of phase formation processes in model systems [92–96].  
 1526 The respective analyses show that critical clusters do have  
 1527 properties, in general, significantly different from the prop-  
 1528 erties of the newly evolving macroscopic phases (although  
 1529 in some particular cases also results are obtained which  
 1530 are in agreement with the classical Gibbs approach). In this  
 1531 way, computer simulation methods support, in general, the  
 1532 van der Waals or alternative density functional approaches  
 1533 for the description of heterogeneous systems.

1534 Consequently, we can conclude that the majority of exist-  
 1535 ing theoretical approaches for the determination of the work  
 1536 of critical cluster formation gives strong support to the point  
 1537 of view that the state of the critical clusters may significantly  
 1538 differ from the state of the newly evolving macroscopic  
 1539 phases. Consequently, in order to obtain correct expressions  
 1540 for the work of critical cluster formation in the interpreta-  
 1541 tion of experimental results one has to account for a cluster  
 1542 size dependence not only of the surface properties of the crit-  
 1543 ical clusters but also of their bulk properties.

#### 1544 5.4.3. A generalization of Gibbs' classical theory

1545 Having reached such conclusion, immediately the ques-  
 1546 tion arises whether it is necessary to abandon the classical  
 1547 Gibbs approach at all or whether it is possible to modify it  
 1548 in such a way that it retains its advantages (use of macro-  
 1549 scopic properties of the phases of interest for a determination  
 1550 of the work of critical cluster formation) but overcomes its  
 1551 shortcomings (incorrect determination of the bulk proper-  
 1552 ties of the critical clusters) discussed above. As it turns out  
 1553 such generalization of Gibbs' thermodynamic theory can  
 1554 be really performed. It was initiated several years ago based  
 1555 initially on a generalization of Ostwald's rule of stages in  
 1556 application to nucleation. This generalization of Ostwald's  
 1557 rule was formulated as follows [97]: 'Those classes of critical  
 1558 clusters determine the process of the transformation, which  
 1559 correspond to a minimum work of critical cluster formation  
 1560 (as compared with all other possible alternative structures  
 1561 and compositions, which may be formed at the given thermo-  
 1562 dynamic constraints)'. This concept was then employed in  
 1563 order to develop a new approach for the determination of  
 1564 the work of critical cluster formation and the determination  
 1565 of critical cluster properties based on a generalization of  
 1566 Gibbs' classical approach [79,98].

1567 In such a generalization of Gibbs' theory, we followed  
 1568 again Gibbs' method of dividing surfaces but started with  
 1569 the analysis of the question how to formulate a thermody-  
 1570 namic description of heterogeneous systems (clusters or  
 1571 ensembles of clusters in the otherwise homogeneous ambi-  
 1572 ent phase) for well-defined non-equilibrium states, when  
 1573 both the clusters and the ambient phase are in an internal  
 1574 thermodynamic equilibrium but the system as a whole is  
 1575 not. Having a look at Eq. (49), immediately the question  
 1576 arises then, how to determine the values of the superficial  
 1577 temperature and chemical potentials for any well-defined  
 1578 non-equilibrium states of the heterogeneous systems under

consideration. Since these parameters cannot be determined independently of the parameters of the coexisting bulk phases, we postulated long ago [99] that generally the conditions

$$T_\beta = T_\sigma, \quad \mu_{i\beta} = \mu_{i\sigma}, \quad i = 1, 2, \dots, k, \quad (53)$$

must hold. In other words, it is assumed that the superficial temperature and chemical potentials are determined widely by the properties of the ambient phase (with known properties). *Note that the bulk state parameters of the cluster phase may vary independently and may have so far arbitrary values.* Employing such condition and the fundamental equation for the superficial quantities Eq. (46) as formulated by Gibbs, the interfacial tension (referred to the surface of tension) becomes then a function of the state parameters of the ambient phase exclusively. However, for non-equilibrium states the interfacial tension has to depend, in general, not only on the properties of the ambient but also on all intensive state parameters of the cluster phase. This set of intensive state parameters of the cluster phase we denote here as  $\{\varphi_{ix}\}$ . In order to be able to describe such additional dependence, Gibbs' fundamental equation Eq. (46) has to be generalized resulting in (see also [79,82] for further details)

$$dU_\sigma = T_\sigma dS_\sigma + \sum \mu_{i\sigma} dn_{i\sigma} + \sigma dA + C dc + \sum \phi_{ix} d\varphi_{ix}, \quad (54)$$

where  $\phi_{ix}$  are parameters determining the magnitude of variations of the superficial internal energy with respect to variations of the bulk state of the cluster phase.

Since all parameters  $\varphi_{ix}$  of the cluster phase, entering Eq. (54), are intensive quantities, the expression for the superficial internal energy Eq. (47) and also for the thermodynamic potentials are formally not changed as compared with Gibbs' original approach. In contrast, the generalized Gibbs' adsorption equation reads now

$$S_\sigma dT_\beta + \sum n_{i\sigma} d\mu_{i\beta} + A d\sigma = C dc + \sum \phi_{ix} d\varphi_{ix}. \quad (55)$$

In the generalization of Gibbs' approach, the interfacial tension can and must be considered consequently as a function both of the intensive state variables of the ambient and the cluster phases and curvature. For the surface of tension (defined also in the generalized Gibbs approach via  $C = 0$ ) an explicit curvature dependence of the surface tension does not occur, again.

Having at ones disposal the thermodynamic potentials for the respective non-equilibrium states, the equilibrium conditions are obtained by known procedures employed already by Gibbs in his classical model approach [4]. They differ from the equilibrium conditions derived by Gibbs and read, in general,

$$r_* = 2\sigma / \left[ p_\alpha - p_\beta - \sum \rho_{ix} (\mu_{ix} - \mu_{i\beta}) - s_\alpha (T_\alpha - T_\beta) \right], \quad (56)$$

$$\mu_{ix} - \mu_{i\beta} = (3/r_*) (\partial\sigma / \partial\rho_{ix}), \quad (57)$$

$$T_\alpha - T_\beta = (3/r_*) (\partial\sigma / \partial s_\alpha). \quad (58)$$

Here  $p$  is the pressure,  $\rho$  the volume density of the ( $i = 1, 2, \dots, k$ ) different components in the system,  $s$  is the volume density of the entropy. The subscript  $\alpha$  specifies, again, the parameters of the cluster, while  $\beta$  refers to the parameters of the ambient phase.

In order to determine the parameters of the critical clusters, one has to know the values of the surface tension (or the specific interfacial energy). In the simplest case [79,82,98,100], it can be expressed as a quadratic form in the differences of the state parameters of the ambient ( $\{\varphi_{i\beta}\}$ ) and cluster ( $\{\varphi_{ix}\}$ ) phases as

$$\sigma = \sum \sum \Xi_{ij} (\varphi_{ix} - \varphi_{i\beta}) (\varphi_{j\alpha} - \varphi_{j\beta}). \quad (59)$$

The values of the parameters  $\Xi_{ij}$  can be determined then from the knowledge of the specific interfacial energy for phase coexistence at planar interfaces.

As it turns out, the work of critical cluster formation can be written generally again in the well-known classical form

$$W_* = \frac{1}{3} \sigma A_*, \quad (60)$$

where  $A_*$  is the surface area of the critical cluster. Note however that the results for the numerical values for the work of critical cluster formation are different in both discussed classical and generalized Gibbs' approaches since the state parameters of the clusters differ in these two methods.

In general, the parameters of the critical clusters as obtained via the generalized Gibbs approach differ significantly from the parameters obtained following the classical Gibbs method. However, for phase equilibrium of macroscopic systems, the equilibrium conditions derived in the generalized Gibbs approach coincide with Gibbs' classical expressions (here the radius of the critical clusters tends to infinity and the classical Gibbs equilibrium conditions are obtained as a special case). Note that Gibbs' classical equilibrium conditions are retained in the above given generalized equations also as a limiting case when the derivatives of the interfacial specific energy with respect to the intensive state parameters of the cluster phase are set equal to zero.

Employing the generalized Gibbs' approach to the determination of critical cluster properties for a variety of phase-separating systems (segregation in solutions [80], condensation and boiling in one-component fluids [81], boiling in multi-component fluids [82]) it has been shown that the predictions concerning the properties of critical clusters and the work of critical cluster formation, derived in the generalized Gibbs' approach, are in agreement with van der Waals' and more advanced density functional methods of determination retaining, on the other hand, the simplicity in applications similarly to the classical Gibbs method as an additional advantage. For example, in Fig. 16 the composition of the critical clusters as obtained via the generalized Gibbs approach is shown by a dashed curve (curve 1). For small supersaturations, the results of all mentioned approaches agree, however, when

1688 the whole range of initial supersaturations is considered  
1689 and especially for large supersaturations the results of the  
1690 generalized Gibbs' approach are similar to the results  
1691 obtained via square gradient density functional computa-  
1692 tions and deviate significantly from the results of Gibbs'  
1693 classical approach. Such kind of behavior is essential in  
1694 order to guarantee the vanishing of the surface free energy  
1695 and of the work of critical cluster formation near the clas-  
1696 sical spinodal curve, two features commonly considered as  
1697 essential for a correct description of nucleation and which  
1698 are not described by the classical approach when the capil-  
1699 larity approximation is utilized [88]. It can be shown fur-  
1700 ther in a general way [99] that the classical Gibbs  
1701 approach employing in addition the capillarity approxima-  
1702 tion as a rule overestimates the work of critical cluster for-  
1703 mation and, in general, significantly.

1704 Recently the generalized Gibbs' approach was further  
1705 extended [91,101–104] to allow the description not only  
1706 of nucleation but also of growth and dissolution processes  
1707 taking into account changes of the bulk and surface state  
1708 parameters of the clusters as a function of supersaturation  
1709 and size. Hereby a criterion was advanced to allow one the  
1710 quantitative determination of the changes in the bulk and  
1711 surface properties of the clusters in the course of their  
1712 growth. As a first application, this new theory of growth  
1713 and dissolution processes was applied to the analysis of  
1714 segregation in solutions. However, the method is generally  
1715 applicable. In the framework of this approach, the change  
1716 of a variety of thermodynamic and kinetic properties with  
1717 cluster size has been determined for the first time such as  
1718 the change of the surface tension, the driving force of clus-  
1719 ter growth, the dependence of the effective diffusion coeffi-  
1720 cients on cluster size, etc. As it turns out the respective  
1721 thermodynamic and kinetic parameters may change signif-  
1722 icantly in dependence on cluster size. In this way, the esti-  
1723 mates of these parameters obtained from nucleation data  
1724 may not be appropriate for the description of growth pro-  
1725 cesses of clusters of macroscopic sizes and vice versa. This  
1726 result gives a new key to the solution of the problems posed  
1727 by Granasy and James [105] that growth rates computed  
1728 with values of kinetic coefficients obtained from nucleation  
1729 data may lead to deviations between theory and experiment  
1730 reaching several orders of magnitude. Even peculiarities in  
1731 the evolution of the cluster size distributions – like the  
1732 development of bimodal distributions in intermediate  
1733 states of the nucleation-growth process and unexpected  
1734 properties – may be explained straightforwardly based on  
1735 these concepts [102,104,106,107]. Thus, in a correct theo-  
1736 retical treatment not only deviations of the composition  
1737 of the critical nuclei from those of the respective macro-  
1738 scopic phases, but also variations in the composition of  
1739 the sub- and supercritical crystals have to be and can be  
1740 accounted for.

1741 The extension of these concepts in application to crystal-  
1742 lization is in progress. Here, in addition to changes in com-  
1743 position and density also possible differences in the  
1744 structure of the critical clusters (and their mutual interde-

1745 pendence with concentration fluctuations [12,88,108,109]),  
1746 as compared with the state of the crystalline macro-phase,  
1747 and its possible change in the course of the growth of the  
1748 supercritical crystallites have to be taken into consideration  
1749 (cf., e.g., [110–112]).

#### 1750 5.4.4. Discussion

1751 Let us first briefly summarize the results of the preceding  
1752 subsection: In order to develop a consistent theoretical  
1753 method of determination of the properties of the critical  
1754 clusters, we have generalized Gibbs' theory starting with  
1755 the thermodynamic description of non-equilibrium states  
1756 and including in this way into the theoretical schema the  
1757 possibility of description of clusters of sub- and supercriti-  
1758 cal sizes in the ambient phase. In order to realize such task,  
1759 Gibbs' fundamental equation for the superficial thermody-  
1760 namic state parameters was generalized to allow one, in  
1761 particular, an incorporation into the theory of the depen-  
1762 dence of the interfacial or surface tension both on the state  
1763 parameters of the ambient and the newly evolving cluster  
1764 phases, respectively. Such essential additional step in the  
1765 generalization of Gibbs' classical approach was not done  
1766 in earlier own work [99] and also not in the two (to the  
1767 knowledge of the authors) existing alternative generaliza-  
1768 tions of Gibbs' theory to non-equilibrium states (see  
1769 [113]). By this reason, in latter mentioned approaches  
1770 [99,113] the equilibrium conditions retain the same form  
1771 as in the classical Gibbs' approach.

1772 Following the generalized Gibbs' approach, it is possible  
1773 to determine the properties of the critical clusters in a new  
1774 way. We arrive at relations, which are, in general, different  
1775 as compared with the predictions of the classical Gibbs  
1776 approach. The respective results are – for model systems  
1777 – in agreement with density functional computations and  
1778 results of computer simulations. Moreover, since we have  
1779 formulated a consistent description of clusters in thermo-  
1780 dynamically non-equilibrium states, regular methods can  
1781 be and are developed to determine also the properties of  
1782 clusters of sub- and supercritical sizes in dependence on  
1783 supersaturation and their sizes. In this way, a new tool  
1784 for the description of nucleation-growth processes, in gen-  
1785 eral, and crystallization processes in glass-forming liquids,  
1786 in particular, has been developed allowing one to interpret  
1787 a variety of experimental findings from a new point of view  
1788 [91,102–104,111].

1789 As an alternative non-classical method of theoretical  
1790 treatment of crystallization going back already to van der  
1791 Waals [83,84], the van der Waals and Cahn–Hilliard square  
1792 gradient density functional approach is employed presently  
1793 intensively for the interpretation of nucleation in crystalli-  
1794 zation processes [77,87–89,114]. These studies are supple-  
1795 mented by the analysis of nucleation-growth processes  
1796 based on so-called phase field models, a dynamic extension  
1797 of the van der Waals and Cahn–Hilliard approach  
1798 [78,87,115–118], allowing one the determination of the evo-  
1799 lution of the order-parameter fields with time. These types  
1800 of analyses are confronted, however, with one principal

1801 problem, which has to be taken into consideration – as it  
1802 seems to us – more carefully in future. This problem is  
1803 the prediction – in the framework of mentioned van der  
1804 Waals and Cahn–Hilliard type approaches – of spinodal  
1805 curves in melt-crystallization.

1806 More than three decades ago, Skripov and Baidakov  
1807 [119], based on the analysis of experimental and computer  
1808 simulation data – advanced the conjecture about the non-  
1809 existence of a spinodal curve in one-component melt crys-  
1810 tallization processes (or widely equivalent to them poly-  
1811 morphic transformations where liquid and crystal phases  
1812 have the same composition). It was emphasized that this  
1813 statement is in agreement with the point of view of the  
1814 non-existence of a critical point in liquid–solid phase equi-  
1815 libria and of a necessarily discontinuous transition  
1816 between liquid and crystal [120]. A further detailed proof  
1817 of this statement in a period of about 30 years resulted in  
1818 a confirmation of its validity [74,121]. An additional sup-  
1819 port of such point of view can be obtained from the anal-  
1820 ysis of experimental data on crystallization processes of  
1821 liquids, in general, and glass-forming melts, in particular.  
1822 Such analysis does not give any indication on the existence  
1823 of spinodal curves in crystallization processes of the con-  
1824 sidered type [12]. The latter conclusion is supported, for  
1825 example, by Oxtoby [87,88] and Granasy and James [77].

1826 However, density functional theories of crystallization  
1827 predict in a variety of cases the existence of spinodal  
1828 curves. Since such kind of behavior is not found by exper-  
1829 iments, parameters are chosen that transfer the spinodal  
1830 into parameter regions, where – due to the high viscosity  
1831 – phase formation processes cannot occur [77,87,122,123].  
1832 A spinodal type behavior is also predicted in some cases  
1833 by Granasy’s so-called diffuse interface theory and even  
1834 close to the glass transition temperature [124]. Provided –  
1835 as we believe – the conjecture of Skripov and Baidakov is  
1836 correct, the prediction of a spinodal in the mentioned the-  
1837 ories leads to some serious doubts into their applicability to  
1838 melt crystallization, at least, in the present form. A theory  
1839 cannot be correct if it predicts – not as an exception but as  
1840 a rule – phenomena, which are absolutely not observed in  
1841 nature. By the above discussed reasons, a further detailed  
1842 analysis of the basic ideas and limitations of density func-  
1843 tional approaches in application to melt crystallization  
1844 seems to be absolutely essential.

1845 Completing the discussion on the limitations of the clas-  
1846 sical Gibbs approach to the description of the properties of  
1847 critical clusters, we would like to add a few comments on  
1848 the so-called ‘nucleation theorem’ [125–128] employed fre-  
1849 quently in order to determine the properties of critical clus-  
1850 ters based on nucleation rate data [88,94,96,129,130]. In an  
1851 approximate form and for one-component systems, the  
1852 content of this theorem can be formulated as [125]

$$1853 \quad dW_*/d\Delta\mu \approx -n_*, \quad (61)$$

1856 i.e., derivatives of the work of critical cluster formation (or  
1857 the steady-state nucleation rate) with respect to the state

1858 parameters of the ambient phase allow one to determine  
1859 the parameters of the critical clusters. Relations of this type  
1860 – derived in the framework of Gibbs’ classical theory and  
1861 employing the capillarity approximation – have been  
1862 known for a long time. The increased interest in dependen-  
1863 cies of such type resulted from the statements by Kashchiev  
1864 [125] that the nucleation theorem is valid independent of  
1865 the method employed for the thermodynamic description  
1866 and valid for any kind of phase transformation and size  
1867 of the critical clusters considered. However, the indepen-  
1868 dence of the mentioned relation on the way of description  
1869 of the clusters is questionable already on general argumen-  
1870 tations. For example, Einstein noted in a conversation with  
1871 Heisenberg on the foundations of quantum mechanics that  
1872 *it is the theory which determines what can be measured*. In a  
1873 detailed analysis of the results of Ref. [125] it has been  
1874 shown recently in detail [127,128] that all above mentioned  
1875 statements concerning Eq. (61) are not correct.

1876 In an extension of the analysis of Ref. [125], Oxtoby and  
1877 Kashchiev developed similar relations in application to  
1878 multi-component systems [126]. In this analysis, Gibbs’  
1879 classical theory of thermodynamically heterogeneous sys-  
1880 tems was employed without introducing any additional  
1881 assumptions like the capillarity approximation, i.e., the  
1882 assumption that the surface tension of critical clusters is  
1883 equal to the respective value for an equilibrium coexistence  
1884 of both phases at planar interfaces. Consequently, the men-  
1885 tioned generalizations of the nucleation theorem are of the  
1886 same level of validity in application to experiment as the  
1887 classical Gibbs approach. They can describe the parameters  
1888 of the real critical clusters correctly only as far as Gibbs’  
1889 classical method is adequate to the considered particular  
1890 situation. Having in mind the above discussed limitations  
1891 of Gibbs’ classical approach in the description of the  
1892 parameters of critical clusters, mentioned generalizations  
1893 of the nucleation theorem do not supply us, in general, with  
1894 a description of the real critical clusters but merely with a  
1895 description of Gibbs’ model clusters resulting in the same  
1896 value of the work of critical cluster formation as for the  
1897 real critical clusters. Consequently, also the correctly  
1898 derived – in the framework of the classical Gibbs’ approach  
1899 – versions of the nucleation theorem do not describe, in  
1900 general, the parameters of the real critical clusters.

1901 Since the generalized Gibbs approach allows one a  
1902 determination of the parameters of the critical clusters, that  
1903 is, for model systems, in agreement with density functional  
1904 computations and computer simulation studies, it is of  
1905 interest to prove whether dependencies similar to the  
1906 ‘nucleation theorem’ can be formulated also in this gener-  
1907 alization of the classical Gibbs approach. The respective  
1908 work is in progress.

1909 Finally, we would like to note that there exist also  
1910 approaches connecting the deviations of the experimental  
1911 data on crystallization and growth with the effect of static  
1912 disorder in the melts [131] or the existence of so-called  
1913 floppy and rigid modes in glasses [132–134].

1914 5.5. Compositional changes of the crystal nuclei at  
1915 nucleation-growth process: some experimental findings

1916 The formation of solid solutions is a common phenom-  
1917 enon in silicate systems. By this reason, it is important to  
1918 keep in mind that the critical nuclei can be a proper solid  
1919 solution with thermodynamic properties, which may differ  
1920 considerably from those of the finally evolving macroscopic  
1921 phase. Thus, we can expect that contradictions between  
1922 experimental results and theoretical predictions concerning  
1923 nucleation rates and growth kinetics in such systems would  
1924 be considerably diminished even neglecting for some time  
1925 possible deviations in the critical nuclei structure as com-  
1926 pared with the evolving macro-phase.

1927 The following reasons could generally lead to a difference  
1928 in the bulk properties of the critical and near-critical crystal-  
1929 lites as compared with the respective newly evolving macro-  
1930 scopic phase and to a reduction of the thermodynamic  
1931 driving force: (a) It is reasonable to assume that near-critical  
1932 nuclei are less ordered than the material in the corresponding  
1933 bulk phase and it is possible to show that, in this case,  
1934  $\Delta G_V < \Delta G_\infty$  holds [69]. (b) According to the model of ideal  
1935 associated solutions [135,136], a glass-forming melt can be  
1936 considered as a solution of oxide components and salt-like  
1937 (stoichiometric) phases. Then, critical cluster formation  
1938 could be represented as a segregation process in a multi-com-  
1939 ponent solution. As shown in Ref. [97], in this case, the driv-  
1940 ing force may be smaller than for the macroscopic phase. (c)  
1941 The deviation of the critical nuclei composition from that of  
1942 the evolving macro-phase (e.g., owing to the formation of  
1943 metastable phases or solid solutions) has also to reduce the  
1944 thermodynamic driving force, as compared with that for  
1945 the stable macro-phase. This effect, i.e., the deviation of  
1946 the critical nuclei composition from those of the evolving  
1947 macro-phase and the parent stoichiometric glass was  
1948 recently observed [137] and is discussed in detail below.

1949 Within certain limits, addition, removal or replacement  
1950 of different components can continuously change the com-  
1951 position of a given crystallographic system. Hence, gener-  
1952 ally speaking, compositional variations of critical nuclei  
1953 of a new phase and, consequently, variations of their prop-  
1954 erties as compared with those of the corresponding macro-  
1955 phase could be expected. Indeed such deviations were  
1956 observed in both stoichiometric  $\text{Na}_2\text{O} \cdot 2\text{CaO} \cdot 3\text{SiO}_2$  glass  
1957 and glasses belonging to the solid solution (s/s) region  
1958 between  $\text{Na}_2\text{O} \cdot 2\text{CaO} \cdot 3\text{SiO}_2$  ( $\text{N}_1\text{C}_2\text{S}_3$ ) and  $\text{Na}_2\text{O} \cdot \text{CaO} \cdot 2\text{SiO}_2$  ( $\text{N}_1\text{C}_1\text{S}_2$ ) [137]. Ref. [137] shows that the formation  
1959 of stoichiometric crystals occurs via nucleation of s/s whose  
1960 composition continuously approaches the stoichiometric  
1961 one and arrives at that in the final stage of crystallization.  
1962 Figs. 17 and 18 show the evolution of crystal and glassy  
1963 matrix compositions and the corresponding change of the  
1964 lattice parameter, respectively. An extrapolation of the  
1965 change of crystal composition to zero time (or zero volume  
1966 fraction,  $\alpha = 0$ , of the crystallized phase) gives a strong  
1967 indication that the critical clusters are also enriched in  
1968 sodium.  
1969

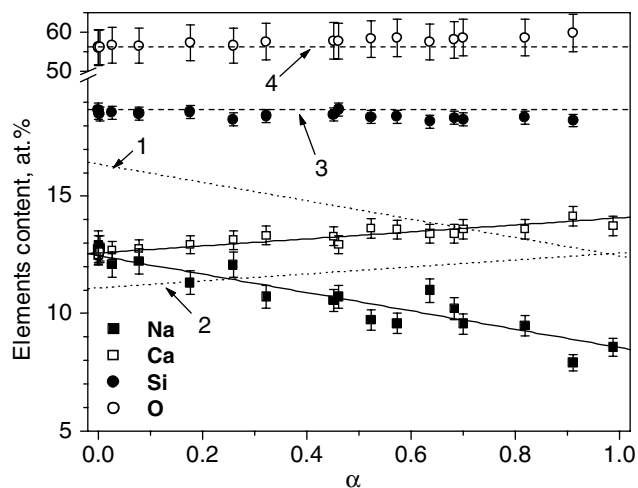


Fig. 17. Composition of the glassy matrix, measured by EDS (points), and of crystals calculated from the parent glass composition,  $\text{N}_1\text{C}_2\text{S}_3$  (dotted lines 1 and 2 – Na and Ca, respectively) versus volume fraction crystallized at  $T = 650^\circ\text{C}$ . Solid lines fit the experimental data. Dashed lines 3 (Si) and 4 (O) refer to the parent glass composition [137].

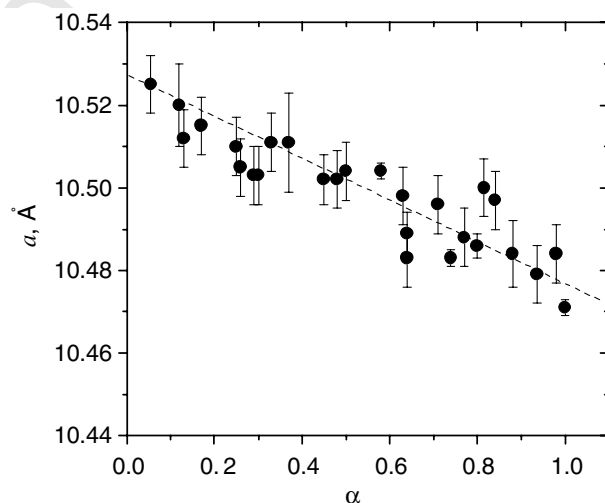


Fig. 18. Lattice parameter of the hexagonal crystal cell of the solid solutions against volume fraction of crystalline phase in stoichiometric  $\text{N}_1\text{C}_2\text{S}_3$  glass heat-treated at  $650^\circ\text{C}$  [137].

1970 The exhaustion of sodium in the glassy matrix during  
1971 crystallization leads to an inhibition of nucleation and crystal  
1972 growth. According to an analysis of the overall crystal-  
1973 lization kinetics using crystal growth data [137], the  
1974 nucleation process is terminated if about 20% of the volume  
1975 is crystallized. Fig. 19(a) and (b) shows the volume fraction  
1976 of crystals and the size of the largest crystals as a function of  
1977 heat treatment time at  $T = 650^\circ\text{C}$  for a glass of stoichiomet-  
1978 ric composition  $\text{N}_1\text{C}_2\text{S}_3$ . Nucleation takes place up to  
1979  $t \sim 150$  min ( $\ln(t) = 5$ ):  $n \approx 4$ ,  $m \approx 1$ ,  $k = n - 3m \approx 1$   
1980 ( $n = k + 3m$ ) (see Eq. (24)). This conclusion is confirmed  
1981 by a  $N(t)$ -plot obtained by the ‘development’ method (see  
1982 Fig. 19(c)). But, at  $\ln(t) > 5$  crystallization proceeds only  
1983 by crystal growth with  $m \approx 0.33$ ,  $n \approx 1$ ,  $k \approx 0$  ( $n = 3m$ ).

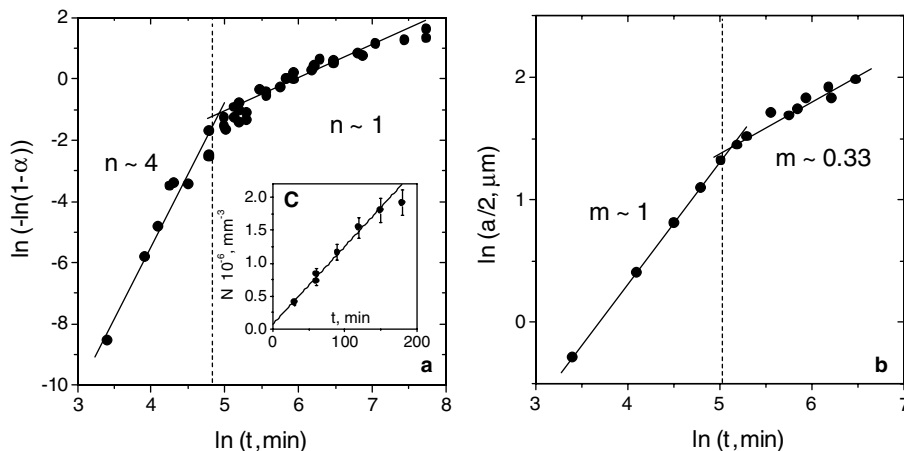


Fig. 19. Volume fraction of crystals (a), size of largest crystals (b), and number of crystals (c) as a function of heat treatment time at  $T = 650\text{ }^{\circ}\text{C}$  for stoichiometric glass  $\text{N}_1\text{C}_2\text{S}_3$  [137].

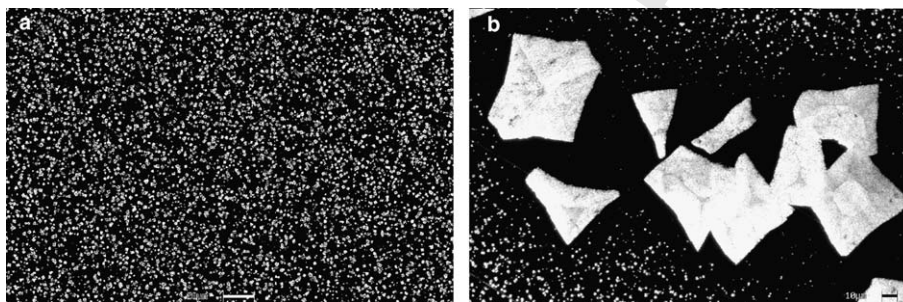


Fig. 20. SEM micrographs of  $\text{N}_1\text{C}_2\text{S}_3$  glass subjected to single (a) and double (b) stage heat treatments: (a)  $T = 590\text{ }^{\circ}\text{C}$ ,  $t = 1560\text{ min}$ ; (b)  $T_1 = 720\text{ }^{\circ}\text{C}$ ,  $t_1 = 20\text{ min}$  and  $T = 590\text{ }^{\circ}\text{C}$ ,  $t = 1560\text{ min}$ . The bars have a length of (a)  $20\text{ }\mu\text{m}$  and (b)  $10\text{ }\mu\text{m}$ .

1984 Na-depleted diffusion fields around the growing crystals  
 1985 can be visualized by a second heat treatment at a tempera-  
 1986 ture corresponding to reasonable values of nucleation  
 1987 and growth rates. A comparison of the samples subjected  
 1988 to single-stage (cf. Fig. 20(a)) and double-stage (cf.  
 1989 Fig. 20(b)) heat treatments reveals that pre-existing crystals  
 1990 (formed in first heat treatment) diminish the number of  
 1991 crystals nucleated in the subsequent treatment. Refs.  
 1992 [48,138] show that the nucleation rate decreases with  
 1993 decreasing sodium content in the glass. Hence, it is appar-  
 1994 ent that the areas observed around the large crystals refer  
 1995 to diffusion fields. A similar transformation path was  
 1996 observed for glasses of compositions between  $\text{N}_1\text{C}_2\text{S}_3$  and  
 1997  $\text{N}_1\text{C}_1\text{S}_2$ , with the only difference that fully crystallized  
 1998 glasses are s/s with compositions of the parent glasses.

1999 According to the results presented in Fig. 21, the differ-  
 2000 ence between the compositions of the critical nuclei and the  
 2001 parent glass diminishes as the latter approaches the bound-  
 2002 ary of s/s formation. The deviation of the nuclei composi-  
 2003 tion from stoichiometry (glass  $\text{N}_1\text{C}_2\text{S}_3$ ) or from the initial  
 2004 glass compositions (glasses of the s/s region) diminishes  
 2005 the thermodynamic driving force for crystallization,  $\Delta G_V$ ,  
 2006 and increases the thermodynamic barrier for nucleation.  
 2007 Moreover, this deviation also may lead to an increase of  
 2008 the kinetic barrier. Nevertheless, nucleation of crystals with

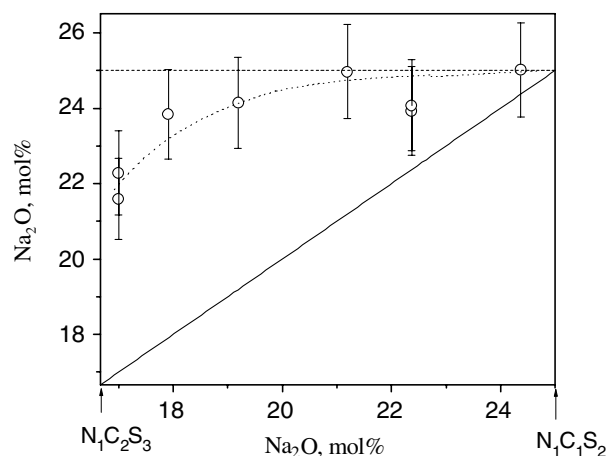


Fig. 21. Sodium oxide content in the critical nuclei versus composition of the parent glass. The solid line represents the case when the compositions of the critical nuclei and the parent glasses are the same.

2009 changed compositions (as compared with those of the par-  
 2010 ent glasses) actually takes place. Hence, the decrease in  
 2011  $\Delta G_V$  must be compensated by a decrease in surface energy  
 2012 in Eq. (4). However, the determination of the variation of  
 2013 the surface energy with composition is not a trivial problem  
 2014 and warrants further study.

2015 Deviations of the composition of the smallest crystals  
 2016 (50 nm) from that of the ambient glass have also been  
 2017 observed for surface crystallization of  $\mu$ -cordierite in a  
 2018 glass of cordierite composition. But the composition of  
 2019 the largest  $\mu$ -cordierite crystals ( $>1 \mu\text{m}$ ) was equal to that  
 2020 of the parent glass [139]. Variations of the crystal composi-  
 2021 tions during phase transformation were also found in  
 2022 CaO–Al<sub>2</sub>O<sub>3</sub>–SiO<sub>2</sub> glasses [140]. A direct experimental  
 2023 proof of changes of crystal composition with size in crystal-  
 2024 lization of Ni(P)-particles in hypoeutectic Ni–P amorphous  
 2025 alloys was recently reported in Refs. [106,107].

2026 All mentioned results give a further experimental confir-  
 2027 mation of the thesis of a considerable variation of the prop-  
 2028 erties of the clusters in the course of their evolution  
 2029 corroborating the predictions of the generalized Gibbs'  
 2030 approach.

### 2031 5.6. Independent estimate of the time-lag for nucleation 2032 from nucleation and growth kinetics

2033 It was correctly claimed in Ref. [141] that another prob-  
 2034 lem may occur in the treatment of nucleation-growth pro-  
 2035 cess in glasses. For a glass with a composition close to  
 2036 lithium disilicate, it was shown in Ref. [141] that the induc-  
 2037 tion time for crystal growth,  $t_{\text{gr}}$ , estimated (as illustrated by  
 2038 Fig. 22) from a  $R \sim t$  plot, where  $R$  is the size of the largest  
 2039 crystal experimentally observed, and  $t$  the time elapsed  
 2040 from the beginning of the nucleation-growth process,  
 2041 strongly exceeds the induction period for nucleation  
 2042 ( $t_{\text{ind}} = \frac{6}{\pi^2} \tau$ , see Eq. (11)). Latter value was estimated from  
 2043 an  $N \sim t$  plot obtained by the 'development' method. How-  
 2044 ever, if crystal nucleation and growth rates refer to the for-  
 2045 mation of the same phase,  $t_{\text{gr}}$  and  $t_{\text{ind}}$  are expected to be  
 2046 similar [21]. In other words, it is reasonable to assume that  
 2047 after an elapsed time  $t_{\text{gr}}$  the first supercritical nuclei have

2048 formed, which then deterministically grow up to sizes visi-  
 2049 ble under an optical microscope.

2050 The discrepancy in induction times reported in Ref.  
 2051 [141] has also been observed for lithium silicate glasses con-  
 2052 taining 32.6–38.4 mol% Li<sub>2</sub>O [142] belonging to the compo-  
 2053 sition range where solid solution crystals precipitate via  
 2054 homogeneous nucleation [143,144]. An example of  $N \sim t$   
 2055 and  $R \sim t$  plots for lithium silicate glass with 35.1 mol%  
 2056 Li<sub>2</sub>O at  $T = 460 \text{ }^\circ\text{C}$  is shown in Fig. 22, while Fig. 23 shows  
 2057 the time parameters  $t_{\text{ind}}$  and  $t_{\text{gr}}$  estimated at different tem-  
 2058 peratures for lithium silicate glasses with 33.5 and  
 2059 32.6 mol% Li<sub>2</sub>O. Since the  $N \sim t$  curve was obtained by  
 2060 the 'development' method (see Section 3.2),  $t_{\text{ind}}$  is overesti-  
 2061 mated as compared with the correct value corresponding to  
 2062 the nucleation temperature. (In Ref. [145] measurements of  
 2063 nucleation and growth rates and corresponding time-lags  
 2064 in lithium disilicate glass were undertaken using single-  
 2065 stage heat treatments at a relatively high temperature,  
 2066  $500 \text{ }^\circ\text{C} > T_{\text{max}} = 455 \text{ }^\circ\text{C}$ . The estimated (extrapolated)  
 2067 nucleation time-lag was considerably higher than that  
 2068 obtained by the 'development' method. We now think that  
 2069 this result was probably due to insufficient stereological  
 2070 corrections of the crystal number density of the samples  
 2071 subjected to single-stage treatments; see Section 3.4.) Thus,  
 2072 the  $t_{\text{gr}}/t_{\text{ind}}$  ratios experimentally obtained in the cited refer-  
 2073 ences are only a lower bound for the difference between the  
 2074 real induction periods. To correct the value of  $t_{\text{gr}}$  to partly  
 2075 resolve the above discussed problem, an attempt was  
 2076 undertaken in Ref. [141] to account for the effect of a size  
 2077 dependent growth rate. However, the discrepancy between  
 2078 induction times independently estimated from nucleation  
 2079 and growth experiments remained too high. By this reason,  
 2080 it was suggested that initially nucleation of metastable

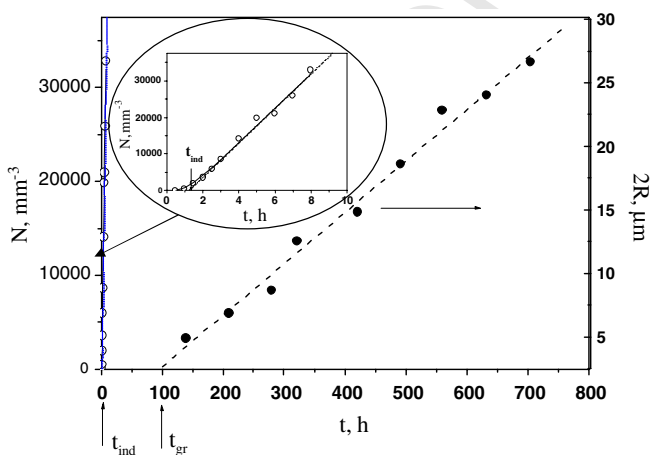


Fig. 22. Number density of crystals,  $N$ , and size of the largest crystals,  $2R$ , versus time of heat treatment at  $T = 460 \text{ }^\circ\text{C}$  for a lithium silicate glass with 35.1 mol% Li<sub>2</sub>O. The inset shows the  $N \sim t$  data on a larger scale. The solid line was plotted with Eq. (10) and the dashed line is a linear fit of the  $2R(t)$ -data [142].

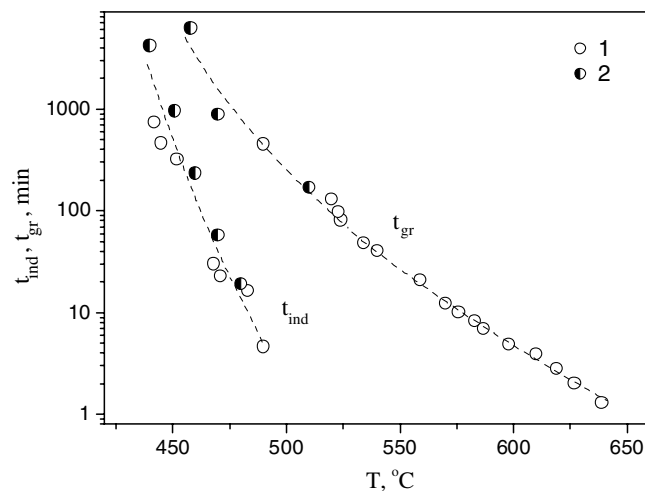


Fig. 23. Induction periods for crystal nucleation,  $t_{\text{ind}}$ , and for crystal growth,  $t_{\text{gr}}$ , versus temperature for lithium silicate glasses with 32.6 mol% (curve 2) Li<sub>2</sub>O [142] and 33.5 mol% (curve 1) Li<sub>2</sub>O [141].  $t_{\text{ind}}$  were taken from  $N$  versus  $t$  plots obtained by the 'development method' (they are thus overestimated, see text) while  $t_{\text{gr}}$  were estimated from single-stage experiments at each temperature.

phase crystals take place, which grow more slowly than the macroscopic crystals of the stable phase.

Weinberg [146] questioned the conclusions of Ref. [141] with the argument that the induction time for growth can not be uniquely determined because it depends on the cluster size for which the measurements are performed. He also stated that the induction time for growth becomes unbounded even for measurements performed at large cluster sizes. Strictly speaking those arguments are correct, but since the growth rate tends to time-independent values fairly rapidly with increasing  $R$  (see, e.g., Eq. (39) or Eq. (62) and Fig. 24), the induction time also tends to a practically finite value when the measurements are extended to large (optical microscopy scale) crystal sizes. Consequently, we believe that the comparison of induction times independently obtained by nucleation and growth experiments can be a useful tool, and, in principle, allows one to draw conclusions similar to those of Ref. [141].

Nevertheless, the results and analysis of induction times for growth deserve some comments. The analysis carried out in Ref. [141] was based on the solution of macroscopic growth equations starting with an initial cluster radius equal to the critical cluster size. With such initial condition, the induction time for growth tends to infinity independently of any particular growth mechanism, since  $U(r_*) = 0$ , and the numerical integration employed in Ref. [141] could not resolve this problem. In other words, the macroscopic growth equation is not valid for  $R = r_*$  and cannot be employed to describe the change of the nuclei size close to the critical one. Recall that according to the Zeldovich–Frenkel equation, in the vicinity of the critical cluster size the ‘motion’ of the clusters in cluster size space is mainly governed by diffusion-like processes in cluster size space under the action of the concentration gradient with respect to the cluster size distribution function, and thus it is not governed by the thermodynamic driving force, as it is the case in deterministic growth. In addition,

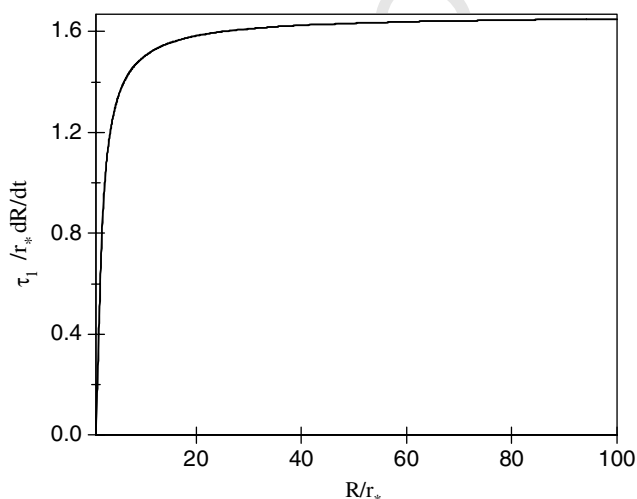


Fig. 24. Crystal growth rate ( $dR/dt$ ) in  $(r_*/\tau_1)$ -units versus reduced crystal size according to Eq. (62).

the discrepancy observed in Ref. [141] could also be explained in different ways, and not only via the assumption of formation of metastable phases.

To reconsider the above mentioned problem from a different perspective, we employed an analytical solution of the Fokker–Planck or Frenkel–Zeldovich equation describing nucleation-growth process (cf. Ref. [147]). According to this analysis, for nuclei with sizes larger than two critical sizes,  $R > 2r_*$ , the following relation holds:

$$\hat{\tau} = \frac{3}{5} \left[ \hat{R} + \ln(\hat{R} - 1) + \frac{2}{3} \right]. \quad (62)$$

In Eq. (62) the following dimensionless variables are used:

$$\hat{R} \equiv \frac{R}{r_*}, \quad \hat{\tau} \equiv \frac{t}{\tau_1}. \quad (63)$$

Here  $\tau_1$  is the period of time needed to establish a steady-state cluster size distribution in a range of cluster sizes slightly exceeding the critical size, i.e., it is practically equal to the time required to establish a steady-state nucleation rate for clusters of critical sizes. Recall that, according to Eq. (9) or (10), to practically establish a steady-state nucleation rate a time period about  $5\tau$  is required (see Fig. 6(b)). Hence the following relation between  $\tau_1$  and  $\tau$  exists

$$\tau_1 \cong 5\tau. \quad (64)$$

It should be emphasized that Eq. (62) was derived with the following (strong) assumptions commonly employed in CNT:

- (i) The bulk state of the clusters is independent on their sizes and is identical to that of the newly evolving macroscopic phase;
- (ii) The mechanism of cluster growth does not depend on cluster size, and growth is kinetically limited.

The term ‘kinetically limited’ refers to the ballistic growth mechanism, where the growth process is only limited by diffusion across the interface, and does not depend on bulk diffusion, as it is the case, for instance, for significant compositional differences between the liquid phase and growing crystal.

The experimental  $R(t)$  data were fitted to Eq. (62) using  $\tau_1$  and  $r_*$  as fit parameters [142]. Fig. 25 shows the result of such calculations. In this way, in order to arrive at the  $R(t)$ -dependence we did not use any macroscopic growth equation, but relied instead on an analytical solution of the Frenkel–Zeldovich equation, which gives a correct description of the evolution of the cluster ensemble. In addition, in our approach, we do not determine an induction time for growth, but instead determine the time-lag for nucleation by fitting experimental growth data to the nonlinear Eq. (62). Hence, even if Weinberg’s comments [146] about the impossibility of defining  $t_{gr}$  from  $R(t)$  curves are strictly correct, they do not affect our analysis.

The value of  $\tau_1$  exceeds the corresponding nucleation induction time,  $5\tau$ , estimated from the  $N \sim t$  curve, by

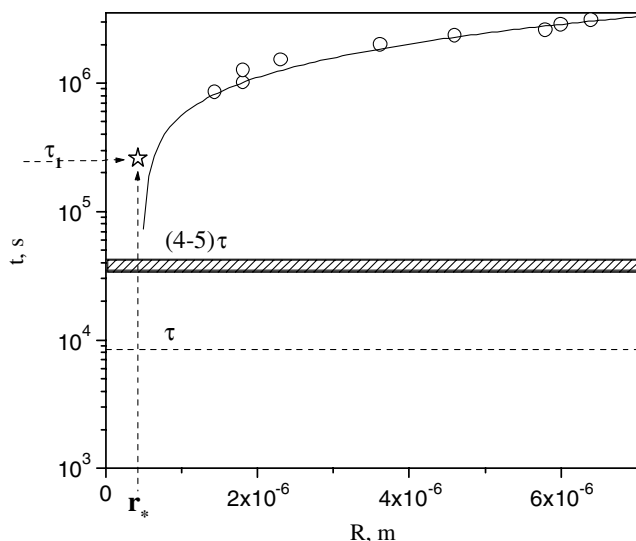


Fig. 25. Time necessary for a crystal to achieve a size  $R$  in a lithium silicate glass with 32.6 mol%  $\text{Li}_2\text{O}$  at 460 °C. The full curve was plotted by Eq. (62) using  $\tau_1$  and  $r_*$  as fit parameters. The coordinates of the open star show the fit parameters  $\tau_1$  and  $r_*$ . The circles refer to the experimental data. The dashed horizontal line shows the value of the time-lag for nucleation  $\tau$  estimated by a fit of the  $N \sim t$  data to Eq. (10). The crosshatched band corresponds to the time when the nucleation rate achieves 95–99% of its steady-state value [142].

2174 about one order of magnitude (see Fig. 25). However, pro-  
 2175 vided the conditions (i) and (ii) are fulfilled, one expects  
 2176 that  $\tau_1$  must be equal to about  $5\tau$ , see Eq. (64), since both  
 2177  $\tau_1$  and  $\tau$  refer to nucleation kinetics. This discrepancy leads  
 2178 to the following conclusion: *at least one or both of the*  
 2179 *assumptions underlying the derivation of Eq. (62) are not*  
 2180 *valid.*

2181 In order to explain the present results, one should recall  
 2182 the assumptions made in the derivation of the above equa-  
 2183 tions. In particular, one can assume that the compositions  
 2184 of near-critical clusters deviate from those of the macro-  
 2185 scopic crystals to which the crystal size measurements refer.  
 2186 Since in the advanced stages of crystallization the compo-  
 2187 sition of the macro-crystals coincides with those of the  
 2188 ambient melt, this assumption leads to the conclusion that  
 2189 growth of near-critical nuclei is limited by diffusion and is  
 2190 thus not kinetically determined. Moreover, as shown in the  
 2191 analysis of a model system [102], the size dependence of the  
 2192 cluster composition results in a cluster size dependence of a  
 2193 variety of thermodynamic and kinetic parameters (driving  
 2194 force, surface tension, effective diffusion coefficients, and  
 2195 growth rates). These deviations are not taken into account  
 2196 in the derivation of Eq. (62).

2197 Consequently, the mentioned deviations can be inter-  
 2198 preted as an additional indication that the classical  
 2199 approach to the description of nucleation-growth processes  
 2200 is insufficient for an interpretation of experimental results  
 2201 on crystallization in lithium disilicate glasses. One of the  
 2202 possible solutions is the assumption of a size (and eventu-  
 2203 ally structure) dependent composition of the crystallites.  
 2204 For completeness we should also to mention an alternative

2205 approach [148,149] connecting the possible deviations with  
 2206 possible (cluster-size dependent) solute depletion and vol-  
 2207 ume diffusion in nucleation. Taking into account the results  
 2208 of the generalized Gibbs' approach, density functional  
 2209 studies and computer simulation methods of the properties  
 2210 of critical clusters, the first interpretation of the deviations  
 2211 between the time-lag established in two independent ways  
 2212 (being the result of the change of both cluster properties  
 2213 and growth kinetics in dependence on their sizes) seems  
 2214 to us to be a more convincing explanation.

2215 The questions under which conditions and in what way  
 2216 nuclei change their properties and the growth mechanism  
 2217 are not trivial to answer, especially if these changes occur  
 2218 in the early stages of crystallization. However, the transfor-  
 2219 mation must finally lead to the formation of a stable mac-  
 2220 rophase with well-defined properties. One of the possible  
 2221 and often assumed ways to account for such effects – the  
 2222 formation of metastable phases – will be discussed in Sec-  
 2223 tion 5.7 However, metastable phase formation is not the  
 2224 only possible but a very particular explanation for such  
 2225 kind of behavior (see, e.g., Section 5.5). The analysis of  
 2226 already mentioned model system (segregation in regular  
 2227 solutions [102]) shows that clusters may continuously  
 2228 change their properties with their sizes and do not have  
 2229 the properties of some fictive metastable phase. Such expla-  
 2230 nation for the observed discrepancy is more general and  
 2231 could be ascribed to the formation of different transient  
 2232 phases more or less continuously changing their properties  
 2233 in dependence on cluster size.

### 2234 5.7. On the possible role of metastable phases in 2235 nucleation

2236 As mentioned in Sections 5.3 and 5.5 the precipitation of  
 2237 metastable phases in the early stages of nucleation may be  
 2238 one of the reasons for the deviation of the critical nuclei  
 2239 properties (e.g., composition) from that of the evolving  
 2240 (stable) macro-phase. The formation of metastable phases  
 2241 is consistent with the original formulation of Ostwald's  
 2242 *Rule of Stages* according to that, 'if the supersaturated  
 2243 state has been spontaneously removed then, instead of a  
 2244 solid phase, which under the given conditions is thermody-  
 2245 namically stable, a less stable phase will be formed' [150].  
 2246 Note that Ostwald restricted his formulation to the possi-  
 2247 ble result of the transformation not specifying the bulk  
 2248 state of the critical clusters as done in the generalization  
 2249 of this rule as given above (see Section 5.4). Implicitly it  
 2250 is assumed in his formulation – and also in its theoretical  
 2251 foundation as developed first by Stranski and Totomanov  
 2252 [151] – that the critical clusters have properties equivalent  
 2253 to the properties of one of the finite number of phases  
 2254 which can exist in a macroscopic form, at least, in a meta-  
 2255 stable state at the given conditions.

2256 Ostwald's rule is corroborated by the following thermo-  
 2257 dynamic considerations. Employing the Skapski–Turnbull  
 2258 equation, Eq. (31), to estimate the crystal/liquid interfacial  
 2259 energy, one can show that the thermodynamic barrier for

2260 nucleation is proportional to the melting enthalpy. Hence,  
 2261 higher nucleation rates of metastable phases than those of  
 2262 the stable phase could be expected due to its lower melting  
 2263 enthalpy and correspondingly lower thermodynamic barrier.  
 2264 But a higher nucleation rate of a metastable phase  
 2265 must be accompanied by a lower growth rate, since the latter  
 2266 is proportional to the thermodynamic driving force.  
 2267 This is especially true if the composition of the metastable  
 2268 phase is similar to that of the parent glass.

2269 Once crystallites of a metastable phase form, they may  
 2270 favor nucleation of crystallites of the stable phase if its formation  
 2271 is followed by transformation into aggregates of the  
 2272 more stable phase as discussed in Ref. [152]. Thus, metastable  
 2273 crystals can, in principle, catalyze in one or the other  
 2274 way nucleation processes of the stable phase. Some authors  
 2275 suggested that such crystallization path occurs in  $\text{Li}_2\text{O}\cdot 2\text{-}$   
 2276  $\text{SiO}_2$  ( $\text{LS}_2$ ) glass, which has been used for many years as  
 2277 a model system to study homogeneous nucleation (see,  
 2278 e.g., [153,154]). An article by Deubener et al. [141] (discussed  
 2279 in Section 5.6) reawakened the interest in this problem  
 2280 and stimulated an intensive search for metastable  
 2281 phase formation in  $\text{LS}_2$ -glass [155–157], mainly by transmission  
 2282 electron microscopy (TEM) and X-ray diffraction (XRD)  
 2283 methods. In addition to stable lithium disilicate and  
 2284 metastable metasilicate crystals, other, so far unknown,  
 2285 phases were found. However, the observations of different  
 2286 authors were often in contradiction to each other. But,  
 2287 in general, the probability of observing such new phases  
 2288 in  $\text{LS}_2$  glass increases with a decrease in time and temperature  
 2289 of heat treatment [158]. Due to low nucleation rates and  
 2290 correspondingly low crystal number densities, and extremely  
 2291 small areas observed by TEM, the statistics of such measurements  
 2292 are quite poor. Moreover, the electron beam can degrade the  
 2293 crystals under study in a short time. As an example, however,  
 2294 the results of Ref. [159] show that at  $T = 454^\circ\text{C}$  (close to the  
 2295 nucleation rate maximum), only  $\text{Li}_2\text{O}\cdot 2\text{SiO}_2$  ( $\text{LS}_2$ ) and  
 2296  $\text{Li}_2\text{O}\cdot \text{SiO}_2$  ( $\text{LS}$ ) crystals were detected in the early stages  
 2297 of crystallization (less than 1% crystallized fraction), but  
 2298  $\text{LS}$  crystals were not detected in the most advanced stages  
 2299 (5–10% crystallized fraction). It should be emphasized that,  
 2300 according to the data collected in a time interval 0–100 h at  
 2301  $454^\circ\text{C}$ , the  $\text{LS}$  crystals sizes practically do not change, while  
 2302 the  $\text{LS}_2$  crystals significantly grow (see Fig. 26). This result  
 2303 agrees with calculations according to which the thermodynamic  
 2304 driving force for  $\text{LS}$  crystallization in lithium disilicate  
 2305 glass is lower than for  $\text{LS}_2$  crystals [160], because a higher  
 2306 thermodynamic driving force also results in higher growth  
 2307 rates. Since there was no evidence of heterogeneous nucleation  
 2308 of lithium disilicate on lithium metasilicate crystals, it was  
 2309 concluded that  $\text{LS}$  nucleates concurrently with the stable  
 2310 phase  $\text{LS}_2$  and disappears with time. Recall that lithium  
 2311 disilicate has a wide range of solid solutions (s/s) formation  
 2312 [143,144]; hence, one can suppose that the critical nuclei  
 2313 are also s/s. Here it should be noted that the technique  
 2314 employed in Ref. [159] did not allow them to distinguish  
 2315 stoichiometric compounds from solid solutions.  
 2316

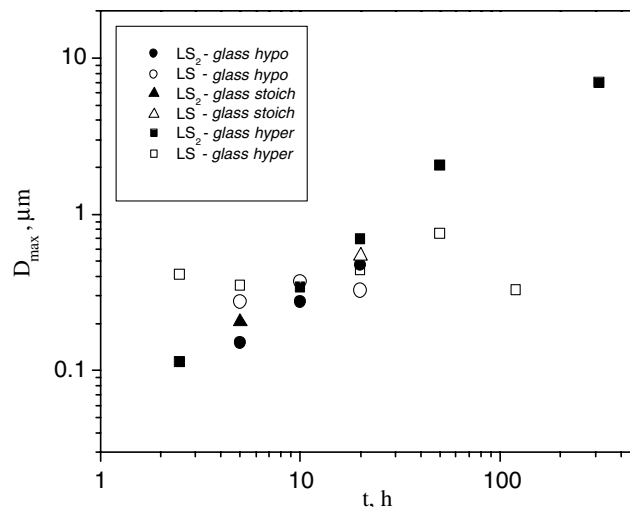


Fig. 26. Maximum dimension ( $D_{\max}$ ) of the largest crystals observed by TEM in samples of *hypo*, *stoich*, and *hyper* lithium disilicate glasses versus heat treatment time at  $454^\circ\text{C}$  [159]. Solid and opened points refer to  $\text{LS}_2$  and  $\text{LS}$  crystals, respectively.

The assumption of s/s nucleation does not contradict the results presented above, but allows one to consider changes of composition of the evolving nuclei with size, such as those demonstrated in Section 5.5 for soda-lime-silica glasses and assumed in Section 5.6. Thus, in some cases, it is possible that the role of metastable phases in nucleation could be simply a continuous variation of nuclei composition (and properties) during the phase transformation. However, there is another factor that has not been taken into consideration so far, but may be of considerable influence. That is the possible effect of elastic stress on nucleation in glass-forming melts. This effect will be analyzed in the next section.

### 5.8. Effect of elastic stresses on the thermodynamic barrier for nucleation

As it follows from Section 5.1, the thermodynamic barrier for nucleation,  $W_*$ , can be calculated in the framework of CNT by a fit of experimental data employing Eq. (34). For such computations, no additional assumptions are needed apart from the validity of CNT. In addition, one has to make some choice concerning the value of the surface energy in the pre-exponential term. However, this choice only weakly affects the final results.

According to Eq. (4), the work of critical cluster formation,  $W_*$ , monotonically decreases with decreasing temperature. Nevertheless, the value of  $W_*(T/T_n)$ , calculated from nucleation data for lithium disilicate glass at temperatures close to  $T_g$  shows an anomalous increase with decreasing temperature (cf. Fig. 27). A similar behavior of  $W_*$  was observed in other systems, e.g., for wollastonite glass [162]. The above mentioned deviations of the  $W_*(T)$ -dependence from the expected (according to CNT) may be caused by elastic stresses. Since, in most cases of interest, the crystal densities differ from those of the corresponding

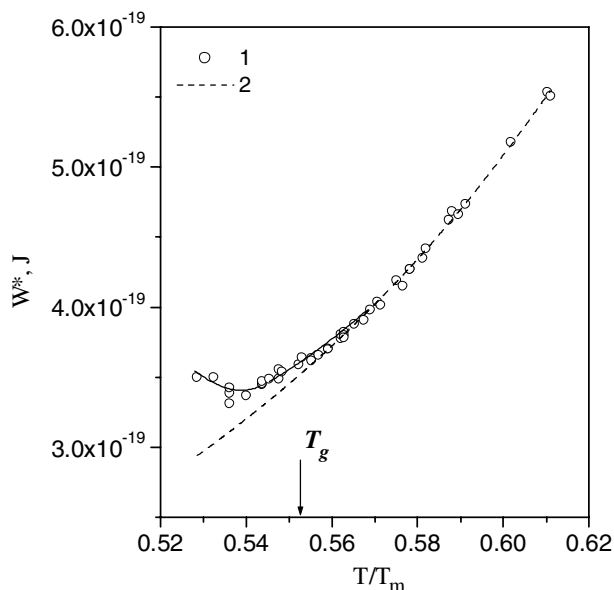


Fig. 27. Thermodynamic barrier for nucleation in  $\text{Li}_2\text{O}\cdot 2\text{SiO}_2$ -glass (curve 1) estimated from a fit of experimental  $I_{st}(T)$  and  $t_{ind}(T)$  to Eq. (32), and (curve 2) calculated with Eq. (4) [161].

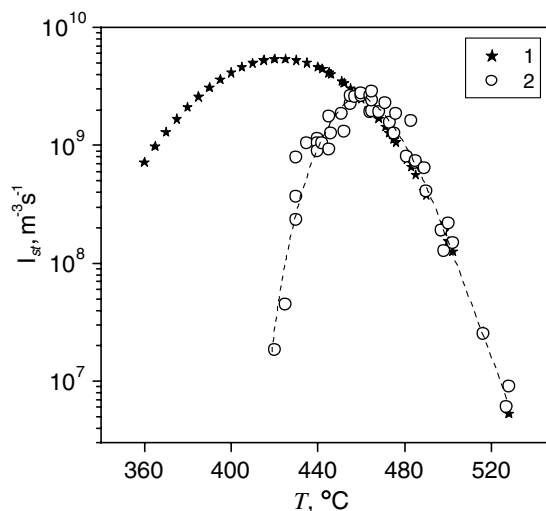


Fig. 28. Temperature dependence of the steady-state nucleation rates in lithium disilicate glass [161]. (Curve 1)  $I_{st}$  calculated with Eq. (34) for the case when elastic stresses do not play any role; (Curve 2) experimental values of  $I_{st}$ . The dashed line is just to guide the eyes.

2351 glasses, glass crystallization is accompanied by volume  
 2352 changes. Such changes may result in stress development  
 2353 which, in turn, diminishes the thermodynamic driving force  
 2354 for the phase transformation by a term connected with the  
 2355 elastic strain energy. This energy can partly or even fully  
 2356 [12,14,163,164] suppress the nucleation-growth process.  
 2357 This effect may be the origin not only of the anomalous  
 2358 behavior of the work of critical cluster formation,  $W_*(T)$ ,  
 2359 but also of a number of well-known additional experimen-  
 2360 tal facts, e.g., the preference of surface to volume nucle-  
 2361 ation [12,163,164], or the existence of a correlation  
 2362 according to which glasses having densities much lower  
 2363 than those of the corresponding crystals usually reveal only  
 2364 surface crystallization [165].

2365 A theory of nucleation in viscoelastic bodies has been  
 2366 developed recently [166,167] which takes into account both  
 2367 stress development and relaxation in phase formation in  
 2368 glass-forming melts (an analysis of the effect of elastic stres-  
 2369 ses on crystal growth – based on the same theoretical pre-  
 2370 mises – is given in Ref. [168]). It was concluded that the  
 2371 effect of elastic stresses on nucleation can be remarkable  
 2372 if the time of stress development (estimated as time-lag  
 2373 for nucleation) is smaller than the characteristic time of  
 2374 stress relaxation, which is governed by viscous flow. Such  
 2375 a situation is possible at temperatures lower than the so-  
 2376 called decoupling temperature  $T_d \sim 1.2T_g$ , when the  
 2377 Stokes–Einstein equation may no longer be valid, i.e.,  
 2378 when the nucleation kinetics is not governed by viscous  
 2379 flow. A detailed analysis, performed for lithium disilicate  
 2380 glass, shows that elastic stresses may decrease the steady-  
 2381 state nucleation rate by up to two orders of magnitude  
 2382 [169]. In this analysis, the work of critical cluster formation  
 2383 in the absence of elastic stresses was determined following  
 2384 classical nucleation theory.

2385 Recently an attempt was made to estimate the elastic  
 2386 stress energy directly using the deviation of  $W_*(T)$ -curves  
 2387 from the theoretical one [161] for the same lithium disilicate  
 2388 glass. The obtained values of elastic strain energy were  
 2389 comparable in magnitude with those calculated using the  
 2390 elastic constants of glass and crystals. It should be noted  
 2391 that in the extrapolation of the  $W_*(T)$ -dependence from  
 2392 relatively high temperatures, at which elastic stress effects  
 2393 can be neglected, to low temperatures, where the minimum  
 2394 of experimental  $W_*$ -values is observed, both thermody-  
 2395 namic driving force and crystal/melt surface energy were  
 2396 considered as fit parameters. The fitting procedure pro-  
 2397 duced, in accordance with the conclusions of Section 5.2,  
 2398 values of effective surface energy that decrease with  
 2399 decreasing temperature. Moreover, the thermodynamic  
 2400 driving force turned out to be considerably less than that  
 2401 for the respective macroscopic phase.

2402 Fig. 28 shows experimental steady-state nucleation rates  
 2403 versus temperature together with the theoretical curve cal-  
 2404 culated by neglecting elastic stresses, employing values for  
 2405 the driving force and surface tension obtained via above  
 2406 discussed fitting procedure. At low temperatures, the calcu-  
 2407 lated  $I_{st}$ -values considerably exceed the experimental data  
 2408 giving an indirect evidence of the essential role of elastic  
 2409 stresses in nucleation.

## 6. Concluding remarks

2410  
 2411 We presented an overview of experimental results on  
 2412 crystal nucleation in silicate glasses and their theoretical  
 2413 interpretation in the framework of CNT. Different modifi-  
 2414 cations and alternative theoretical approaches of CNT do  
 2415 exist and the importance of the correct determination of  
 2416 the properties of critical clusters and, in particular, of  
 2417 the work for their formation has been known since the

2418 formulation of the basic concepts of CNT. However, fol- 2475  
2419 lowing Gibbs' ideas in the description of thermodynami- 2476  
2420 cally heterogeneous systems, in the search for the 2477  
2421 solution of this problem the properties of the critical clus- 2478  
2422 ters have been commonly identified with the properties of 2479  
2423 the newly evolving macroscopic phases. Exclusively under 2480  
2424 such assumption, the supersaturation (or driving force) 2481  
2425 can be considered – at constant pressure – as a function 2482  
2426 only of temperature. As a consequence, in most attempts 2483  
2427 to reconcile theoretical and experimental results attention 2484  
2428 was predominantly directed to the determination of the 2485  
2429 size-dependence of the specific interfacial energy. In con- 2486  
2430 trast, it follows from the present review that the main prob- 2487  
2431 lem regarding the application of CNT for a quantitative 2488  
2432 description of nucleation kinetics in glass-forming liquids 2489  
2433 consists primarily in the adequate description of the bulk 2490  
2434 properties of the critical nuclei. Of course, a deviation of 2491  
2435 the bulk properties of the critical clusters as compared with 2492  
2436 the newly evolving macroscopic phases also leads to mod- 2493  
2437 ifications of the specific interfacial energy. However, the 2494  
2438 resulting variation of the specific interfacial energy – due 2495  
2439 to changes in the bulk properties of the critical clusters as 2496  
2440 compared with the newly evolving macroscopic phase – is 2497  
2441 only a secondary factor that must be, of course, also ade- 2498  
2442 quately incorporated into the theory. Therefore, the circle 2499  
2443 of problems one has to solve for the theoretical description 2500  
2444 of nucleation is enlarged. On the other hand, a new meth- 2501  
2445 odology – the generalized Gibbs approach – that allows 2502  
2446 one to overcome the mentioned problems, which cannot 2503  
2447 be resolved following the classical concepts of Gibbs, has 2504  
2448 been recently developed. 2505

2449 Direct experimental methods usually employed to study 2506  
2450 micron-sized or larger crystals cannot be used for nuclei of 2507  
2451 critical sizes, which are only of a few nanometers in the 2508  
2452 temperature range of interest. This is one of the reasons 2509  
2453 why one typically follows Gibbs' description of heteroge- 2510  
2454 neous systems and assigns the thermodynamic properties 2511  
2455 (particularly the thermodynamic driving force for crystalli- 2512  
2456 zation) of the macro-phases to the critical nuclei, thus 2513  
2457 assuming that the critical nuclei and the evolving stable 2514  
2458 macro-phase can be characterized by similar bulk state 2515  
2459 parameters. However, since the thermodynamic barrier 2516  
2460 for nucleation includes both the thermodynamic driving 2517  
2461 force and the nucleus-melt surface energy, a maximum 2518  
2462 thermodynamic driving force (corresponding to the stable 2519  
2463 phase) is not a necessary condition to attain the lowest 2520  
2464 value of the thermodynamic barrier and, correspondingly, 2521  
2465 the highest value of the nucleation rate. Moreover, the 2522  
2466 thermodynamic properties of the critical nuclei can be 2523  
2467 affected by elastic stresses arising from differences between 2524  
2468 the densities of the nucleus and the melt. Hence, one can 2525  
2469 suppose that, in some cases, the deviation of the composi- 2526  
2470 tion of the nuclei from those of the stable phase may be 2527  
2471 accompanied by an approach of the nuclei density to that 2528  
2472 of the melt. In such cases, the effect of elastic stresses is 2529  
2473 reduced and, correspondingly, a decrease in the thermody- 2530  
2474 namic barrier for formation of such nuclei (as compared

with the respective value for the stable phase) could be 2475  
expected. Thus, elastic stress effects can considerably com- 2476  
plicate the thermodynamics of nucleation and extend the 2477  
variety of possible structures and compositions of the crit- 2478  
ical nuclei. 2479

Since, with rare exceptions, direct measurements of the 2480  
characteristic properties of critical nuclei are inaccessible, 2481  
it is rather difficult or impossible to attribute the measured 2482  
nucleation rates to defined crystal phases. It seems that 2483  
such situation will not change in the near future. Moreover, 2484  
taking into account density functional studies, computer 2485  
simulations and theoretical analyses connected with the 2486  
generalization of Ostwald's rule of stages, it is even ques- 2487  
tionable whether the critical clusters have structures and 2488  
compositions resembling those of the possible macroscopic 2489  
phases that may evolve in the system under consideration. 2490  
As shown here, there is some remarkable evidence – partly 2491  
presented in this review – for the existence of considerable 2492  
differences between the properties of near-critical nuclei 2493  
and those of the respective stable macroscopic phases. 2494

Glasses of stoichiometric compositions have been used 2495  
as model systems in a variety of studies of crystal nucle- 2496  
ation. Such choice was made hoping that it should be possi- 2497  
ble to treat such systems as one-component systems. 2498  
However, it now became clear that a stoichiometric glass 2499  
composition, equal to the composition of the evolving crys- 2500  
talline phase, does not guarantee that the nuclei have the 2501  
same composition. Therefore, systematic investigations of 2502  
nucleation rates versus glass compositions are of great 2503  
interest allowing us to understand the true nature of nucle- 2504  
ation in glasses. The great value of such analysis is rein- 2505  
forced if the crystal growth rates are also measured in the 2506  
same temperature range. In this way, additional informa- 2507  
tion can be accumulated allowing one to reveal both the 2508  
crystal nucleation and growth mechanisms operating in 2509  
the systems under study. 2510

On the other hand, further development of the classical 2511  
theories of nucleation and growth – aimed to describe not 2512  
only critical nuclei formation, but also its subsequent 2513  
growth, including the possible evolution of their composi- 2514  
tion – may allow us to develop a more adequate description 2515  
of phase transformation kinetics. Here we drew attention 2516  
to a new approach to the description both of nucleation 2517  
and growth – *the generalized Gibbs' approach* – which has 2518  
been developed in recent years and already demonstrated 2519  
its power in the analysis of phase formation in different sys- 2520  
tems. Existing different alternative theories and modifica- 2521  
tions of CNT and their further developments will show 2522  
which of them will be most successful in treating nucle- 2523  
ation-growth phenomena in crystallization. However, in 2524  
order to be successful in the description of experimental 2525  
data on nucleation and growth, any of the proposed theo- 2526  
ries – and this is one of the main conclusions of the present 2527  
review – must be able to appropriately describe the depen- 2528  
dence of the properties of the critical clusters on the state of 2529  
the ambient glass-forming melt and the change of the state 2530  
of the crystallites with their sizes both in dissolution and 2531

2532 growth processes. We believe the analysis of the size-dependence of the cluster properties and their theoretical interpretation may lead to new exciting developments in the field of crystal nucleation of glasses, with a variety of new applications. Thus, despite the fact that numerous analyses of crystallization kinetics and mechanisms of silicate and other glasses have been performed for decades, they are expected to remain a highly interesting subject for both fundamental and applied research on nucleation and phase transformations in general.

## 2542 Acknowledgements

2543 The authors would like to express their deep gratitude to Professor Ivan Gutzow (Sofia, Bulgaria) for helpful discussions and critical comments. Financial support by Fapesp, Capes and CNPq (Brazil) is fully appreciated.

## 2547 Appendix A

2548 The experimental values of the thermodynamic driving force for crystallization given by Eq. (5) is bounded by a linear approximation (Eq. (6)), commonly denoted as Turnbull's formula, and by the approximation of Hoffman (Eq. (7)), see Fig. A1(b), (d), and (f). Eq. (6) directly fol-

lows from Eq. (5) in the case of  $\Delta C_p = 0$ . The Hoffman equation assumes  $\Delta C_p = \text{constant}$  and some additional simplifications. There are other approximations that predict values of  $\Delta G_V$  located inside the range given by Eqs. (6) and (7). Some of them, taken from Ref. [13], are

$$\Delta G_V = \frac{\Delta H_V \Delta T}{T_m} \left[ \frac{7T}{T_m + 6T} \right], \quad (\text{A.1})$$

$$\Delta G_V = \frac{\Delta H_V \Delta T}{T_m} - \gamma \Delta S_m \left[ \Delta T - T \ln \left( \frac{T_m}{T} \right) \right], \quad (\text{A.2})$$

$$\Delta G_V = \frac{\Delta H_V \Delta T}{T_m} \frac{2T}{T_m + T}. \quad (\text{A.3})$$

2561 Fig. A1(b), (d), (f), and (h) shows the values of  $\Delta G_V$  versus temperature calculated with Eqs. (6), (A.1), (A.2), (A.3), and (7). The value of  $\gamma$  in Eq. (A.2) was chosen equal to 0.8. Experimental data on  $\Delta G_V$  are also shown for  $\text{Li}_2\text{O} \cdot 2\text{SiO}_2$ ,  $\text{Na}_2\text{O} \cdot 2\text{CaO} \cdot 3\text{SiO}_2$  and  $2\text{Na}_2\text{O} \cdot 1\text{CaO} \cdot 3\text{SiO}_2$  glasses. Different approximations for the thermodynamic driving force were used to plot the nucleation rates as shown in Fig. 23(a), (c), (e), and (g). The intercepts and slopes of the linear fits at  $T > T_g$  were employed to estimate  $I_o^{\text{exp}}$  and  $\sigma_{\text{cm}}^*$ . These parameters are listed in Table A1.

2571 According to Table A1 the discrepancy between experimental and theoretical values of  $I_o$  is always drastic and becomes even stronger when the  $\Delta G_V(T)$ -function becomes

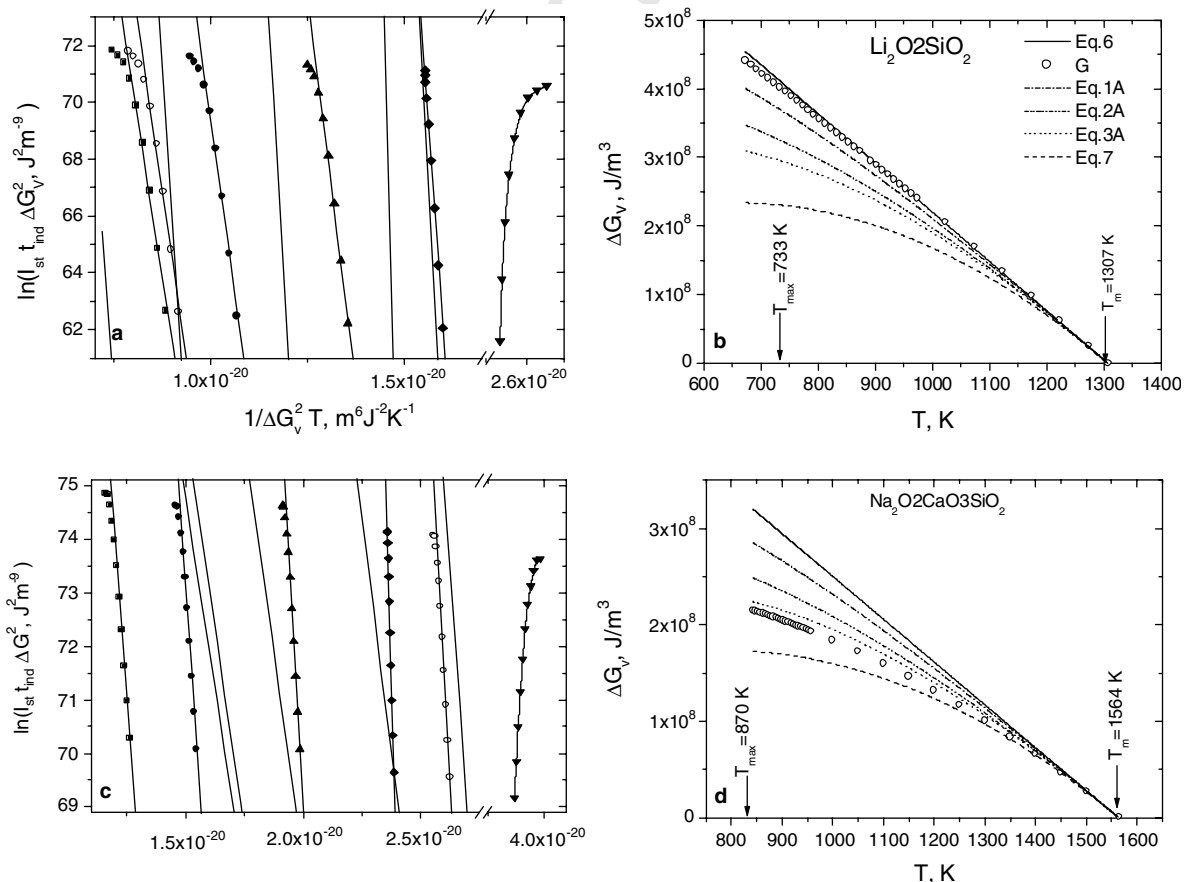


Fig. A1. Analysis of nucleation data with different expressions for the thermodynamic driving force. (b,d,f,h): thermodynamic driving force versus temperature; (a,c,e):  $\ln(I_{\text{st}} t_{\text{ind}} \Delta G_V^2)$ ; (g):  $\ln(I_{\text{st}} \eta)$  versus  $1/\Delta G_V^2 T$ .

Table A1

Ratio of experimental and theoretical pre-exponential terms, and surface energy for different glasses [40] calculated by fitting nucleation data to CNT employing experimental and approximate values of the thermodynamic driving force

	Li <sub>2</sub> O·2SiO <sub>2</sub>		Na <sub>2</sub> O·2CaO·3SiO <sub>2</sub>		2Na <sub>2</sub> O·CaO·3SiO <sub>2</sub>		BaO·2SiO <sub>2</sub> <sup>a</sup>	
	$\sigma_{cm}^*$	$\log\left(\frac{I_0^{exp}}{I_0^{theo}}\right)$	$\sigma_{cm}^*$	$\log\left(\frac{I_0^{exp}}{I_0^{theo}}\right)$	$\sigma_{cm}^*$	$\log\left(\frac{I_0^{exp}}{I_0^{theo}}\right)$	$\sigma_{cm}^*$	$\log\left(\frac{I_0^{exp}}{I_0^{theo}}\right)$
Eq. (6)	0.19	15	0.17	18	0.15	27	0.13	8
Eq. (A.1)	0.20	27	0.18	30	0.16	46	0.13	14
Eq. (A.2)	0.20	45	0.19	51	0.17	79	0.13	23
Eq. (A.3)	0.25	113	0.22	156			0.14	43
Experiment	0.20	19	0.19	72	0.17	139		

The specific interfacial energy is given in J m<sup>-2</sup>.

<sup>a</sup> Viscosity was used to calculate  $I_0^{exp}$  and  $\sigma_{cm}^*$ .

2574 weaker, while  $\sigma_{cm}^*$  depends only weakly on the choice of a  
2575 particular expression for the thermodynamic driving force.

## 2576 References

- 2577 [1] J.W.P. Schmelzer, in: J.W.P. Schmelzer, G. Röpke, V.B. Priezhev  
2578 (Eds.), Nucleation Theory and Applications, Joint Institute for  
2579 Nuclear Research Publishing Department, Dubna, Russia, 1999, p.  
2580 1.
- 2581 [2] J.M.F. Navaro, El Vidrio, CSIC, Madrid, Spain, 1991.
- 2582 [3] W. Höland, G. Beall, Glass-ceramic technology, American Ceramic  
2583 Society, 2002.
- 2584 [4] J.W. Gibbs, The Collected Works, Thermodynamics, vol. 1,  
2585 Longmans & Green, New York, 1928.
- 2586 [5] R. Kaischew, I.N. Stranski, Z. Phys. Chem. B 26 (1934) 317.
- 2587 [6] M. Volmer, A. Weber, Z. Phys. Chem. 119 (1926) 277.
- 2588 [7] R. Becker, W. Döring, Ann. Phys. 24 (1935) 719;  
2589 R. Becker, W. Döring, Ann. Phys. 32 (1938) 128.
- 2590 [8] M. Volmer, Kinetik der Phasenbildung, Steinkopf, Dresden, 1939.
- 2591 [9] J. Frenkel, Kinetic Theory of Liquids, Oxford University Press,  
2592 Oxford, 1946.
- 2593 [10] D. Turnbull, J.C. Fisher, J. Chem. Phys. 17 (1949) 71.
- 2594 [11] H. Reiss, J. Chem. Phys. 18 (1950) 840.
- 2595 [12] I. Gutzow, J. Schmelzer, The Vitreous State: Thermodynamics,  
2596 Structure, Rheology and Crystallization, Springer, Berlin, 1995.
- 2597 [13] K.F. Kelton, Solid State Phys. 45 (1991) 75.
- 2598 [14] J.W. Christian, The Theory of Transformations in Metals and  
2599 Alloys. Part I, Pergamon Press, Oxford, 1981.
- 2600 [15] F.C. Collins, Z. Electrochem. 59 (1955) 404.
- 2601 [16] D. Kashchiev, Surf. Sci. 14 (1969) 209.
- 2602 [17] V.N. Filipovich, V.M. Fokin, N.S. Yuritsyn, A.M. Kalinina,  
2603 Thermochim. Acta 280&281 (1996) 205.
- 2604 [18] G. Tammann, Z. Phys. Chem. 25 (1898) 441.
- 2605 [19] M. Ito, T. Sakaino, T. Moriya, Bull. Tokyo Inst. Technol. 88 (1968)  
2606 127.
- 2607 [20] V.N. Filipovich, A.M. Kalinina, Izv. Akad. Nauk USSR, Neorgan.  
2608 Mat. 4 (1968) 1532 (in Russian).
- 2609 [21] I. Gutzow, Contemp. Phys. 21 (1980) 121, 243.
- 2610 [22] S. Toschev, I. Gutzow, Phys. Status Solidi 24 (1967) 349.
- 2611 [23] U. Köster, Mater. Sci. Eng. 97 (1988) 183.
- 2612 [24] V.M. Fokin, N.S. Yuritsyn, V.N. Filipovich, A.M. Kalinina, J. Non-  
2613 Cryst. Solids 219 (1997) 37.
- 2614 [25] E.D. Zanotto, P.F. James, J. Non-Cryst. Solids 124 (1990) 86.
- 2615 [26] E.D. Zanotto, J. Mater. Res. 13 (1998) 2045.
- 2616 [27] S. Toschev, in: P. Hartman (Ed.), North-Holland Publishing  
2617 Company, Amsterdam, 1973, p. 1.
- 2618 [28] V.P. Skripov, V.P. Koverda, Spontaneous Crystallization of Super-  
2619 cooled Liquids, Nauka, Moscow, 1984 (in Russian).
- 2620 [29] A.N. Kolmogorov, Izv. Akad. Nauk USSR, Ser. Mathem. 3 (1937)  
2621 355 (in Russian).
- 2622 [30] W.A. Johnson, R.F. Mehl, Trans. AIME 135 (1939) 416.
- [31] M. Avrami, J. Chem. Phys. 7 (1939) 1103. 2623
- [32] V.N. Filipovich, A.M. Kalinina, V.M. Fokin, E.K. Shishchikina, D.D.  
2624 Dmitriev, Fiz. Khim. Stekla 9 (1983) 58 [English trans.: Soviet J.  
2625 Glass Phys. Chem. 9 (1983) 45]. 2626
- [33] E.D. Zanotto, A.C. Galhardi, J. Non-Cryst. Solids 103 (1982) 73. 2627
- [34] A.A. Cabral, V.M. Fokin, E.D. Zanotto, J. Non-Cryst. Solids 330  
2628 (2003) 174. 2629
- [35] V.M. Fokin, A.M. Kalinina, V.N. Filipovich, J. Cryst. Growth 52  
2630 (1980) 115. 2631
- [36] A.M. Kalinina, V.M. Fokin, V.N. Filipovich, J. Non-Cryst. Solids  
2632 38&39 (1980) 723. 2633
- [37] U. Schiffrer, W. Pannhorst, Glastechn. Ber. 60 (1987) 211. 2634
- [38] A.M. Kalinina, V.M. Fokin, V.N. Filipovich, Fiz. Khim. Stekla 2  
2635 (1976) 298 [English trans.: Soviet J. Glass Phys. Chem. 2 (1976) 294]. 2636
- [39] I. Gutzow, S. Toschev, M. Marinov, E. Popov, Kristall Technik 3  
2637 (1968) 337. 2638
- [40] E.D. Zanotto, V.M. Fokin, Phil. Trans. R Soc. Lond. A 361 (2002)  
2639 591. 2640
- [41] V.M. Fokin, A.M. Kalinina, V.N. Filipovich, Fiz. Khim. Stekla 3  
2641 (1977) 122 [English trans.: Soviet J. Glass Phys. Chem. 3 (1977) 113]. 2642
- [42] S.C. Glotzer, J. Non-Cryst. Solids 274 (2000) 342. 2643
- [43] V.M. Fokin, A.M. Kalinina, V.N. Filipovich, Fiz. Khim. Stekla 3  
2644 (1977) 129 [English trans.: Soviet J. Glass Phys. Chem. 3 (1977) 119]. 2645
- [44] Z. Kozisek, Cryst. Res. Technol. 23 (1988) 1315. 2646
- [45] K.F. Kelton, A.L. Greer, Phys. Rev. B 38 (1988) 10089. 2647
- [46] A.L. Greer, K.F. Kelton, J. Am. Ceram. Soc. 74 (1991) 1015. 2648
- [47] J. Deubener, in: Proc. XIX Int. Cong. on Glass, vol. 2, Extended  
2649 Abstracts, Soc. Glass Technology, Edinburgh, 2001, p. 66. 2650
- [48] O.V. Potapov, V.M. Fokin, V.L. Ugolkov, L.Y. Suslova, V.N.  
2651 Filipovich, Glass Phys. Chem. 26 (2000) 39. 2652
- [49] D. Turnbull, J. Chem. Phys. 18 (1950) 769. 2653
- [50] A.S. Skapski, Acta Metall. 4 (1956) 576. 2654
- [51] A.M. Kalinina, V.N. Filipovich, V.M. Fokin, G.A. Sycheva, in:  
2655 Proc. XIV Int. Cong. on Glass, vol. 1, New Delhi, 1986, p. 366. 2656
- [52] O.V. Potapov, V.M. Fokin, V.N. Filipovich, J. Non-Cryst. Solids  
2657 247 (1999) 74. 2658
- [53] R. Müller, E.D. Zanotto, V.M. Fokin, J. Non-Cryst. Solids 274  
2659 (2000) 208. 2660
- [54] G. Tammann, Z. Elektrochemie 10 (1904) 532. 2661
- [55] P.F. James, in: M.H. Lewis (Ed.), Glasses and Glass-Ceramics,  
2662 Chapman and Hall, London, 1989, p. 59. 2663
- [56] E.D. Zanotto, J. Non-Cryst. Solids 89 (1987) 361. 2664
- [57] J. Deubener, J. Non-Cryst. Solids 274 (2000) 195. 2665
- [58] V.M. Fokin, E.D. Zanotto, J.W.P. Schmelzer, J. Non-Cryst. Solids  
2666 321 (2003) 52. 2667
- [59] M.H. Lewis, J. Metacalf-Johanson, P.S. Bell, J. Am. Ceram. Soc. 62  
2668 (1979) 278. 2669
- [60] D. Turnbull, in: J.A. Prins (Ed.), Physics of Non-Crystalline Solids,  
2670 North Holland Publishing Company, Amsterdam, 1965, p. 41. 2671
- [61] G. Tammann, Der Glaszustand, Leopold Voss Verlag, Leipzig,  
2672 1933. 2673

- 2674 [62] G.L. Mikhnevich, J.F. Browko, *Phys. Sowjetunion* 13 (1938) 113.
- 2675 [63] P.F. James, in: J.H. Simmons, D.R. Uhlmann, G.H. Beall (Eds.),
- 2676 *Advances in Ceramics*, vol. 4, American Ceramic Society, Colum-
- 2677 bus, Ohio, 1982, p. 1.
- 2678 [64] M.C. Weinberg, E.D. Zanotto, *J. Non-Cryst. Solids* 108 (1989) 99.
- 2679 [65] Y. Miyazawa, G.M. Pound, *J. Cryst. Growth* 23 (1974) 45.
- 2680 [66] D. Turnbull, *J. Chem. Phys.* 20 (1952) 411.
- 2681 [67] L. Shartsis, S. Spinner, *J. Res. Nat. Bur. Stand.* 46 (1951) 385.
- 2682 [68] A.A. Appen, K.A. Schishov, S.S. Kaylova, *Silikattechnik* 4 (1953)
- 2683 104.
- 2684 [69] V.M. Fokin, E.D. Zanotto, J.W.P. Schmelzer, *J. Non-Cryst. Solids*
- 2685 278 (2000) 24.
- 2686 [70] J. Stefan, *Ann. Phys.* 29 (1886) 655.
- 2687 [71] V.M. Fokin, E.D. Zanotto, *J. Non-Cryst. Solids* 265 (2000) 105.
- 2688 [72] I. Gutzow, D. Kashchiev, I. Avramov, *J. Non-Cryst. Solids* 73
- 2689 (1985) 477.
- 2690 [73] A.I. Rusanov, *Phasengleichgewichte und Grenzflächenerscheinun-*
- 2691 *gen*, Akademie-Verlag, Berlin, 1978.
- 2692 [74] V.P. Skripov, M.Z. Faizulin, in: J.W.P. Schmelzer (Ed.), *Nucleation*
- 2693 *Theory and Applications*, Wiley-VCH, Berlin-Weinheim, 2005, p. 4.
- 2694 [75] F. Spaepen, *Solid State Phys.* 47 (1994) 1.
- 2695 [76] V.N. Filipovich, T.A. Zhukovskaya, *Fiz. Khim. Stekla* 14 (1988) 300
- 2696 (in Russian).
- 2697 [77] L. Granasy, P. James, *J. Non-Cryst. Solids* 253 (1999) 210.
- 2698 [78] L. Granasy, T. Börzsony, T. Pusztai, *J. Cryst. Growth* 237 (2002)
- 2699 1813.
- 2700 [79] J.W.P. Schmelzer, G.Sh. Boltachev, V.G. Baidakov, in: J.W.P.
- 2701 Schmelzer (Ed.), *Nucleation Theory and Applications*, Wiley-VCH,
- 2702 Berlin-Weinheim, 2005, p. 418.
- 2703 [80] V.G. Baidakov, G.Sh. Boltachev, J.W.P. Schmelzer, *J. Colloid*
- 2704 *Interface Sci.* 231 (2000) 312.
- 2705 [81] V.G. Baidakov, J.W.P. Schmelzer, *J. Phys. Chem. B* 105 (2001)
- 2706 11595.
- 2707 [82] J.W. P Schmelzer, V.G. Baidakov, G.Sh. Boltachev, *J. Chem. Phys.*
- 2708 119 (2003) 6166.
- 2709 [83] J.D. van der Waals, Ph. Kohnstamm, *Lehrbuch der Thermodyn-*
- 2710 *amik*, Johann-Ambrosius-Barth Verlag, Leipzig und Amsterdam,
- 2711 1908.
- 2712 [84] J.D. van der Waals, *Z. Phys. Chem.* 13 (1893) 657 (in German) [J.S.
- 2713 Rowlinson, Translation of J.D. van der Waals': *The thermodynamic*
- 2714 *theory of capillarity under the hypothesis of a continuous variation*
- 2715 *of density*, *J. Stat. Phys.* 20 (1979) 197].
- 2716 [85] J.W. Cahn, J.E. Hilliard, *J. Chem. Phys.* 28 (1959) 258;
- 2717 J.W. Cahn, J.E. Hilliard, *J. Chem. Phys.* 31 (1959) 688.
- 2718 [86] D.W. Oxtoby, R. Evans, *J. Chem. Phys.* 89 (1988) 7521.
- 2719 [87] C.K. Bagdassarian, D.W. Oxtoby, *J. Chem. Phys.* 100 (1994) 2139.
- 2720 [88] D.W. Oxtoby, *Acc. Chem. Res.* 31 (1998) 91.
- 2721 [89] L. Granasy, *J. Mol. Struct.* 485&486 (1999) 523.
- 2722 [90] L. Granasy, T. Pusztai, P. James, *J. Chem. Phys.* 117 (2002) 6157.
- 2723 [91] J.W.P. Schmelzer, A.S. Abyzov, J. Möller, *J. Chem. Phys.* 121 (2004)
- 2724 6900.
- 2725 [92] B.N. Hale, in: M. Kasahara, M. Kulmala (Eds.), 16th Int. Conf. on
- 2726 *Nucleation and Atmospheric Aerosols*, Kyoto, Japan, August 2004,
- 2727 compact disk.
- 2728 [93] P.R. ten Wolde, D. Frenkel, *J. Chem. Phys.* 109 (1998) 9919.
- 2729 [94] V.K. Shen, P.G. Debenedetti, *J. Chem. Phys.* 111 (1999) 3581.
- 2730 [95] K. Laasonen, S. Wonzak, R. Strey, A. Laaksonen, *J. Chem. Phys.*
- 2731 113 (2000) 9741.
- 2732 [96] B. Chen, J.I. Siepmann, K.J. Oh, M.L. Klein, *J. Chem. Phys.* 115
- 2733 (2000) 10903.
- 2734 [97] J.W.P. Schmelzer, J. Schmelzer Jr., I. Gutzow, *J. Chem. Phys.* 112
- 2735 (2000) 3820.
- 2736 [98] J.W.P. Schmelzer, in: J.W.P. Schmelzer (Ed.), *Nucleation Theory*
- 2737 *and Applications*, Wiley-VCH, Berlin-Weinheim, 2005, p. 447.
- 2738 [99] H. Ulbricht, J.W.P. Schmelzer, R. Mahnke, F. Schweitzer, *Ther-*
- 2739 *modynamics of Finite Systems and the Kinetics of First-Order Phase*
- 2740 *Transitions*, Teubner, Leipzig, 1988.
- [100] J.W.P. Schmelzer, V.G. Baidakov, *J. Chem. Phys.*, submitted for
- publication.
- [101] J.W.P. Schmelzer, *Phys. Chem. Glasses* 45 (2004) 116.
- [102] J.W.P. Schmelzer, A.R. Gokhman, V.M. Fokin, *J. Colloid Interface*
- Sci.* 272 (2004) 109.
- [103] J.W.P. Schmelzer, in: XX Int. Cong. on Glass, Kyoto, 2004,
- compact disk.
- [104] J.W.P. Schmelzer, A.S. Abyzov, in: J.W.P. Schmelzer, G. Röpke,
- V.B. Priezhev (Eds.), *Nucleation Theory and Applications*, Joint
- Institute for Nuclear Research Publishing Department, Dubna,
- Russia, 2006, p. 4.
- [105] L. Granasy, P.F. James, *J. Chem. Phys.* 113 (2000) 9810.
- [106] D. Tatchev, G. Goerigk, E. Valova, J. Dille, R. Kranold, S.
- Armyanov, J.-L. Delplancke, *Appl. Crystallogr.* 38 (2005) 787.
- [107] D. Tatchev, A. Hoell, R. Kranold, S. Armyanov, *Physica B* 369
- (2005) 8.
- [108] P.J. Desre, E. Cini, B. Vinet, *J. Non-Cryst. Solids* 288 (2001) 210.
- [109] W. Pan, A.B. Kolomeisky, P.G. Vekilov, *J. Chem. Phys.* 122 (2005)
- 174905.
- [110] G. Medeiros-Ribeiro, A.M. Bratkovski, T.I. Kamins, D.A.A.
- Ohlberg, R.S. Williams, *Science* 286 (1998) 353.
- [111] F.M. Ross, R.M. Tromp, M.C. Reuter, *Science* 286 (1999) 1931.
- [112] A. Rastelli, M. Kummer, H. van Käse, *Phys. Rev. Lett.* 87 (2001)
- 256101.
- [113] P.G. Debenedetti, H. Reiss, *J. Chem. Phys.* 108 (1998) 5498, and
- references cited therein.
- [114] D.W. Oxtoby, *Nature* 347 (1990) 725.
- [115] L. Granasy, T. Börzsony, T. Pusztai, *Phys. Rev. Lett.* 20 (2002)
- 206105.
- [116] L. Granasy, T. Pusztai, J.A. Warren, *J. Phys.: Cond. Matter.* 16
- (2004) R1205.
- [117] T. Pusztai, G. Bortel, L. Granasy, *Europhys. Lett.* 71 (2005) 131.
- [118] T. Pusztai, G. Bortel, L. Granasy, *Mater. Sci. Eng. A* 413&414
- (2005) 412.
- [119] V.P. Skripov, V.G. Baidakov, *High Temp. Thermal Phys.* 10 (1972)
- 1226 (in Russian).
- [120] L.D. Landau, I.M. Lifschitz, *Statistische Physik*, Akademie-Verlag,
- Berlin, 1976.
- [121] V.P. Skripov, M.Z. Faizullin, *Solid-Liquid-Gas Phase Transitions*
- and Thermodynamic Similarity*, Wiley-VCH, Berlin-Weinheim,
- 2006.
- [122] L. Granasy, T. Wang, P. James, *J. Chem. Phys.* 108 (1998) 7317.
- [123] L. Granasy, D.W. Oxtoby, *J. Chem. Phys.* 112 (2000) 2410.
- [124] L. Granasy, T. Pusztai, *J. Chem. Phys.* 117 (2002) 10121.
- [125] D. Kashchiev, *J. Chem. Phys.* 76 (1984) 5098.
- [126] D.W. Oxtoby, D. Kashchiev, *J. Chem. Phys.* 100 (1994) 7665.
- [127] J.W.P. Schmelzer, *J. Colloid Interface Sci.* 242 (2001) 354.
- [128] J.W.P. Schmelzer, *Russ. J. Phys. Chem.* 77 (2003) 143.
- [129] Y. Viisanen, R. Strey, H. Reiss, *J. Chem. Phys.* 99 (1993) 4680.
- [130] Y. Viisanen, R. Strey, *J. Chem. Phys.* 105 (1996) 8293.
- [131] V.G. Karpov, D.W. Oxtoby, *Phys. Rev.* 54 (1996) 9734.
- [132] M.F. Thorpe, *J. Non-Cryst. Solids* 57 (1983) 355.
- [133] M.F. Thorpe, M.I. Mitkova (Eds.), *Amorphous insulators and*
- semiconductors*, NATO ASI, Kluwer, Dordrecht, 1997.
- [134] I. Avramov, R. Keding, C. Rüssel, R. Kranold, *J. Non-Cryst. Solids*
- 278 (2001) 13.
- [135] B.A. Shakhmatkin, N.M. Vedishcheva, *J. Non-Cryst. Solids* 171
- (1994) 1.
- [136] B.A. Shakhmatkin, N.M. Vedishcheva, M.M. Shultz, A.C. Wright,
- J. Non-Cryst. Solids* 177 (1994) 249.
- [137] V.M. Fokin, O.V. Potapov, E.D. Zanotto, F.M. Spiandorello, V.L.
- Ugolkov, B.Z. Pevzner, *J. Non-Cryst. Solids* 331 (2003) 240.
- [138] E.N. Soboleva, N.S. Yuritsyn, V.L. Ugolkov, *Glass Phys. Chem.* 30
- (2004) 481.
- [139] G. Völksch, T. Kittel, F. Siegelin, H.-J. Kleebe, in: XIX Int. Cong.
- on Glass, Edinburgh, 2001.
- [140] M. Roskosz, M.J. Toplis, P. Besson, P. Richet, *J. Non-Cryst. Solids*
- 351 (2005) 1266.
- 2741  
2742  
2743  
2744  
2745  
2746  
2747  
2748  
2749  
2750  
2751  
2752  
2753  
2754  
2755  
2756  
2757  
2758  
2759  
2760  
2761  
2762  
2763  
2764  
2765  
2766  
2767  
2768  
2769  
2770  
2771  
2772  
2773  
2774  
2775  
2776  
2777  
2778  
2779  
2780  
2781  
2782  
2783  
2784  
2785  
2786  
2787  
2788  
2789  
2790  
2791  
2792  
2793  
2794  
2795  
2796  
2797  
2798  
2799  
2800  
2801  
2802  
2803  
2804  
2805  
2806  
2807  
2808

- 2809 [141] J. Deubener, R. Brückner, M. Sternitzke, *J. Non-Cryst. Solids* 163 (1993) 1. 2836
- 2810 [142] N.S. Yuritsyn, J.W.P. Schmelzer, V.M. Fokin, E.D. Zanotto, In preparation. 2837
- 2811 [143] A.R. West, F.P. Glasser, in: L.L. Hench, S.W. Freiman (Eds.), *Advances in Nucleation and Crystallization in Glasses*, American Ceramic Society, Columbus, Ohio, 1971, p. 151. 2838
- 2812 [144] I. Hasdemir, R. Brückner, J. Deubener, *Phys. Chem. Glasses* 39 (1998) 253. 2839
- 2813 [145] E.D. Zanotto, M.L.G. Leite, *J. Non-Cryst. Solids* 202 (1996) 145. 2840
- 2814 [146] M.C. Weinberg, *J. Non-Cryst. Solids* 170 (1994) 300. 2841
- 2815 [147] V.V. Slezov, J.W.P. Schmelzer, in: J.W.P. Schmelzer, G. Röpke, V.B. Priezhev (Eds.), *Nucleation Theory and Applications*, Joint Institute for Nuclear Research Publishing Department, Dubna, Russia, 1999, p. 6. 2842
- 2816 [148] K.S. Russell, *Acta Metall.* 16 (1968) 761. 2843
- 2817 [149] K.F. Kelton, *Acta Mater.* 48 (2000) 1967. 2844
- 2818 [150] W. Ostwald, *Z. Phys. Chem.* 22 (1897) 289. 2845
- 2819 [151] I. Stranski, D. Totomanov, *Z. Phys. Chem. A* 163 (1933) 399. 2846
- 2820 [152] A.S. Milev, I.S. Gutzow, *Bulg. Chem. Commun.* 29 (1996/1997) 597. 2847
- 2821 [153] A.M. Kalinina, V.N. Filipovich, V.A. Kolesova, I.A. Bondar, in: E.A. Porai-Koshits (Ed.), *The Structure of Glass*, vol. 3, Consultants Bureau, New York, 1964, p. 53. 2848
- 2822 [154] D.L. Kinser, L.L. Hench, *J. Am. Ceram. Soc.* 12 (1971) 58. 2849
- 2823 [155] P.C. Soares Jr., Initial stages of crystallization in lithium disilicate glass revisited, MSc thesis, Universidade Federal de São Carlos, Brazil, 1997 (in Portuguese). 2850
- 2824 [156] Y. Iqbal, W.E. Lee, D. Holland, P.F. James, *J. Non-Cryst. Solids* 224 (1998) 1. 2851
- 2825 [157] L.I. Burger, P. Lucas, M.C. Weinberg, P.C. Soares Jr., E.D. Zanotto, *J. Non-Cryst. Solids* 274 (2000) 188. 2852
- 2826 [158] J. Deubener, *Homogene Volumenkeimbildung in Silicatschmelzen: Theorie und Experiment*, Habilitationsschrift, Berlin, 2001. 2853
- 2827 [159] P.C. Soares Jr., E.D. Zanotto, V.M. Fokin, H.J. Jain, *J. Non-Cryst. Solids* 331 (2003) 217. 2854
- 2828 [160] B.A. Shakhmatkin, N.M. Vedishcheva, Private communication, 2001. 2855
- 2829 [161] V.M. Fokin, E.D. Zanotto, J.W.P. Schmelzer, O.V. Potapov, *J. Non-Cryst. Solids* 351 (2005) 1491. 2856
- 2830 [162] L. Granasy, T. Pusztai, P.F. James, *J. Chem. Phys.* 117 (2002) 6157. 2857
- 2831 [163] J.W.P. Schmelzer, R. Pascova, J. Möller, I. Gutzow, *J. Non-Cryst. Solids* 162 (1993) 26. 2858
- 2832 [164] J.W.P. Schmelzer, J. Möller, I. Gutzow, R. Pascova, R. Müller, W. Pannhorst, *J. Non-Cryst. Solids* 183 (1995) 215. 2859
- 2833 [165] E.D. Zanotto, E.J. Müller, *J. Non-Cryst. Solids* 130 (1991) 220. 2860
- 2834 [166] J.W.P. Schmelzer, R. Müller, J. Möller, I.S. Gutzow, *Phys. Chem. Glasses* 43C (2002) 291. 2861
- 2835 [167] J.W.P. Schmelzer, R. Müller, J. Möller, I.S. Gutzow, *J. Non-Cryst. Solids* 315 (2003) 144. 2862
- 2836 [168] J.W.P. Schmelzer, E.D. Zanotto, I. Avramov, V.M. Fokin, *J. Non-Cryst. Solids*, in press. 2863
- 2837 [169] J.W.P. Schmelzer, O.V. Potapov, V.M. Fokin, R. Müller, S. Reinsch, *J. Non-Cryst. Solids* 333 (2004) 150. 2864